Order Number 9218279

Structure/function and conformation/activity relationships for biologically significant peptides

Tallon, Michael Anthony, Ph.D.

City University of New York, 1992

U·M·I

300 N. Zeeb Rd.
Ann Arbor, MI 48106

STRUCTURE/FUNCTION AND CONFORMATION/ACTIVITY RELATIONSHIPS FOR BIOLOGICALLY SIGNIFICANT PEPTIDES

By

Michael A. Tallon

A dissertation submitted to the Graduate Faculty in Biochemistry in partial fulfillment of the requirements for the degree of Doctor of Philosophy, The City University of New York.

1992

This manuscript has been read and accepted for the Graduate Faculty in Biochemistry in satisfaction of the dissertation requirement for the degree of Doctor of Philosophy.

August 8, 1991
Date

Fred Naider
Chair of Examining Committee

Date

Horst Schuster
Executive Officer

Ruth Stark

Supervisory Committee

The City University of New York

ABSTRACT

STRUCTURE/FUNCTION AND CONFORMATION/ACTIVITY RELATIONSHIPS FOR BIOLOGICALLY SIGNIFICANT PEPTIDES

By

Michael A. Tallon

Advisor: Professor Fred Naider

Peptides corresponding to putative loop regions 107-125, 191-206, and 350-372, for the α-factor receptor of the yeast *Saccharomyces cerevisiae* were synthesized by solid phase methods in purified yields ranging from 15 to 44% of theoretical. These peptides were greater than 98% homogeneous as judged by gradient reversed phase HPLC, and were characterized by either FAB-MS, amino acid analysis, or 200 MHz ^{1}H-NMR spectroscopy. The synthetic peptides were used to generate polyclonal antisera which will be utilized as topological probes for the α-factor receptor in future studies.

Peptide based probes for the α-factor binding site within the STE-2 receptor were synthesized by incorporation of either a biotin, fluorescein, or the Bolton Hunter group into the [Nle^{12}]-α-factor pheromone, or into the tetradecapeptide analog, [Lys^{-1}, Nle^{12}]-α-factor. All of these peptides are within one order of magnitude as active as the native pheromone, and therefore represent a class of reagents that will be useful in identifying the pheromone binding site.

In addition to the synthesis of receptor probes, detailed conformational analyses on $cyclo^{7,10}$ [Nle^{12}]-α-factor and on a biologically active analog of the mammalian peptide hormone Substance P, [$pGlu^{6}$-Phe-$NMePhe^{8}$-Aib^{9}-Leu-Met^{11}-NH_2] SP^{6-11}, were performed in DMSO-d_6 at 25°C, utilizing 2D NMR techniques. The results indicate that a mixture of type I and type II β-turns, spanning residues 7-10 in the cyclic α-factor, is present in DMSO. Long range interactions were also observed, indicating the ends of this molecule are in close proximity. The NMR results on the NK3 selective Substance P analog indicate that [$pGlu^{6}$,$NMePhe^{8}$, Aib^{9}]SP^{6-11} exhibits cis/trans isomerism about the Phe^{7}-$NMePhe^{8}$ peptide bond. This results in a 60/40 mixture of *cis* and *trans* forms

of this hexapeptide in DMSO at 25°C. Long range interactions were observed which indicate that both the *cis* and *trans* isomers are bent in solution. In each molecule, the amide and terminal carboxamide of methionine[11] are hydrogen bonded. Our results suggest that the Substance P analog is conformationally restricted and that consecutive C_7 conformations may span residues Aib[9]-Leu-Met[11]-NH_2.

To Susan

Whose Love, Support, and Encouragement

were instrumental in completing this

dissertation.

ACKNOWLEDGEMENT

At this point, I would like to acknowledge the many people who have given me advise and training during the period of my graduate studies. First and foremost, I am truly indebted to my mentor Dr. Fred Naider, whose enthusiasm, dedication and passion for his work, has not only instilled these qualities in myself, but has also taught me how to be objective and critical of my own work. He is a fine chemist and an excellent mentor. I would like to thank Dr. Ponniah Shengbagamurthi for training me in the field of peptide chemistry, and for synthesizing several of the peptide analogs used in this study. The efforts of Dr. Jeffrey M. Becker, Effimia Eriotou-Bariota, Steven Marcus, David Miller, and Dusty Hill can not be underscored, their biological results were essential for this dissertation. Special thanks to Dr. Chu-Biao Xue for contributing the cyclo^{7,10}[Nle^{12}]-α-factor and [Lys^{7}-Acetyl, Nle^{12}]-α-factor for this study, his synthetic expertise has been an inspiration to me during these studies. I would like to thank John Gounarides, Sean Cahill, Linda Jelicks, Paula Longo, Michael Blumenstein, and Dr. Michelle Briodo, for not only allowing me to use the NMR facilities at Hunter College, but for their helpful and insightful discussions as well.

I would like to specially thank the members of my thesis committee: Dr. Ruth Stark; Dr. Peter Lipke; Dr. Robert Bittman; and Dr. Jeffrey Becker, for their time, suggestions, and helpful criticism, during the course of my graduate studies. And finally but most importantly, I would like to thank my wife Susan, your support, encouragement, and devotion have made the creation of this text possible.

TABLE OF CONTENTS

LIST OF TABLES

LIST OF ILLUSTRATIONS

Abbreviations:

Ac	-	Acetyl
BHA	-	Benzhydrylamine (resin)
Boc	-	*tert*-butyloxycarbonyl
Bop	-	Benzatriazol-1-yl-oxy-tris-(dimethylamino)phosphonium hexafluorophosphate
2-Br-Cbz	-	2-Bromobenzyloxycarbonyl
Bzl	-	Benzyl
n-BuOH	-	1-Butanol
$CHCl_3$	-	Chloroform
2-Cl-Cbz	-	2-Chlorobenzyloxycarbonyl
COSY	-	Correlation spectroscopy
DCC	-	1,3-Dicyclohexylcarbodiimide
DCHA	-	Dicyclohexylamine
DCM	-	Dichloromethane
DCU	-	1,3-Dicyclohexylurea
DIEA	-	N,N'-Diisopropylethylamine
DIPC	-	1,3-Diisopropylcarbodiimide
DIPU	-	1,3-Diisopropylurea
DMF	-	N,N'-Dimethylformamide
DMS	-	Dimethyl sulfide
DMSO	-	Dimethyl sulfoxide
DQF	-	Double-Quantum-Filtered (spectroscopy)

Et_2O	-	Diethyl ether
EtOAc	-	Ethyl acetate
EtOH	-	Ethanol
FAB-MS	-	Fast Atom Bombardment-Mass Spectrometry
FMOC	-	9-Fluorenylmethyloxycarbonyl
For	-	Formyl
HF	-	Hydrogen fluoride
HOAc	-	Acetic acid
HOBt	-	1-hydroxybenzotriazole
HPPA	-	β-(4-hydroxyphenyl)propionate
HPLC	-	High Performance Liquid Chromatography
*i*PrOH	-	2-propanol
MBHA	-	4-methylbenzhydrylamine (resin)
MeCN	-	Acetonitrile
MeOH	-	Methanol
Nle	-	Norleucine
NMR	-	Nuclear magnetic resonance (spectroscopy)
NOESY	-	Nuclear Overhauser Enhancement Spectroscopy
ONp	-	4-nitrophenyl ester
OSu	-	N-hydroxysuccinimide ester
PAM	-	Phenylacetamidomethyl (resin)
Pyr	-	Pyridine
ROESY	-	Rotating-frame Overhauser Enhancement Spectroscopy
SPPS	-	Solid-Phase Peptide Synthesis
SUBP	-	Substance P

TEA - Triethylamine

TFA - Trifluoroacetic acid

TLC - Thin-layer chromatography

TMS - Tetramethylsilane

Tos - 4-toluenesulfonyl

UV - Ultraviolet (spectroscopy)

YEPD - Yeast extract-peptone-dextrose medium

YNB - Yeast nitrogen base medium

Standard abbreviations for amino-acid derivatives and peptides are according to IUPAC-IUB joint commission on Biochemical Nomenclature(1983)(1)

I) Introduction

Introduction:

Many cells of higher eukaryotic organisms communicate with one another through the use of sophisticated intercellular messengers. These signaling molecules serve to control a variety of cellular processes such as growth, differentiation, reproduction, and metabolism.

Understanding the molecular basis for control of these processes is critically important, and has remained a central goal in many fields of science. Ultimately one must focus on the signaling molecule itself to get a true picture of its biological relevance in the control of these processes. Furthermore, this messenger provides a major focal point to manipulate the process under investigation, through the use and design of agonists and/or antagonists.

As varied as are the processes controlled by these intercellular messengers, so are the types of signaling molecules themselves. These include inorganic ions, steroids, peptides, proteins, phospholipids and many other complex organic molecules. Most pertinent to this dissertation are the peptide hormones. In the chemical structure of a peptide hormone resides the information necessary to interact with its cognate receptor. A great deal of effort has been expended to elucidate the secondary and tertiary structure of peptide hormones, with the aim of

relating the solution-state conformation of these molecules to the biologically-active state. The results of these types of studies not only lead to a better understanding on how the peptide hormone invoke activity, but also aid in the design of analogs which are agonists or antagonists. This approach has been successfully applied to a number of peptide hormones, such as human growth hormone(2), somatostatin(3), and the enkephalins(4).

Numerous classes of peptide hormones have been defined, and many seem to share common signal-transduction systems(5-7). Association of the peptide messenger with its receptor can trigger an amplified biochemical cascade, either mediated through a G-protein complex or directly to the effector system. Several cell-surface receptors interact with guanine nucleotide binding proteins(G-proteins), and these G-proteins mediate signal transduction from receptor to intracellular effectors(8-13). In addition, the genes for several cell-surface receptors have been cloned and sequenced, and according to the hydropathy profile for the primary gene product, many receptors appear to have similar structural models for their overall folding patterns (14-17). In these models, the cell surface receptor contains several transmembrane helices, which are connected by hydrophilic loops as one of the major structural features.

This structural motif was observed for mammalian receptors such as rhodopsin(18), the β_2-andernergic receptor(19), and the acetylcholine receptor(20).

The unicellular yeast *Saccharomyces cerevisiae* provides an excellent model system to study peptide hormone/cell interactions. The signal transduction system in this yeast possesses many characteristics found in higher eukaryotic organisms. For example, models for the folding pattern of the pheromone receptors in this yeast resemble those for mammalian receptors, such as the rhodopsin/β_2-adrenergic receptor family(61-63). The yeast pheromone receptors are believed to interact with G-proteins, which mediate signal transduction to an as yet undefined effector system(21,22). Signal transduction mediated through a G-protein complex was also found for several mammalian receptors, such as the nicotinic acetylcholine receptor(23), rhodopsin(24), and the β_2-adrenergic receptor(25). Furthermore, the genes coding for these yeast G-proteins have been cloned and sequenced, and their predicted primary structures are highly homologous to mammalian G-protein sequences(26,27). Moreover, recent studies have reported on the insertion of mammalian β_2-adrenergic receptor and a mammalian G_α-protein into yeast cells using recombinant DNA methods(28). Mutant yeast cells expressing both the β_2-adrenergic receptor and the G_α-subunit responded to adrenergic agonists and their

antagonists(29). This result clearly suggests a biochemical similarity between simple yeast cells and cells of complex eukaryotic organisms. Since *S. cerevisiae* is easy to manipulate genetically and to grow in the laboratory, and shares overall biochemical similarity with other yeast and eukaryotic cells, this model system should permit great insights to be gained into the mode of action of peptide hormones and their receptors.

A major interest of this research group is the analysis of peptide/cell interactions. This topic has been approached by examining structure/function relationships for peptide hormones as well as attempting to relate the conformation of a peptide to its specific activity. The goals of my dissertation were to develop tools which could be useful in localizing the binding site of the α-factor receptor, the receptor's overall topology in the membrane, and to examine the structure of a constrained analog of α-factor which was biologically active. These studies should provide insights into the structural requirements for binding of α-factor to its receptor.

In addition to studies on α-factor, I conducted a detailed conformational analysis on a biologically active analog of a mammalian peptide hormone. Substance P is a undecaneuropeptide, Arg-Pro-Lys-Pro-Gln-Gln-Phe-Phe-Gly-Leu-Met-NH_2, which is believed to be involved in pain

perception. A conformationally restricted analog was synthesized by Dr. Michael Chorev at the Hebrew University, Jerusalem, Israel. This analog is a potent agonist of Substance P, but interacts with only one of three possible Neurokinin receptor subtypes, specifically NK-3 (30).

A complete conformational analysis for this analog, utilizing two-dimensional nuclear magnetic resonance techniques, was performed. The goal of these studies was to elucidate structural characteristics for the solution-state conformation of this analog in DMSO. The results of these studies may provide insights into the structural requirements for binding of this analog to its specific receptor subtype.

Background:

A) Mating in Yeast:

In the yeast *S. cerevisiae*, there exists two haploid cell-types, designated as **a** or α (32,33). Either haploid cell-type can asexually reproduce through the process of budding, or in the presence of its opposite cell-type, can sexually reproduce(34). During sexual conjugation an **a** and α-cell fuse to form an **a**/α diploid cell. This diploid can grow asexually or can undergo a series of meiotic events, to generate four haploid progeny spores, as depicted in Figure 1.

Sexual mating is initiated through the reciprocal exchange of diffusible peptide pheromones. α-Cells secrete a tridecapeptide α-factor pheromone, Trp-His-Trp-Leu-Gln-Leu-Lys-Pro-Gly-Gln-Pro-Met-Tyr, which targets **a**-cells (35), whereas **a**-cells secrete a dodecapeptide **a**-factor pheromone,Tyr-Ile-Ile-Lys-Gly-Val-Phe-Trp-Asp-Pro-Ala-Cys[S-farnesyl]-$COOCH_3$(36,37), which targets α-cells. Similar physiological responses are evoked by both pheromones from their target cell. These include changes in gene expression and increased agglutinability to the opposite cell-type, which aids in the cell fusion process.

Figure 1. Life cycle of the yeast *Saccharomyces cerevisiae* **(31).**

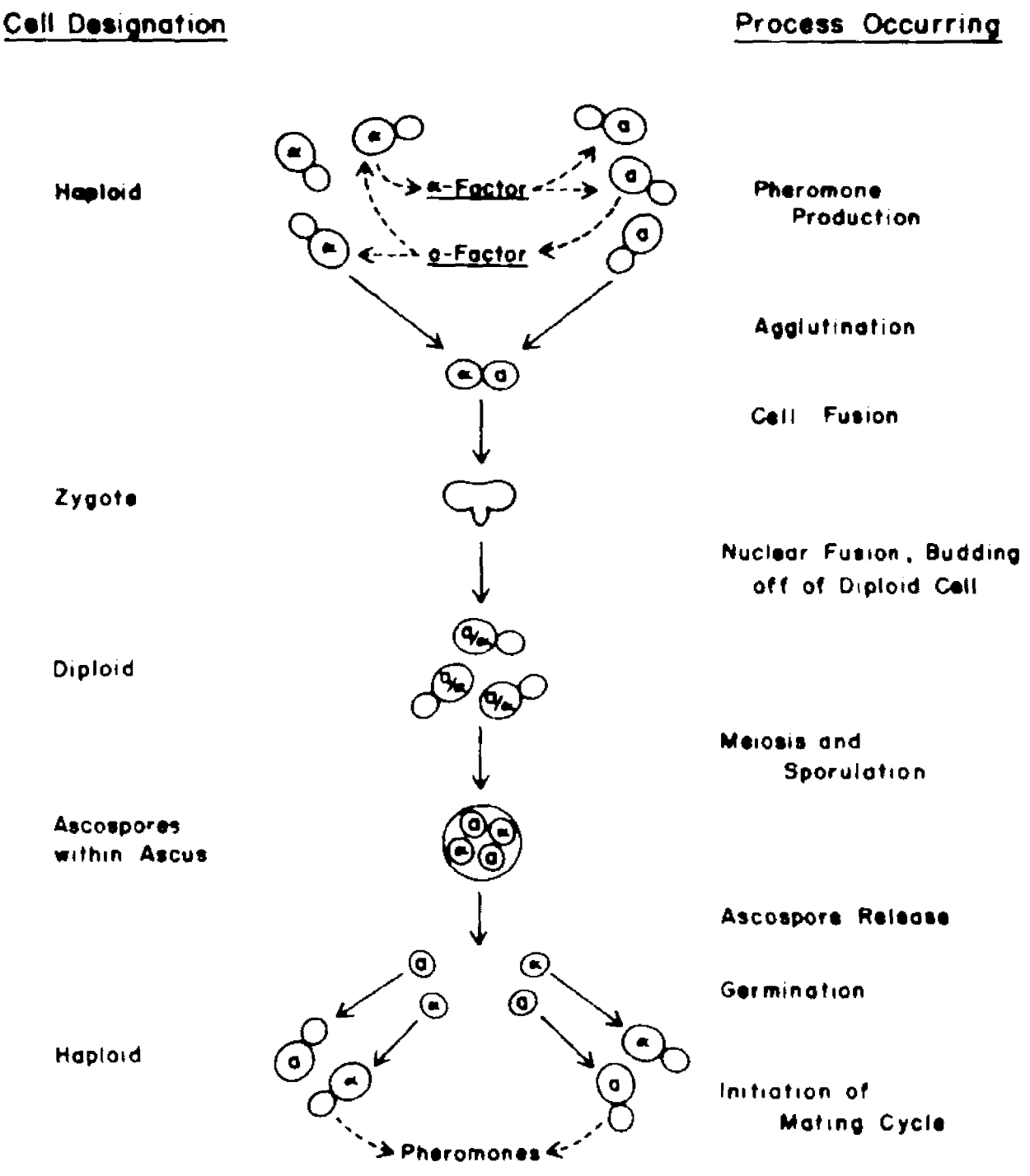
Cell Designation
Process Occurring
Haploid
α-Factor
a-Factor
Pheromone Production
Agglutination
Cell Fusion
Zygote
Nuclear Fusion, Budding off of Diploid Cell
Diploid
Meiosis and Sporulation
Ascospores within Ascus
Ascospore Release
Germination
Haploid
Initiation of Mating Cycle
Pheromones

Cessation of DNA synthesis in the G1-phase of the growth cycle, which synchronizes both cell-types for the ensuing meiotic events, as well as changes in the biosynthesis of cell-wall components, and pronounced morphological changes known as "shooming", which enable cells to seek out their opposite mating partners(38).

The **a** or α-phenotype is conferred by the mating-type locus, **MAT**, localized to chromosome three in the yeast genome(39). The **MAT** locus codes for a number of master-regulatory proteins, which control cell-type specific gene expression in *S. cerevisiae*. A variety of structural gene products are known to be under the control of the **MAT** locus. In particular, *MFα1* and *MFα2* code for pre-pro-α-factor; two different polypeptides each containing multiple copies of the pheromone(40). Pre-pro-α-factor undergoes a series of proteolytic processing events to generate the mature tridecapeptide α-factor pheromone, Trp-His-Trp-Leu-Gln-Leu-Lys-Pro-Gly-Gln-Pro-Met-Tyr(41).

Figure 2. Proteolytic processing of biosynthetic precursors of pre-pro-α-factor.

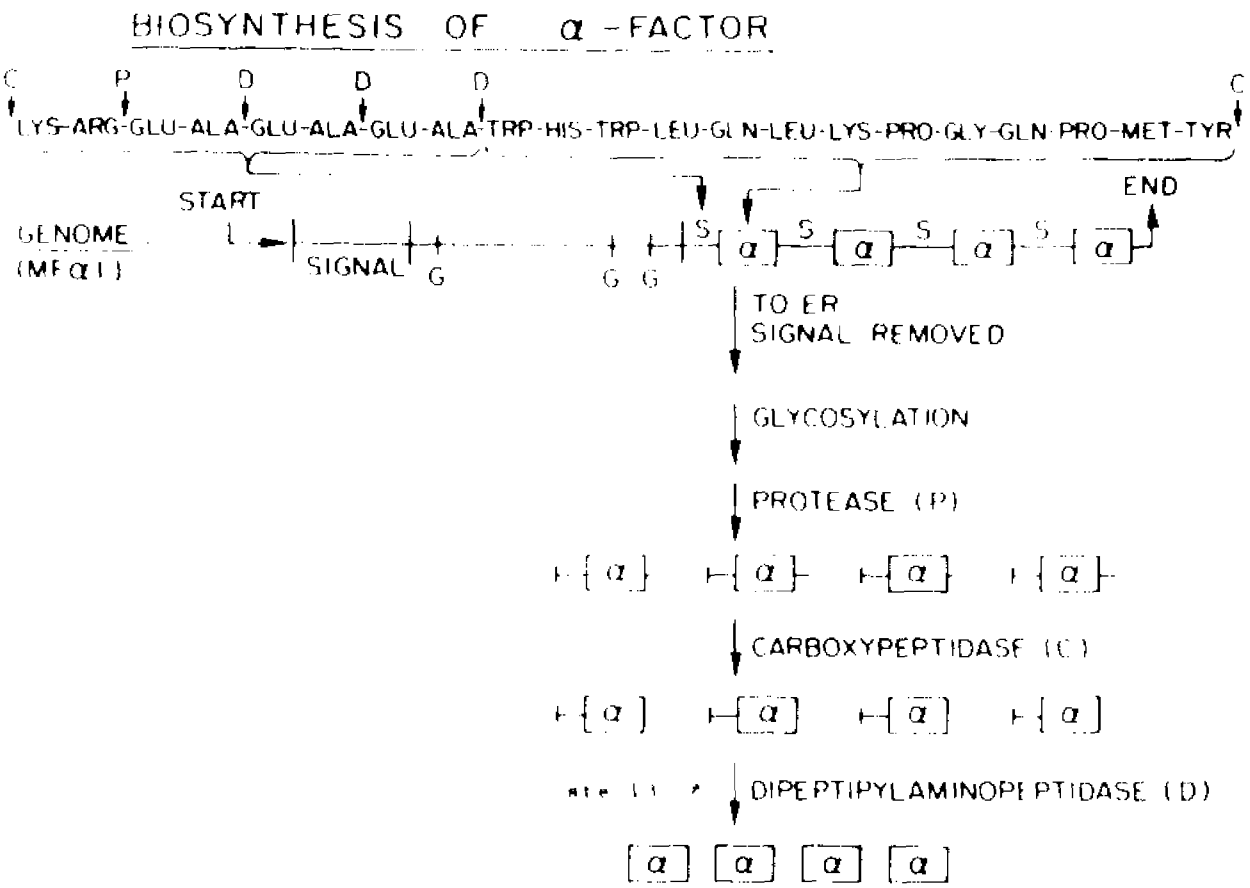
BIOSYNTHESIS OF α-FACTOR
C P D D D C
LYS-ARG-GLU-ALA-GLU-ALA-GLU-ALA-TRP-HIS-TRP-LEU-GLN-LEU-LYS-PRO-GLY-GLN-PRO-MET-TYR
START
END
GENOME
(MFα1)
SIGNAL
G
G G
S
α
TO ER
SIGNAL REMOVED
GLYCOSYLATION
PROTEASE (P)
CARBOXYPEPTIDASE (C)
DIPEPTIPYLAMINOPEPTIDASE (D)

As depicted in Figure 2 (see p.12), the *MFα1* precursor contains four identical tandem repeats of the mature α-factor pheromone sequence, each separated from the other by spacer regions of six or eight residues of nearly identical sequence; Lys-Arg-Glu-Ala-Glu-Ala and Lys-Arg-Glu-Ala-[Glu or Asp]-Ala-Glu-Ala(45). Several reports provide strong evidence that the first proteolytic processing event in α-factor maturation is cleavage at the carboxyl side of the Lys-Arg pair of the spacer regions (42,43). This cleavage results in four propheromone fragments, with either Glu-Ala-Glu-Ala or Glu-Ala-[Glu or Asp]-Ala-Glu-Ala sequences attached to the *N*-terminus of the mature α-factor. In addition, three of the propheromone fragments would also contain an additional Lys-Arg sequence attached to their carboxyl ends. The final processing events to generate the mature tridecapeptide are the results of the combined action of carboxypeptidase YSC, which removes the Lys-Arg sequence, and dipeptidyl aminopeptidase YSC IV, which removes X-Ala sequences (44).

A **STE-13** mutant which lacks a functional dipeptidyl aminopeptidase processing enzyme for processing the α-factor was reported (43). This mutant was expected to secrete improperly processed forms of the α-factor pheromone which would have additional residues located on the *N*-terminus of the α-factor(42). An α-factor analog with an additional alanine residue on the amino-terminus of the pheromone

possessed the same biological activity as the native pheromone. However, an additional Glu-Ala sequence on the *N*-terminus, resulted in a decrease in biological activity by two orders of magnitude(43). In contrast, research in our laboratory indicated that an extended α-factor analog which contained a Glu-Ala-Glu-Ala sequence on the *N*-terminus exhibited only a modest reduction in its activity. Both growth-arrest and cell-shape assays on this extended α-factor analog indicated a slightly less than ten-fold decrease in its activity. Shorter analogs with an additional Ala, Glu-Ala, or Glu-Ala-Glu sequence on the amino-terminus were 1-5 fold less active than the native pheromone(45).

The regulatory proteins of the **MAT** locus also influence the transcription of *MFa1* and *MFa2* genes. These genes code for pre-pro-**a**-factor. Pre-pro-**a**-factor also is proteolytically processed, but in addition it undergoes post-translational modification of the C-terminal cysteine residue(37). In the mature dodecapeptide **a**-factor pheromone, a trans-farnesyl group is attached to the sulfhydryl side-chain, and a methyl ester to its α-carboxyl group(37). Intensive studies are currently underway on the **a**-factor pheromone, Tyr-Ile-Ile-Lys-Gly-Val-Phe-Trp-Asp-Pro-Ala-Cys[S-farnesyl]-$COOCH_3$, as it is a unique example of a new class of peptide hormone which has been recently identified(40). It is interesting to note that farnesylation of a cysteine residue in the *ras* gene product is associated

with its oncogenesis(47). Thus the **a**-factor model system may prove to be useful in determining characteristics associated with intestinal carcinomas invoked by *ras*(48,49).

Several mutants have been isolated and have proven to be very useful in mating assays. These are super-sensitive mutants (**SST**) to the yeast pheromones. **SST1**, also designated **BAR1**, codes for a membrane-associated α-factor-degrading peptidase found in **a**-cells(50). This peptidase cleaves on the carbonyl-side of Leu^6 of α-factor, thereby inactivating the α-factor(51). Since *sst1* mutants can not destroy α-factor pheromone in the medium, they are more sensitive to α-factor. The function of the **SST2** gene product is still not discerned; however, mutation of this gene confers super-sensitivity to pheromone-induced mating in both haploid cell-types. A recent review has suggested that the **SST2** gene product may act to promote desensitization by inactivating another component of the response pathway rather than the receptor(33).

Based on their inefficient mating ability, a number of sterile mutants (**STE**) have also been isolated. Among these **STE**-mutants, one would expect several to involve structural gene products influencing the mating process. In particular, **STE-2** and **STE-3** mutants have allowed elucidation of the α-factor and **a**-factor receptors, respectively

(52,53). **GPA1**, also known as **SCG1**, as well as **STE-4** and **STE-18**, show sequence homology to the G-protein subunits, of α, β, and γ,respectively(26,27). Studies on these mutants indicate that guanine-nucleotide binding G-proteins are essential participants in the mating scheme for this yeast(54,26,27). There is evidence to suggest that the $\beta\gamma$-subunits of the G-protein complex in this yeast may serve to carry the message from receptor to effector. This trait has long been attributed to only the α-subunit in many other signal transduction systems(6,26,55,56).

Direct evidence that the **STE-2** gene product is the ligand-binding component of the α-factor receptor has been presented. Studies have demonstrated that α-factor cannot only be crosslinked into the STE-2 gene product, but that when synthetic STE-2 mRNA is injected into *Xenopus* oocytes, these cells also bind α-factor(57,58). A model for STE-2 is illustrated in Figure 3. The primary structure for this 431 residue receptor has been deduced by cloning and sequencing the STE-2 gene(21,22). Several reports have also demonstrated that this receptor has 2-4 *N*-linked core oligosaccharide chains(57,22). According to the hydropathy profile for the deduced primary structure, a model has been proposed for the "folding" pattern of this protein(21,22). It is believed that the receptor folds as seven transmembrane helices, which are separated by short "hydrophilic loops"(60). In addition, the C-terminal domain

of 135 hydrophilic residues is located intracellularly and is responsible for the adaptive response observed upon prolonged exposure to α-factor(61-63). Although there is a basal level of phosphorylation for this receptor, the adaptive-response is associated with phosphorylation at two new distinct sites(62). Genetic analyses have also demonstrated that the C-terminal region of 135 residues is not required for pheromone binding and subsequent signal transduction(61). However, a shorter fragment of this receptor containing only the first 261 residues was inactive in mating. Interestingly, this fragment did not contain the proposed seventh transmembrane helix(63). It appears that all the information required for ligand binding and signal transduction for the STE-2 gene product is contained within the amino-terminal 305 residues.

Figure 3. Model for the folding pattern of the STE-2 receptor(59).

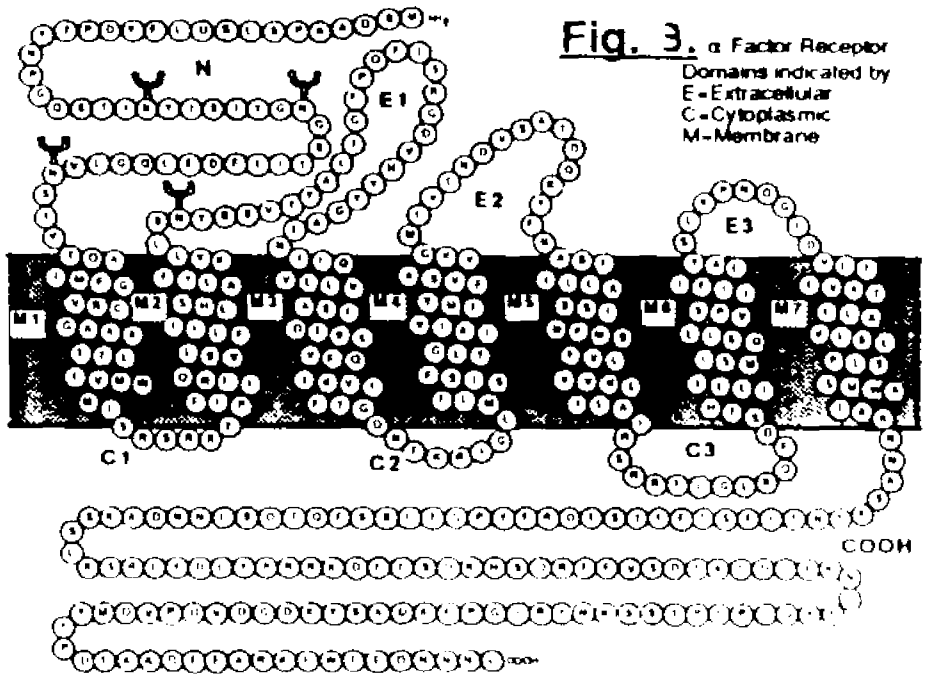

Fig. 3. α Factor Receptor
Domains indicated by
E-Extracellular
C-Cytoplasmic
M-Membrane

Although a model has been proposed for the STE-2 receptor, the location of the hydrophilic loops has not at present been discerned. In order to determine whether these loops face toward the cytosol or toward the exterior of the cell, goal one of this dissertation was to develop tools that could be utilized to determine the topology of the STE-2 receptor in its membrane-bound state. The results of these studies may not only provide supporting evidence for the model of STE-2(Figure 3), but also provide major constraints on the possible folding pattern for the α-factor receptor.

B) Structure/activity relationships in the α-factor:

It has long been accepted that the function of a peptide or protein can be directly related to its primary structure. For peptide hormones, peptide-based derivatives can be utilized to define structural domains necessary for recognition and/or biological activity. Furthermore, these peptide analogs can be used to dissect various steps in the biological response to a peptide hormone. Specifically, peptide hormone processing can be followed by use of a tagged synthetic precursor, which can result in the elucidation of the order and identity of those enzymes involved in the processing scheme (37). In addition, peptide analogs have been used to distinguish different types of receptors involved in the recognition of

biologically active peptide hormones (30,64,65). Moreover, peptide agonists and antagonists can be employed to select for receptor mutants, and possibly delineate essential structural features required by the peptide for its function. The ultimate goal of these types of studies is to relate the biological activity of a peptide hormone to its three-dimensional structure. Therefore, structure/function studies are necessary and important components for the overall understanding of the mode of action of α-factor and other peptide hormones. Most of the studies on the relationship between the structure of α-factor and its activity have come from the laboratory of Dr. Y. Masui and from the laboratories of Dr. Fred Naider and Dr. Jeffrey M. Becker. These laboratories have concentrated their efforts on the tridecapeptide pheromone and on the dodecapeptide lacking the *N*-terminal tryptophan, [des-Trp^1]-α-factor respectively(31,66).

Early reports on the tridecapeptide and dodecapeptide α factor pheromones suggested that both peptides have equal activity in the cell-shape or "shmoo" assay (67-69). In contrast, Shengbagamurthi et al.(70) reported the tridecapeptide was 16 fold more active than the homologous dodecapeptide. Nevertheless, both pheromones have activity in the nanogram per milliliter range. In comparison, removal of any other residue drastically reduces the activity of the resulting peptide. In particular,

removal of Tyr^{13} from the native tridecapeptide α-factor sequence resulted in decreased activity by three orders of magnitude(68). Removal of His^{2} from the dodecapeptide [des-Trp^{1}, des-His^{2}]-α-factor drastically lowered the activity (68). In addition, a variety of fragments containing partial sequences of the native tridecapeptide possessed one-millionth of the normal activity. Furthermore, Trp^{1}-Leu^{6} and Lys^{7}-Tyr^{13} fragments were virtually inactive(71,72). This latter result is significant since the BAR1 protease cleaves the intact α-factor molecule at the Leu^{6}-Lys^{7} peptide bond(71), resulting in desensitization towards the pheromone.

Recent studies from our laboratory have demonstrated that biologically inactive, truncated analogs of α-factor either antagonized or synergized the activity of the native pheromone(73). An *N*-terminal truncated pheromone [des-Trp^{1}, des-His^{2}, Nle^{12}]-α-factor acted as an antagonist by competing with binding and activity for the native pheromone. In contrast, a carboxyl terminal truncated pheromone, [des-Tyr^{13},des-Nle^{12}]-α-factor acted as a synergist, by a marked and early increase in activity of α-factor. This result is a unique example of peptide synergism and has not been reported previously.

Although removal of two residues at either end of the α-factor molecule results in a dramatic decrease in

activity, additional residues on the *N*-terminus of the pheromone appears to be tolerated by the α-factor receptor. An additional alanine residue on the *N*-terminus is as active as the native pheromone, whereas an additional Glu-Ala-Glu-Ala sequence on the *N*-terminus resulted in a ten-fold decrease in activity when compared against the native α-factor(45). These results suggest that an extended binding site within the α-factor receptor may be present for the *N*-terminal region of the pheromone.

In contrast, modification of the terminal carboxyl group results in a dramatic decrease in activity. Esterification of Tyr^{13} or conversion of the carboxyl terminus to the carboxamide decreased the potency by 10^3 and 10^4, respectively(66,74). Furthermore, an analog with a poly(ethylene glycol) protecting group attached to the C-terminus was devoid of activity(70). Hence it appears that extensions or modifications of the C-terminus of the pheromone are not acceptable for activity.

Numerous amino-acid substitutions have been made within positions 1, 2, 3, 6, 7, 8, 11, 12, and 13 of the α-factor. In every case examined, the substituted derivative was less active than the native pheromone, and in two-thirds of these analogs, activity decreased a minimum of 10,000-fold(31). Replacement of His^2 with either its enantiomeric (D)-homolog, or Lys, Phe, or Leu, resulted in

at least a 10^6 decrease in activity(66,68). These results suggest that His^2 is extremely important for activity. Despite the sensitivity of position 2 within the α-factor for activity, positions 1 and 3 can be substituted by hydrophobic amino-acids or bulky non-polar groups. Replacement of Trp^1 with Phe led only to a ten-fold drop in potency. In contrast, replacement of Trp^1 by Tyr decreased the activity 2500 fold, and replacement by Lys led to an inactive analog(66,68). Replacement of Trp^3 with either Phe, Leu, Ala, Tyr, or (cyclohexylalanine in the dodecapeptide) resulted in analogs with only modest reductions in their activity, approximately 50 fold. Replacement of Trp^3 with acidic or basic residues decreased the activity almost 10,000 fold. Furthermore, a bulky hydrophobic group is essential for activity when Trp^1 is not present. Both a [des-Trp^1, Ala^3]-α-factor and a [des-Trp^1, Phe^3]-α-factor were antagonists, whereas the same tridecapeptide analogs, [Ala^3]-α-factor and [Phe^3]-α-factor, were agonists(70,75).

Replacement of Leu^6 with alanine resulted in an inactive analog, whereas replacement by valine or norleucine resulted in analogs that were ten and si -fold less active than the α-factor, respectively. However, replacement with (D)-leucine resulted in an inactive analog. Hence a minimum hydrophobicity and/or steric bulkiness appears to be required at the position 6 side-chain, and β-branching may lower pheromone potency. Replacement of Lys^7 with ornithine

or norleucine resulted in analogs which were effective pheromones compared with the dodecapeptide, indicating that the side-chain ϵ-amino group is not required for activity(83).

In contrast to all other positions within the α-factor, Gly^9 was the only position where a (D)-amino-acid was more active than its (L)-enantiomer. In particular, replacement of Gly^9 with (D)-alanine or (D)-leucine resulted in analogs with relatively high activity, whereas the (L)-enantiomers were 200-fold less active and completely inactive, respectively(31). Hence a Pro^8-Gly^9 or Pro^8-(D)-X^9 sequence appears to be tolerated whereas Pro^8-(L)-X^9 reduces pheromone potency. According to theoretical considerations, (D)-residues can be tolerated in the (i+2) position of a type II β-turn, whereas (L)-residues are not as stable (76-80). These results suggest that a type II β-turn may be an important structural feature for the α-factor. Furthermore, a constrained α-factor analog generated by cyclizing the side-chains of $Lys^7$and Glu^{10} in the cyclo^{7,10}[Nle^{12}]-α-factor peptide retained high activity(92). Moreover, a cyclic analog in which Lys^7 and Gln^{10} have been replaced with cysteine, and the resultant analog cyclized by oxidizing the cysteines to their disulfide was also an effective pheromone (Xue et al. unpublished results).

Replacement of Met^{12} with norleucine resulted in an analog with an identical activity to that of the native pheromone(66). Hence the thioether of Met^{12} does not appear to be critical for pheromone activity. Despite this finding the [Nle^{12}] analog was not degraded as quickly as the native pheromone by the BAR1 peptidase, which normally degrades the α-factor by cleaving the Leu^{6}-Lys^{7}peptide bond. This result suggests that the BAR1 protease may be more sensitive than the receptor toward this position in the α-factor.

As discussed above, the α-factor has been the subject of numerous structure/activity studies. In order to form a basis for studies that can begin to localize the binding site for the α-factor within the STE-2 receptor, as well as to extend previous structure/activity relationships for the α-factor, goal two of this dissertation was to develop synthetic probes which could be useful in localizing the binding site for the α-factor. These probes may also provide insights into the structural requirements for binding of α-factor to its receptor.

C) Previous conformational analyses on the α-factor:

It has been generally accepted that peptide hormones bind to their receptors in a unique three-dimensional manner. Elucidating this bioactive conformation remains a primary goal in most conformational analyses on peptide

hormones. Despite the flexibility of peptide hormones in solution, many studies have examined the solution-state conformation of these molecules, and have attempted to extend these results to the biologically active state. These approaches have been successful for peptide hormones such as the enkephalins(4), human growth hormone(2), somatostatin(3), and the neurokinins(30). The results of these types of studies not only yield information on the shape of a peptide hormone required for activity, but also aid in the design of analogs with increased potency and/or antagonistic properties.

Despite the wealth of information on structure/activity relationships for the α-factor, conformational analyses on this pheromone are limited. Previous CD profiles for the α-factor in Tris buffer at a pH of 7.2 suggest a random-coil structure(31). In the presence of lipid or small unilamellar vesicles, changes are observed in the CD profile near 220 nm for the α-factor, suggesting a more ordered structure, which is associable with both α-helices and β-structures(81). These results were not observed for an inactive analog of the α-factor. In contrast, results from our laboratory on position 9 analogs of [des-Trp^{1}, Cha^{3}, X^{9}]-α-factor, where X^{9}= Gly^{9}, (L)-Ala^{9}, and (D)-Ala^{9} suggest random coil structures in trifluoroethanol or in Tris buffer(31). However there are noticeable differences between the CD spectrum of the

(L)-Ala^9 analog and those of the Gly^{9}and (D)-Ala^9 peptides(82). Since (D)-X^9 analogs are active whereas (L)-X^9 analogs are almost inactive, we conclude that the Pro^8-Gly^9 sequence may be an important structural determinant for biological activity.

Previous NMR studies on α-factor and several analogs in either lipid, DMSO, or aqueous environments have been reported(84-88). The most comprehensive NMR study to date has utilized a combination of pH profiles of amide chemical shifts, measurement of amide temperature shift coefficients, comparisons of amide coupling constants, and studies of relaxation rates in the presence of Gd(II)(84). This study concluded that the Trp^1-Leu^6 region of the α-factor is helical and that β-turns are located in the central and C-terminal domains for this pheromone in water. In lipid, the same group proposed that the Trp^1-Leu^6 domain of the α-factor is helical and the remainder of the peptide is extended(86,88). In contrast, Jelicks et al.(89,90) reported a compact N-terminal domain for the tridecapeptide in lipid vesicles and a type II β-turn spanning residues Lys^7-Gln^{10}. Furthermore, the proposed turn has been correlated with biological activity; substitution in position 9 by amino acids that are compatible with forming a type II β-turn results in active analogs, whereas destabilizing amino acids

are inactive(90). Similar results were reported by our laboratory for the α-factor in both aqueous and lipid environments(91).

In order to determine the biological significance for a centrally located turn, Xue et al.(92) synthesized a cyclic analog of the α-factor, in which the side-chains of Lys^{7} and Glu^{10} were linked through a covalent amide-bond linkage. This linkage causes a bend to be maintained in the center of the pheromone spanning residues 7-10, and the activity of this cyclo^{7,10}[Nle^{12}]-α-factor is only ten to twenty fold less than that of the native α-factor. The most pertinent consequence of this cyclic agonist for the present study is that cyclization significantly restricts the conformational flexibility for this analog. This flexibility appears to be a shortcoming in all of the previous reports. Since the activity of the cyclic agonist is in the same range as the α-factor, this cyclic analog should provide an excellent model system to study conformational features present in this molecule, which may be extendable to the more flexible α-factor. Consequently, goal three of this disseration was to examine the structure of this constrained analog of α-factor in DMSO, and to hopefully be able to extend these results to the biologically active state for the native α-factor.

D) Conformational analysis on a biologically active analog of a mammalian peptide hormone, Substance P

Substance P is an undecaneuropeptide, Arg-Pro-Lys-Pro-Gln-Gln-Phe-Phe-Gly-Leu-Met-NH_2, which is thought to be involved in pain-perception(93). Substance P is an important member in a family of neuropeptides which are classified as tachykinins(94). Such molecules have been shown to interact with at least three independent receptors classified as NK1, NK2, and NK3, where the preferred agonist is Substance P, NKA and NKB, respectively (95-98). Recently, several groups have independently reported the synthesis and characterization of Substance P analogs which are selective for individual receptors (30,64,65). Two analogs which are highly selective for a particular neurokinin receptor subtype are Ac-Arg^6-Phe-Phe-Gly-Leu-Met^{11}-NH_2 and pGlu^6-Phe-NMePhe- Aib-Leu-Met^{11}-NH_2. These hexapeptide analogs preferentially interact with only one of the three possible neurokinin receptor subtypes. They are 1000 fold and 30,000 fold more active toward the NK1 receptor and the NK3 receptor, respectively(96).

An important problem in the field of membrane-hormone recognition is determining the biologically active conformation of the signal molecule. Many mammalian peptides interact with a multiplicity of receptors, and it is difficult to extend studies on the conformation of such

molecules in solution to the biologically active state. In such cases it would be very advantageous to examine analogs which are highly selective for a given receptor. Since [pGlu^{6}-NMePhe^{8}]SP6-11 has been found to interact specifically with the NK3 receptor, it would be an ideal model for determining the conformation of Substance P bound to this receptor subtype. However, [pGlu^{6},NMe Phe^{8}]SP6-11 is a relatively flexible molecule and probably assumes a distribution of conformations in solution. Recently, a new analog of Substance P, pGlu-Phe-NMePhe-Aib-Leu-Met-NH_2, which is also highly selective for NK3 has been synthesized. Since this molecule contains both Aib and *N*Me-Phe residues, its conformation is expected to be significantly more restricted than that of the other hexapeptide analogs. In addition to NMR studies on the yeast α-factor, goal four of this dissertation was to conduct a detailed NMR analysis on a biologically active analog of a mammalian peptide hormone, pGlu-Phe-NMe-Phe-Aib-Leu-Met-NH_2, in DMSO-$_{d_6}$. The aim is to determine structural characteristics that may be required for binding to the NK3 receptor subtype.

II) Materials and Methods

A. Reagents:

All amino-acid derivatives were of the (L)-configuration, and were purchased from Bachem. Inc., except for Boc-N^{1}(For)-tryptophan which was purchased from Peptides International. All solvents were HPLC-grade supplied from Fisher Scientific. The following chemicals were reagent-grade,and used as received: 1-hydroxybenzotriazole, trifluoroacetic acid, ninhydrin, diisopropylethylamine, dimethyl sulfide, anisole, dicyclohexylcarbodiimide, diisopropylcarbodiimide, fluorescein disodium salt, and piperidine, were supplied from Aldrich. D-Biotin-p-nitrophenyl ester, β-(4-hydroxyphenyl)propionic acid *N*-hydroxysuccinimide ester, and the Merrifield resin were purchased from Sigma. Aminomethyl resin, benzhydrylamine resin, and 4-methylbenzhydrylamine resin were supplied by Peninsula Laboratories. Anhydrous hydrogen fluoride was supplied by Matheson. Yeast nitrogen base without ammonium sulfate or amino acids and noble agar were from Difco. Yeast extract and peptone were from BBL.

B. Solid-Phase Peptide Synthesis:

Synthesis of *t*-Butoxycarbonyl-(L)-isoleucyl-Phenylacetamidomethyl Resin (I)

a) Synthesis of *t*-butoxycarbonyl-(L)-isoleucyl-4-(oxymethyl)phenylacetic acid phenacyl ester (Ia)

Boc-Ile-Pam resin was prepared by the procedure of Mitchell et al.(101). Boc-Ileucine (4.97 g; 2.15 mmol) and DCHA (4.23 ml; 2.16 mmol) were dissolved in 90 ml of DMF. To the solution was added 4-bromomethylphenylacetic acid phenacyl ester(3.75 g; 10.8 mmol). The mixture was stirred at 50°C for 4 h, and overnight at room temperature. At this stage TLC (DCM/MeOH/HOAc 10:0.5:0.5) indicated that no unreacted Boc-Ile was present. The organic salts were removed by filtration, and the solution was evaporated "in-vacuo" to dryness. The residue was taken up in EtOAc (75 ml) and washed with 5% $NaHCO_3$ solution (w/v; 4 x 75 ml) and H_2O (4 x 75 ml), dried over anhydrous $MgSO_4$, and evaporated *in-vacuo* to an oil. The product was obtained from Et_2O/cyclohexane at 0°C. TLC indicated a slight trace of a UV positive impurity. The major product Boc-Ile-4-(oxymethyl)-phenylacetic acid phenacyl ester (4.28 g; 8.6 mmol; 80% yield) was an oil which was both UV and ninhydrin positive (with heating). The structure was

confirmed by 200 MHz ^{1}H NMR.

Boc-Ile-4-(oxymethyl)-phenylacetic acid phenacyl ester was analyzed by TLC(R_{f_a}= 0.95; R_{f_b}= 0.94); $[\alpha]_D^{25}$ = -4.17° (c 0.6 MeOH);NMR(DMSO-d_6) δ 7.95 (m,1,Ar-H); 7.71(m,1,Ar-H); 7.58 (m,2,Ar-H); 7.32 (s,4,C_6H_4); 7.23 (br d,J=7.95 Hz,αNH); 5.51 (s,2,$COOCH_2CO$); 5.09 (m,2,$COOCH_2$); 3.92 (m,1,αCH); 3.84 (s,2,CH_2COO); 1.75 (br m,1,βCH); 1.39-1.20 (m,11,t-C_4H_9 and γCH_2); 0.81 (t,6, β and γCH_3).

Synthesis of t-Butoxycarbonyl-(L)-isoleucyl-4-(oxymethyl)phenylacetic acid (Ib)

Boc-Ile-4-(oxymethyl)phenylacetic acid phenacyl ester (4.28 g; 8.6 mmol) and zinc powder (12.8 g; 195 mmol) were added to an 85% HOAc solution (v/v; 75 ml), and stirred for 6 h. The zinc was filtered off, Et_2O (100 ml) and H_2O (100 ml) were added, and the aqueous phase was adjusted to pH 1-1.5 with 6N HCl. The ether layer was separated and the aqueous phase was extracted with an additional portion of ether (100 ml). The combined ether extracts were washed with H_2O (100 ml), and evaporated *in-vacuo* to an oil. The residue was dried in a desiccator over KOH pellets, and crystallized from Et_2O (25 ml) by addition of DCHA (1.81 ml; 9.5 mmol). The DCHA salt was filtered and washed with cyclohexane (4 x 20 ml), and dried in a desiccator over KOH under high vacuum overnight. The resulting solid (3.6 g; 7.8 mmol) was dissolved in Et_2O (100 ml), and H_2O containing 7.8

mmol of HCl was added. After vigorous mixing, the ether layer was separated, washed with H_2O (5 x 50 ml), dried over anhydrous $MgSO_4$, and reduced to a volume of 10 ml. Addition of petroleum ether resulted in the crystallization of Boc-Ile-4-(oxymethyl)phenylacetic acid, which was obtained as a white solid (2.68 g; 7.1 mmol) in 83% yield. The structure was also confirmed by 200 MHz ^{1}H-NMR spectroscopy.

Pure Boc-Ile-4-(oxymethyl)phenylacetic acid as its dicyclohexylamine salt was analyzed by TLC(R_{f_a}= 0.68; R_{f_b}= 0.78); mp of DCHA salt= 118°C ; $[\alpha]_D^{25}$ = -6.5° (c 1.0 MeOH); NMR of the free acid in (DMSO-d_6) δ 7.28 (m,5,Ar-H and αNH); 5.08 (m,2,$COOCH_2$); 3.91 (m,1,αCH); 3.56 (s,2,CH_2COO); 1.73 (br m,1,βCH); 1.40-1.10 (m,11,t-C_4H_9 and γCH_2); 0.80 (t,6, β and γCH_3).

Synthesis of t-Butoxycarbonyl-(L)-isoleucyl-PAM Resin (Ic)

Aminomethyl-resin as the hydrochloride salt (5.0 g; 3.5 mmol; 0.7 meq.N/g) was washed successively with; DMF (3 x 100 ml, 1 min), DCM (3 x 100 ml, 1 min), 10% DIEA/DCM (2 x 100 ml, 5 min), and DCM (3 x 100 ml, 1 min). The neutralized resin was added to Boc-Ile-4-oxymethyl-phenylacteic acid(1.34 g; 3.5 mmol) and DCC (0.7 g; 3.5 mmol) in 30 ml DCM, and the reaction was allowed to proceed for 2 h. The resin was filtered and washed successively with DCM (3 x 100

ml, 1 min), 5% DIEA/DCM (1 x 100 ml, 10 min),and DCM (3 x 100 ml, 1 min). A qualitative Kaiser test (99) of the derivatized resin was negative, in comparison to an intense positive result obtained on the starting resin. Nevertheless, the above derivatization was repeated using Boc-Ile-4 oxymethyl phenylacetic acid (1.34 g; 3.5 mmol) and DCC (0.7 g; 3.5 mmol) in 30 ml DCM, and the reaction was allowed to proceed overnight. The resin was worked-up by washing successively with DCM (3 x 100 ml, 1 min), DMF (3 x 100 ml, 1 min), MeOH (3 x 100 ml, 1 min), and DCM (3 x 100 ml, 1 min). The Kaiser test was again negative, and the resin was washed with Et_2O (4 x 100 ml, 1 min), and dried in a desiccator for 24 h. Boc-Ile-PAM resin (6.24 g) was obtained, which corresponds to a weight increase of 1.24 g. Based on this weight increase, the derivatized resin contains 3.2 mmol of Boc-Ile-phenylacetic acid (0.55 mmol/g),corresponding to a 91% yield.

Acetylation of t-Butoxycarbonyl-(L)-isoleucyl-PAM Resin (Id)

In order to minimize any side-reaction due to the presence of unreacted amino groups on the resin, the following procedure was performed (100). Boc-Ile-PAM resin (6.2 g; 3.2 mmol) was placed into a solution of 50 ml acetic anhydride (532 mmol) and 50 ml pyridine, and rocked for 30 min at room temperature. The acetylating mixture was removed by filtration, and the resin was washed successively with

DMF (3 x 40 ml, 1 min), DCM (3 x 40 ml, 1 min), and Et_2O (5 x 40 ml, 1 min). The acetylated resin was then dried *in-vacuo* over P_2O_5 for 24 h.

2) Synthesis of

TFA-Thr-Phe-Val-Ser-Glu-Thr-Ala-Asp-Asp-Ile (II)

a) This synthesis was performed manually, by placing Boc-Ile-PAM resin (3.0 g; 1.65 mmol) into a 100 ml reaction vessel, and initiating the synthetic cycles. All residues were double coupled regardless of the Kaiser test results(99), which was performed prior to and after each coupling step. The Boc-group was used exclusively for the N^{α}-protection. The side-chain protecting groups were Thr(Bzl), Ser(Bzl),Glu(Bzl), and Asp(Bzl). A typical cycle was as follows: (1) TFA/DCM/DMS (50:48:2 v/v/v, 50 ml, 1 x 30 min); (2) DCM (40 ml, 3 x 1 min); (3) 8% DIEA/DCM (50 ml, 1 x 10min); (4) DCM (40 ml, 3 x 1 min); (5) Boc-amino-acid (3 equiv.) in 40 ml DCM added to reaction vessel, and shaken at room temperature with DCC (3 equiv.) for 2 h; (6) DCM (40 ml, 3 x 1 min); (7) 5% DIEA/DCM (50 ml, 1 x 10 min); (8) DCM (40 ml, 3 x 1 min); (9) Boc-amino-acid (1 equiv.) and DCC (1 equiv.) in 40 ml DCM were shaken at room temperature for 1 h; (10) DCM (40 ml, 3 x 1 min); (11) MeOH (40 ml, 2 x 1 min); (12) DCM (40 ml, 3 x 1 min). The resin was then suspended in 100 ml DCM and stored overnight. In the cases in which a third coupling was required as

revealed by the Kaiser test(99), 1 equiv. of Boc-amino-acid, DCC, and HOBt in DMF were added, and the reaction was allowed to proceed overnight at room temperature.

Upon completion of the assembly of the decapeptide-PAM resin, the resin was washed with DCM (40 ml, 3 x 1 min) and Et_2O (40 ml, 3 x 1 min). The resin was then dried to a constant weight in a desiccator over P_2O_5 under high vacuum. Boc-decapeptide-PAM resin (5.1 g) was isolated,corresponding to an increase in weight of 2.1 g. The maximum peptide content based on this increase in weight was 1.63 mmol, which reflects an overall yield of 99%. Two-thirds of the Boc-decapeptide-PAM resin (1.7 g; 0.54 mmol) was then stored at -20°C, for future syntheses.

b) The Boc-decapeptide-PAM resin (1.7 g; 0.54 mmol) was treated with TFA/DCM/DMS (50:48:2 v/v/v) for 1 x 30 min, and washed with DCM (40 ml, 3 x 1 min) and Et_2O (40 ml, 3 x 1 min). The resin was then dried to a constant weight in a desiccator over P_2O_5 under high vacuum.

c) The TFA·decapeptide-PAM resin salt was subjected to high HF cleavage, as outlined in Section (*C*) of this chapter. The crude deprotected peptide was extracted into 6% HOAc solution (6 x 15 ml). The extracts were pooled and condensed *in vacuo* to 10 ml. Water(25 ml) was added and the resulting solution was lyophilized overnight. Crude peptide

(180 mg) was obtained, corresponding to a 97% overall crude yield. The crude material was analyzed by isocratic reversed-phase HPLC, as described in Section (D) of this chapter, utilizing a MeOH/H_2O/TFA (43:57:0.025) as eluant. One major peak was observed, which was greater than 98% homogenous, as judged by the UV profile.

The crude decapeptide was purified on a C_{18}-reversed-phase (50 x 300 mm) HPLC column, utilizing a 2% MeOH/H_2O step gradient, as outlined in Section (*D*). Pure decapeptide (149 mg), which was greater than 99% homogenous as judged by analytical gradient reversed-phase HPLC (see section (D), corresponding to an 81% overall yield of TFA·Thr-Phe-Val-Ser-Glu-Thr-Ala-Asp-Asp-Ile was obtained. The purified decapeptide was characterized by amino-acid analysis and 200 MHz ^{1}H-NMR spectroscopy.

Synthesis of

4TFA·Lys-His-Ser-Glu-Arg-Thr-Phe-

-Val-Ser-Glu-Thr-Ala-Asp-Asp-Ile (III)

a) Synthesis was performed manually starting with Boc-decapeptide-PAM resin (3.4 g; 1.09 mmol) using a 100 ml reaction vessel and the same procedure described for decapeptide **(2a)**. The Boc-group was exclusively used for the N^{α}-protection. The side-chain protecting groups were Lys(2-Cl-Cbz), His(DNP), Ser(Bzl), Glu(Bzl, and Arg(Tos).

Boc-pentadecapeptide-PAM resin (4.52 g) corresponding to an increase in weight of 1.1 g was obtained, and reflects (1.08 mmol peptide; 0.24 mmol/g resin; 99% of theoretical). One-half of the Boc-pentadecapeptide (2.25 g; 0.54 mmol) was stored at -20°C for the synthesis of the 23-mer.

b) Boc-pentadecapeptide-PAM resin (2.25 g; 0.54 mmol) was treated with 1 M thiophenol/DMF (50 ml) for 1.5 days to remove the DNP group from histidine, then washed successively with DMF (40 ml, 3 x 1 min), Et_2O (40 ml, 3 x 1 min), and DCM (40 ml, 3 x 1 min), and the Boc-group was removed as described above (**IIb**). A portion (1.6 g; 0.38 mmol) of the dried TFA·resin salt (2.21 g) was then subjected to high HF cleavage. Crude deprotected peptide was extracted into 50% HOAc solution (6 x 15 ml), and the extracts were pooled and evaporated *in-vacuo* to 10 ml, H_2O (50 ml) was added and the resulting solution was lyophilized overnight. The crude product (708 mg), corresponding to a 95% overall crude yield, was one major peak as judged by isocratic reversed-phase HPLC, using MeOH/H_2O/TFA (38:62:0.025) as the eluant.

c) The pentadecapeptide (700 mg) was purified on a C_{18}-reversed-phase (50 x 300 mm) HPLC column, utilizing a 2% MeOH/H_2O step gradient, as outlined in Section (D). Pure material (367 mg) was obtained, which was greater than 99% homogenous as judged by analytical gradient reversed-phase

HPLC, which corresponded to a 49% overall yield of 4TFA·Lys-His-Ser-Glu-Thr-Phe-Val-Ser-Glu-Thr-Ala-Asp-Asp-Ile peptide. The pentadecapeptide was characterized by amino-acid analysis and 200 MHz ^{1}H-NMR spectroscopy.

Synthesis of

7TFA·Arg-Arg-Lys-Glu-Thr-Thr-Ser-Asp-Lys-His-Ser-Glu-Arg-Thr-Phe-Val-Ser-Glu-Thr-Ala-Asp-Asp-Ile (IV)

a) Synthesis was performed manually starting with Boc-pentadecapeptide-PAM resin (2.25 g; 0.55 mmol) following the procedures described for the decapeptide and pentadecapeptide **(IIa,IIIa)**. The protected 23-mer-PAM resin was washed with DCM (40 ml, 3 x 1 min) and Et_2O (40 ml, 3 x 1 min), and dried to a constant weight. Boc-23-mer-PAM resin (2.83 g; 0.39 mmol; 71% yield) was obtained, and both the DNP and Boc groups were removed as described for the pentadecapeptide **(IIIb)**.

b) The dried TFA·23-mer-Pam resin salt (2.7 g; 0.39 mmol)was then subjected to High HF cleavage(see section (C), following procedures outlined for the pentadecapeptide above. After HF cleavage,the TFA·23-mer-PAM resin salt (2.3 g; 0.32 mmol) yielded the crude peptide (1.06 g), which was one major peak as analyzed by isocratic reversed-phase HPLC, utilizing MeOH/H_2O/TFA (27:73:0.025) as eluant.

c) The crude 23-mer peptide (1 g) was purified on a C_{18}-reversed-phase (50 x 300 mm) HPLC column, utilizing a 2% MeOH/H_2O step gradient. Pure peptide (490 mg) which was greater than 99% homogeneous as judged by analytical gradient reversed-phase HPLC was obtained, which corresponded to a 44% yield of 7TFA·Arg-Arg-Lys-Glu-Thr-Thr-Ser-Asp-Lys-His-Ser-Glu-Arg-Thr-Phe-Val-Ser-Glu-Thr-Ala-Asp-Asp-Ile-amide peptide. The 23-mer peptide was characterized by amino-acid analysis and 200 MHz ^{1}H-NMR spectroscopy.

Synthesis of *t*-Butoxycarbonyl-(L)-valyl-Benzhydrylamine Resin (V)

a) The benzhydrylamine resin(3.0 g; 2.62 mmol; 0.87 meq.N/g;)as its hydrochloride salt was washed successively with DMF (2 x 80 ml, 1 min); DCM (3 x 60 ml, 1 min); 10% DIEA/DCM (2 x 60 ml, 5 min); and DCM (3 x 60 ml, 1 min). The neutralized BHA resin was added to Boc-Valine (1.68 g ; 7.75 mmol) and DCC (1.59 g; 7.75 mmol) in 10 ml DCM, and reaction was allowed to proceed for 1 h. The mixture was filtered and the resin was washed successively with DCM (3 x 60 ml, 1 min), 5% DIEA/DCM (1 x 60 ml, 10 min) and DCM (3 x 60 ml, 1 min). A qualitative Kaiser test (99) on the derivatized resin was negative as compared with the intense positive result obtained on the starting resin. Nevertheless, the derivatization was repeated using Boc-Valine (1.68 g; 7.5

mmol) and DCC (1.59 g; 7.5 mmol) in 25 ml DCM, and the reaction was allowed to proceed for 3 h. The resulting solid was worked-up as described for the preparation of the Boc-Ile-PAM-Resin (**Ic**). Boc-Val-BHA resin (3.48 g, 114% yield) was obtained. The high yield obtained might be due to a resin loading slightly higher than the reported value, or to residual DCU in the resin. Consequently, it was presumed that a resin loading of 0.75 mmol/g was the actual value at this stage.

Acetylation of ε-Butoxycarbonyl-(L)-valyl-BHA Resin

b) In order to minimize any side-reaction due to the presence of unreacted amino-groups on the resin, the Boc-Val-BHA resin (3.48 g; 2.6 mmol) was "capped" by a procedure identical to that outlined for the Boc-Ile-Pam resin(**Id**).

Synthesis of

2TFA·Phe-Pro-Gln-Phe-Ile-Ser-Arg-Gly-Asp-Val-amide (VI)

a) Syntheses were performed on a Vega 250C peptide synthesizer in the semi-automatic mode. Boc-Val-BHA resin (3.4 g; 2.55 mmol) was placed in a 250 ml reaction vessel, and the synthetic cycling was initiated. All residues were double coupled even if the Kaiser test(99) performed after the first coupling was negative. The Boc-group was

exclusively used for the N^{α}-protection, and the side-chain protecting groups were Ser(Bzl), Arg(Tos), and Asp(β-cyclohexyl). A typical cycle was as follows: (1) TFA/DCM/DMS (40:58:2 v/v/v, 60 ml, 1 x 1 min); (2) TFA/DCM/DMS (40:58:2, 60 ml, 1 x 30 min); (3) DCM (60 ml, 3 x 1 min); (4) 10% DIEA/DCM (60 ml, 1 x 2 min); (5) 10% DIEA/DCM (60 ml, 1 x 8 min); (6) DCM (60 ml, 3 x 1 min); (7) Boc-amino-acid (3 equiv.) in 15 ml DCM added to reaction vessel, and shaken at room temperature with DIPC (3 equiv.) for 2 h; (8) DCM (60 ml, 3 x 1 min); (9) 5% DIEA/DCM (60 ml, 1 x 1 min); (10) 5% DIEA/DCM (60 ml, 1 x 5 min); (11) DCM (60 ml, 3 x 1 min); (12) Boc-amino-acid (1 equiv.) and DIPC (1 equiv.) in 25 ml DCM were shaken at room temperature for 1 h; (13) DCM (60 ml, 3 x 1 min); (14) DMF (60 ml, 3 x 1 min); (15) DCM (60 ml, 3 x 1 min). The resin was then suspended in 100 ml DCM and stored overnight. For glutamine residues the HOBt/DIPC-accelerated active ester coupling procedure was utilized in DMF. DMF washes also replaced steps 6,8,11, and 13.

The procedures of the cycle immediately following the incorporation of Boc-Gln were different from the above protocol: (1) Dioxane (60 ml, 3 x 1 min); (2) 4N HCl/dioxane (60ml, 1 x 1 min); (3) 4N HCl/Dioxane (60 ml, 1 x 30 min); (4) Dioxane (60 ml, 3 x 1 min); (5) $CHCl_3$ (60 ml, 3 x 1 min) (6) 10% DIEA/$CHCL_3$ (60 ml, 1 x 2 min); (7) 10% DIEA/$CHCL_3$ (60 ml, 1x 8 min); (8) $CHCL_3$ (60 ml, 3 x 1 min);

c) In order to check the synthetic progress for this peptide the TFA·decapeptide resin (0.3 g; 0.117 mmol) was then subjected to High HF cleavage, as previously outlined for the TFA·decapeptide-Pam resin (**IIc**). Crude product (16 mg; 10% yield)was obtained, which was one major peak as judged by gradient reversed-phase HPLC. The crude decapeptide-amide was also analyzed by amino-acid analysis, and acceptable amino-acid ratios were obtained.

Since a low yield of crude peptide was obtained, although the increase in resin weight and good homogeneity of the crude peptide indicated a satisfactory synthesis, the HF-treated decapeptide resin was recleaved. In addition, the concentration of HOAc was increased from 6 to 50% to extract the crude product from the resin. This same resin yielded an additional 49 mg of crude peptide, with the same homogeneity as the previously cleaved material, as judged by analytical gradient reversed-phase HPLC. A portion of the TFA·decapeptide-BHA resin (1.0 g; 0.39 mmol) was stored at -20°C, and the synthesis was resumed with the remaining TFA·decapeptide-BHA resin (6.3 g; 2.46 mmol).

Synthesis of

TFA·Ala-Leu-Thr-Gly-Phe-Pro-Gln-Phe-Ile-Ser(Bzl)-Arg(Tos)-Gly-Asp(β-cyclohexyl)-Val-BHA Resin (VII)

a) The synthesis was again performed on a Vega 250C peptide synthesizer, in the semi-automatic mode. The TFA·decapeptide resin (6.3 g; 2.46 mmol) was placed in the 250-ml reaction vessel, and the coupling cycles were identical to those described for the decapeptide above (**VIa**). The side-chain protecting group for threonine was its benzyl ester.

Upon completion of the assembly of the TFA·tetradecapeptide resin, the Boc-group was removed as previously described (**VIb**). TFA·tetradecapeptide-BHA resin (6.17 g; 1.89 mmol; 77% of theoretical) was obtained, a portion (2.0 g; 0.62 mmol) was stored at -20°C, and the synthesis was resumed with the remaining peptide-resin (4.68 g; 1.45 mmol) to generate the nonadecapeptide.

Synthesis of

2TFA·Ser-Ser-Val-Thr-Tyr-Ala-Leu-Thr-Gly-Phe-Pro-Gln-Phe-Ile-Ser-Arg-Gly-Asp-Val-amide (VIII)

a) The syntheses were performed on a Vega 250C peptide synthesizer, in the semi-automatic mode. The assembly of the protected nonadecapeptide from

TFA·tetradecapeptide-BHA resin (4.68 g; 1.45 mmol) followed the identical synthetic protocol outlined for the decapeptide (**VIa**). The side-chain protecting group for Tyr was (2-Br-Cbz). After completion of the final synthetic cycle, the assembled nonadecapeptide resin was washed with DCM (60 ml, 4 x 1 min) and Et_2O (60 ml, 4 x 1 min), and the resin was dried to a constant weight. Boc-nonadecapeptide resin (5.94 g; 1.3 mmol) was obtained in 98% yield and used to prepare the free 19-peptide.

b) The assembled nonadecapeptide-BHA resin (1.54 g; 0.34 mmol) was treated with TFA/DCM/DMS (40:58:2 v/v/v) for 1 x 1 min, and 1 x 30 min, washed with DCM (60 ml, 4 x 1 min) and Et_2O (60 ml, 4 x 1 min), and dried to a constant weight (1.5 g; 0.34 mmol). One-third of the TFA·nonadecapeptide resin salt (0.5 g; 0.11 mmol) was subjected to High HF cleavage, as previously outlined above (**IIc**), however a 10% HOAc solution was used to extract the crude peptide from the resin. Crude nonadecapeptide (122 mg; 52% yield) was obtained, and was one major peak as analyzed by gradient reversed-phase HPLC. This material (120 mg) was purified on a C_{18}-reversed-phase (25.4 x 300 mm) column, utilizing a 2% MeOH/H_2O step gradient. Three liters of 54% MeOH, 2 L of 56% MeOH, and 2 L of 58% MeOH was sufficient to elute the purified nonadecapeptide (32 mg; 13% of theoretical), which was approximately 95% homogeneous as judged by analytical gradient reversed-phase HPLC.

Since this peptide was to be utilized as a synthetic antigen to generate a polyclonal antisera, it was decided to insure that antibodies were not preferentially raised against the impurities rather than the peptide. Therefore, additional material was cleaved and the yield of the product was sacrificed in order to obtain peptide that was of spectroscopic purity.

The remaining TFA·nonadecapeptide-BHA resin (1.0 g; 0.22 mmol) was subjected to High HF cleavage as described above. Additional nonadecapeptide(225 mg; 47% yield) was obtained as one major peak as analyzed by gradient reversed-phase HPLC, comigrating with the previously purified nonadecapeptide. This crude nonadecapeptide (215 mg) was purified on a C_{18}-reversed-phase (25.4 x 300 mm) column, utilizing a 2% MeOH/H_2O step gradient. Three liters of 54% MeOH, 2 L of 56% MeOH, and 2 L of 58% MeOH was sufficient to elute pure nonadecapeptide (66 mg; 14% of theoretical), which was greater than 99 homogeneous as judged by analytical gradient reversed-phase HPLC. This batch of purified 2TFA·Ser-Ser-Val-Thr-Tyr-Ala-Leu-Thr-Gly-Phe-Pro-Gln-Phe-Ile - Ser-Arg-Gly-Asp-Val-amide peptide was characterized by amino-acid analysis and 200 MHz ^{1}H-NMR spectroscopy.

Synthesis of t-Butoxycarbonyl-(L)-alanyl-4-Methyl-Benzhydrylamine Resin (IX)

a) 4-Methylbenzhydrylamine (3.15 g; 3.1 mmol; 0.87 meq.N/g) as its hydrochloride salt was washed as described for the benzhydrylamine resin **(Va)**. The neutralized MBHA resin was added to Boc-Alanine (1.17 g; 6.2 mmol) and DIPC (0.95 ml; 6.1 mmol) in 20 ml DCM,and the reaction was allowed to proceed for 1 h, and worked up as per the synthesis of Boc-Val-BHA resin **(Va)**. The derivatization was repeated using Boc-Alanine (1.17 g; 6.2 mmol) and DIPC (0.95 ml; 6.1 mmol) in 20 ml DCM, and the reaction was allowed to proceed overnight. After washing, the resin was dried over P_2O_5 for 24 h. Boc-Ala-MBHA resin (3.27 g; 3.1 mmol; 99% yield; 0.95 mmol/g)was obtained.

Since quantitative removal of the resin from the reaction vessel is quite difficult, and aliquots of resin are always removed for Kaiser testing during our synthetic cycling, the synthetic yield at this stage may not truly reflect the actual peptide content on the resin. Therefore, the resin loading will be determined at the tetrapeptide stage, based on the increase in resin weight.

Acetylation of t-Butoxycarbonyl-(L)-alanyl-MBHA Resin

b) In order to minimize any side-reaction due to the

presence of unreacted amino groups on the resin, the Boc-Ala-MBHA resin (3.45 g; 3.1 mmol) was acetylated in an identical fashion as the Boc-Val-BHA resin (Id).

Synthesis of

TFA·Tyr(2-Br-Cbz)-Phe-Asn-Ala-MBHA Resin (X)

a) Syntheses were performed on a Vega 250C peptide synthesizer, in the semi-automatic mode. Boc-Ala-MBHA resin (3.45 g; 3.1 mmol) was placed in a 250-ml reaction vessel, and the synthetic cycle was initiated. The Boc group was exclusively used for the N^{α}-protection. The side-chain protecting group for the Tyrosine-OH group was its 2-Br-Cbz. The synthetic protocol for this peptide was identical to that used for the decapeptide-BHA resin (VIa), with the exception that 2 equivalents of Boc-amino-acid and DIPC were used for both couplings. Asparagine residues followed the same protocol as that previously given for Glutamine residues.

b) After completing the assembly of the tetrapeptide-MBHA resin, the Boc-group was removed as outlined for the decapeptide (IIb). The TFA·tetrapeptide-MBHA resin(5.4 g; 2.99 mmol; 99% yield; 0.55 mmol/g) was obtained. An aliquot of the TFA·tetrapeptide-MBHA resin (0.117 g; 0.065 mmol) was then subjected to High HF cleavage as described above, the crude

product was extracted into 6% HOAc, and lyophilized overnight. The crude tetrapeptide-amide (39 mg; 99% of theoretical) was more than 99% homogeneous as judged by gradient reversed-phase HPLC.

Synthesis of TFA·Ser-Ala-Thr-Gln-Asp-Lys-Tyr-Phe-Asn-Ala-amide (XI)

The synthesis of the decapeptide-amide was performed on a Vega 250C peptide synthesizer, in the semi-automative mode starting from TFA·tetrapeptide-MBHA resin (5.2 g; 2.9 mmol). An identical synthetic protocol to that outlined for the tetrapeptide above (**XIa**) was utilized. The side-chain protecting groups were Ser(Bzl), Thr(Bzl), Asp(β-cyclohexyl), and Lys(2-Cl-Cbz).

The Boc-group was removed from a portion(576 mg; 0.16 mmol) of the dried Boc-decapeptide-MBHA resin (8.11 g; 2.24 mmol; 78% yield; 0.276 mmol/g) which was obtained. A portion of the TFA·decapeptide-MBHA resin(255 mg; 0.07 mmol) was then subjected to High HF cleavage as described above, and the crude deprotected peptide was extracted into a 10% HOAc solution,evaporated *in-vacuo*, and lyophilized overnight. The crude decapeptide-amide (90 mg; 99% of theoretical) was one major peak as judged by gradient reversed-phase HPLC. Since the yield and homogeneity of the crude decapeptide-amide

appeared fine, 3.41 g (0.94 mM) of the Boc-decapeptide-MBHA resin was stored at -20°C, and the synthesis continued to the hexadecapeptide stage.

Synthesis of

2TFA·Val-Thr-Tyr-Asn-Asp-Val-Ser-Ala-Thr

-Gln-Asp-Lys-Tyr-Phe-Asn-Ala-amide (XII)

a) The Boc-decapeptide-MBHA resin (4.24 g; 1.17 mmol) was placed in the 250-ml reaction vessel of the Vega 250C synthesizer and the chain extended as described for the decapeptide **(VI a)** For Asparagine residues, procedures described above **(X)** were utilized.

b) After completion of the assembly of the hexadecapeptide resin, the resin was washed with DCM (60 ml, 4 x 1 min) Et_2O (60 ml, 4 x 1 min), and dried to constant weight in a desiccator over P_2O_5 under high vacuum. A portion of this Boc-hexadecapeptide-MBHA resin (2.35 g; 0.48 mmol) was stored at -20°C for future use, the remainder of this resin (3.32 g; 0.68 mmol) was treated with TFA to remove the Boc-group. The total yield of resin was 99% (0.21 mmol/g).

The Boc protecting group was removed from Boc-hexadecapeptide-MBHA resin(3.32 g ; 0.68 mmol) as described above **(IXb)**. A portion of the

TFA·hexadecapeptide-MBHA resin (1.03 g; 0.21 mmol) was then subjected to High HF cleavage, as outlined in Section (C) of this chapter. The crude peptide-amide was extracted into 10% HOAc solution (6 x 15 ml), evaporated *in-vacuo*, and lyophilized overnight. The crude hexadecapeptide-amide (510 mg; 99% of theoretical), was one major peak as judged by gradient reversed-phase HPLC.

A portion of this material (105 mg) was purified on a C_{18}-reversed-phase (9 x 500 mm) column, utilizing semi-preparative gradient HPLC as outlined in Section (D). Pure material (32 mg; 0.016 mmol; 37% yield) was obtained, which was more than 99% homogeneous as judged by analytical gradient reversed-phase HPLC. The purified 2TFA·Val-Thr-Tyr-Asn-Asp-Val-Ser-Ala-Thr-Gln-Asp-Lys-Tyr-Phe-Asn-Ala-amide peptide was characterized by amino-acid analysis as outlined in Section (E), and 200 MHz ^{1}H-NMR spectroscopy.

Synthesis of *t*-butoxycarbonyl-(L)-tyrosyl(2,6 Dichlorobenzyl)-Merrifield Resin (XIII)

Boc-Tyr(2,6-dichlorobenzyl) (4.4 g; 11 mmol) and absolute EtOH (25 ml) were added to 10 g of chloromethyl-polystyrene crosslinked by 2% divinylbenzene, (10 meq. Cl/g). TEA (1.32 ml; 9.5 mmol) was added to the resin suspension to minimize the formation of quaternary ammonium groups on the resin, the mixture was refluxed with stirring

for 28 h, cooled to room temperature, filtered and the resin was washed successively with 3 x 60 ml EtOH, 3 x 60 ml H_2O, 3 x 60 ml EtOH, 3 x 60 ml DCM, 2 x 60 ml Et_2O, and dried. Boc-Tyr(2,6 dichlorobenzyl)-Merrifield resin (11.63 g; 4.02 mmol; 40% yield) was obtained.

Synthesis of

TFA·Trp-His(Tos)-Trp-Leu-Gln-Leu-Lys(2-Cl-Cbz)-Pro-Gly-Gln-Pro-(Nle)-Tyr(2,6 Dichlorobenzyl)-Merrifield Resin (XIV)

a) Syntheses were performed manually, starting with Boc-Tyr(2,6 dichlorobenzyl)-Merrifield resin (3.0 g; 1.21 mmol) in a 100 ml reaction vessel. All residues were double coupled and Kaiser tests (#) were performed prior to and after each coupling step. The Boc-group was exclusively used for the N^{α}-protection. The side-chain protecting groups were His(Tos), Lys(2-Cl-Cbz), and Tyr(2,6 Dichlorobenzyl). After each cycle the resin was suspended in 100 ml DCM and stored overnight. When a third coupling was required, as revealed by the Kaiser test(99), 1 equiv. of Boc-amino-acid, DCC, and HOBt in DMF were added, and the reaction was allowed to proceed overnight at room temperature. Glutamine residues were incorporated as their p-nitrophenyl esters in the presence of 1 equiv. of HOBt in DMF, which replaced the standard coupling step 5. The HOBt/DCC-accelerated active ester coupling procedure in DMF replaced coupling step 9. DMF washes also replaced washing steps 8 and 10.

Upon completion of the assembly of the tridecapeptide resin, the resin was washed with DCM (40 ml, 3 x 1 min), Et_2O (40 ml, 3 x 1 min) and dried to a constant weight in a desiccator, Boc-(Nle^{12})-α-factor-Merrifield resin (4.61 g; 0.88 mmol; 70% yield; 0.19 mmol/g) was obtained. A portion of the Boc-(Nle^{12})-α-factor-Merrifield resin (420 mg; 0.082 mmol) was treated with 40 ml TFA/DCM/DMS (50:48:2 v/v/v) for 1 x 1 min and 3 x 30 min, washed with DCM (40 ml, 3 x 1 min) and Et_2O (40 ml, 3 x 1 min),and then dried to a constant weight in a desiccator over P_2O_5 under high vacuum.

Synthesis of

2TFA·Trp^1(N^{α}-Biotinyl)-His-Trp-Leu-Gln-Leu-Lys-Pro-Gly-Gln-Pro-(Nle^{12})-Tyr (XV)

The TFA·(Nle^{12})-α-Factor-Merrifield resin salt (420 mg; 0.08 mmol) was washed successively with DMF (3 x 50 ml, 1 min), DCM (3 x 50 ml, 1 min), 10% DIEA/DCM (2 x 50 ml, 5 min), DCM (3 x 50 ml, 1 min), and DMF (4 x 50 ml, 1 min). The neutralized resin was added to 3 equivalents of D-Biotin-ONp (92 mg; 0.25 mmol) and 3 equivalents of HOBt (34 mg; 0.25 mmol) in 15 ml of DMF. The reaction was allowed to proceed at room temperature for 18 h, filtered and the resin was washed successively with DMF (3 x 50 ml, 1 min), DCM (3 x 50 ml, 1 min), 10% DIEA/DCM (2 x 50 ml, 5 min), DCM (3 x 50 ml, 1 min), and DMF (4 x 50 ml, 1 min). A qualitative Kaiser test (99) was negative for the

derivatized resin, in comparison to an intense positive result obtained on the starting resin. Nevertheless, the above derivatization was repeated using 3 equivalents of D-Biotin-ONp (92 mg; 0.25 mmol) and 3 equivalents of HOBt (34 mg; 0.25 mmol) in 15 ml of DMF, and the reaction was allowed to proceed overnight. The resin was worked-up by washing successively with DMF (50 ml, 3 x 1 min), DCM (50 ml,3 x 1 min), MeOH (50 ml, 3 x 1 min), and DCM (50 ml, 3 x 1 min). The Kaiser test was again negative, and the resin was washed with Et_2O (4 x 100 ml, 1 min), and dried in desiccator for 24 h. [(N^{α}-Biotinylated)^{1}, Nle^{12}]-α-factor-Merrifield resin (420 mg; 0.08 mmol) was obtained, the Boc group was removed with TFA/DCM/Anisole (40:56:2 v/v/v, 50 ml, 1 x 1 min, 1 x 30 min), the deprotected resin was washed successively with DCM (3 x 50 ml, 1 min), 10% DIEA/DCM (2 x 50 ml, 5 min), DCM (3 x 50 ml, 1 min), and DMF (4 x 50 ml, 1 min), dried and subjected to High HF cleavage as described in Section (C). Crude peptide was extracted into a 10% HOAc solution (6 x 10 ml), evaporated *in-vacuo*, and lyophilized overnight. The crude [(N^{α}-Biotinylated)^{1}, Nle^{12}]-α-factor (132 mg; 0.067 mmol; 82% of theoretical) was one major peak, as judged by analytical reversed-phase HPLC. It was purified on a C_{18}-reversed-phase (25.4 x 300 mm) HPLC column, utilizing a 2% MeOH/H_2O step gradient, as outlined in Section (D). Pure material (27 mg;16.4% yield) was obtained in greater than 99% homogeneity, as judged by analytical gradient

reversed-phase HPLC (see section (D)). The product 2TFA·(N^{α}-Biotinyl-Trp^{1})-His-Trp-Leu-Gln-Leu-Lys-Pro-Gly-Gln-Pro-(Nle^{12})-Tyr peptide (0.013 mmol) was then characterized by amino-acid analysis, 200-MHz ^{1}H-NMR spectroscopy, and FAB-MS.

Synthesis of

3TFA·Lys^{1}(N^{ϵ}-Biotinyl)-Trp-His-Trp-Leu-Gln-Leu-Lys-Pro-Gly-Gln-Pro (Nle^{12})-Tyr (XVI)

TFA·(Nle^{12})-α-Factor-Merrifield resin salt (560 mg; 0.109 mmol) **(XV)** was neutralized as above **(XVI)** and was added to 3 equivalents of Boc-Lys-(N^{ϵ}-FMOC)(154 mg; 0.33 mmol), 3 equivalents of HOBt (51 mg; 0.33 mmol), and 3 equivalents of DIPC (0.051 ml; 0.33 mmol) in 15 ml DMF. The reaction was allowed to proceed at room temperature for 1 h, the resin was filtered and washed successively with DMF (3 x 50 ml, 1 min), DCM (3 x 50 ml, 1 min), 10% DIEA/DCM (2 x 50 ml, 5 min), DCM (3 x 50 ml, 1 min), and DMF (4 x 50 ml, 1 min). A qualitative Kaiser test was slightly positive for the derivatized resin, in comparison to an intense positive result obtained on the starting resin. Consequently the above derivatization was repeated using 3 equivalents of Boc-Lys-(N^{ϵ}-FMOC)(154 mg; 0.33 mmol), 3 equivalents of HOBt (51 mg; 0.33 mmol), and 3 equivalents of DIPC (0.051 ml; 0.33 mmol) in 15 ml of DMF, and the reaction was allowed to proceed for 3h. A negative Kaiser test result was then

obtained. The FMOC-group was then removed by treatment with 10% piperidine/DCM (50 ml, 1 x 1 min, 1 x 30 min), and washed with DMF (50 ml, 3 x 1 min). The tetradecapeptide resin was then coupled with 3 equivalents of D-Biotin-ONp (121 mg; 0.33 mmol) and 3 equivalents of HOBt (45 mg; 0.33 mmol) in 15 ml of DMF. A qualitative Kaiser test was slightly positive for the derivatized resin, in comparison to an intense positive result obtained on the starting resin. Consequently the above derivatization was repeated using an additional 3 equivalents of D-Biotin-ONp (121 mg; 0.33 mmol) and 3 equivalents of HOBt (45 mg; 0.33 mmol) in 15 ml DMF. A negative Kaiser test result was then obtained. The resin was worked-up by washing successively with DMF (50 ml, 3 x 1 min), DCM (50 ml,3 x 1 min), MeOH (50 ml, 3 x 1 min), DCM (50 ml, 3 x 1 min), Et_2O (4 x 100 ml, 1 min), and dried in desiccator for 24 h.

[Lys ^{1}-N^{ϵ}-Biotinyl,(Nle^{12})]-α-factor Merrifield resin (594 mg; 0.108 mmol/g; 98.7% yield) was obtained. The Boc group was removed with TFA/DCM/Anisole (40:56:2 v/v/v, 50 ml, 1 x 1 min, 1 x 30 min), as described above and the deprotected resin was subjected to High HF cleavage,as described in Section (C). The crude peptide was extracted into a 10% HOAc solution (6 x 10 ml), evaporated *in-vacuo*, and lyophilized overnight. The crude [Lys ^{1}-N^{ϵ}-Biotinyl,(Nle^{12})]-α-factor (165 mg; 0.073 mmol; 67% of theoretical) was one major peak, as judged by analytical reversed-phase HPLC. It was purified on a C_{18}-reversed-phase (25.4 x 300 mm) HPLC column,

utilizing a 2% MeOH/H_2O step gradient, as outlined in Section (D). Pure material (47 mg; 18% yield), which was greater than 99% homogeneous as judged by analytical gradient reversed-phase HPLC was obtained. The biotinylated-peptide was characterized by amino-acid analysis, 200-MHz ^{1}H-NMR spectroscopy, and FAB-MS.

Synthesis of *t*-Butoxycarbonyl-(L)-tyrosyl-(2-Br-Cbz)-Phenylacetamidomethyl Resin (XVII)

Synthesis of *t*-Butoxycarbonyl--(L)-tyrosyl-(2-Br-Cbz) 4-(oxymethyl)phenylacetic acid phenacyl ester (XVIIa)

Boc-Tyr(2-Br-Cbz)-PAM resin was prepared by the procedure of Tam et al.(102). Boc-Tyr(2-Br-Cbz) (10.87 g; 22 mmol) and $KF\cdot 2H_2O$ (4.14 g; 44 mmol) were dissolved in 90 ml of MeCN. To the solution was added 4-bromomethylphenylacetic acid phenacyl ester(7.0 g; 20. mmol). The mixture was stirred at room temperature for 48 h. At this stage TLC (DCM/MeOH/HOAc 10:1:0.5) indicated that no unreacted 4-bromomethylphenylacetic acid phenacyl ester was present. The organic salts were removed by filtration, and the solution was evaporated *in-vacuo* to dryness. The residue was taken up in EtOAc (75 ml) and washed with 5% $NaHCO_3$ solution (w/v; 9 x 75 ml) and H_2O (9 x 75 ml), dried over

anhydrous $MgSO_4$, and evaporated *in-vacuo* to an oil. The product was crystallized from Et_2O/cyclohexane at 0°C. TLC indicated a slight trace of a UV positive impurity. The major product Boc-Tyr(2-Br-Cbz)-4-(oxymethyl)phenylacetic acid phenacyl ester (9.62 g; 12.6 mmol; 63% yield) was an off-white powder which was both UV and ninhydrin positive (with heating). The structure was confirmed by 200-MHz ^1H NMR.

Boc-Tyr(2-Br-Cbz)-4-(oxymethyl)phenylacetic acid phenacyl ester was analyzed by TLC(R_{f_a}= 0.97; R_{f_b}= 0.91); mp = 86°C ; $[\alpha]_D^{25}$ = +10.0° (c 0.75 MeOH); NMR(DMSO-d_6) δ 7.95(d,1H,Ar-H); 7.67(t,2H,Ar-H); 7.57(d,2H,Ar-H); 7.52-7.25(m,10H,Ar-H and αNH); 7.16(d,2H,$C_{3,5}H$); 5.53 (s,2H,$COOCH_2CO$); 5.32(s,2H,$CH_2C_4H_4Br$); 5.09 (s,2H,$COOCH_2$); 4.22 (m,1H,αCH); 3.85 (s,2H,CH_2COO); 2.93(m,2H,βCH);1.32,1.25 (s,9H,*cis/trans* t-C_4H_9).

Synthesis of t-Butoxycarbonyl-(L)-tyrosyl (2-Br-Cbz)-4-(oxymethyl)phenylacetic acid(XVIIb)

Boc-Tyr(2-Br-Cbz)-4-(oxymethyl)phenylacetic acid phenacyl ester (9.6 g; 12.5 mmol) and zinc powder (12.8 g; 200 mmol) were added to a 85% HOAc (v/v; 125 ml), and stirred for 6 h. The zinc was filtered off, EtOAc (100 ml) and H_2O (100 ml) were added, the organic layer was separated and the aqueous phase was extracted with an additional

portion of EtOAc (100 ml). The combined EtOAc extracts were washed with H_2O (100 ml), and evaporated *in-vacuo* to an oil. The residue was crystallized from Et_2O (25 ml) by addition of cyclohexane. The product was filtered, washed with cyclohexane (4 x 20 ml), and dried in a desiccator under high vacuum overnight. Boc-Tyr(2-Br-Cbz)phenylacetic acid (6.15 g; 9.56 mmol; 76% yield) was then obtained. The structure was also confirmed by 200-MHz ^{1}H-NMR spectroscopy.

Pure Boc-Tyr(2-Br-Cbz)phenylacetic acid was analyzed by TLC(R_{f_a}= 0.87; R_{f_b}= 0.84); M.p.= 88°C ; $[\alpha]_D^{25}$ = +1.33° (c 0.5 MeOH) NMR(DMSO-d_6) δ 7.69(d,1H,Ar-H); 7.58(d,1H,Ar-H); 7.45(t,1H,Ar-H); 7.40-7.20(m,8H,Ar-H and αNH); 7.14(d,2H,$C_{3,5}$H); 5.33 (s,2H,$CH_2C_4H_4Br$); 5.08(s,2H,$COOCH_2$); 4.23 (m,1H,αCH); 3.57 (s,2H,CH_2COO); 2.93(m,2H,βCH); 1.32,1.23 (s,9H,*cis/trans* *t*-C_4H_9)

Synthesis of *t*-Butoxycarbonyl--Tyr(2-Br-Cbz)-Phenylacetamidomethyl Resin (XVIIc)

Aminomethyl-resin as the hydrochloride salt (5.7 g; 6.89 mmol; 1.2 meq.N/g) was washed successively with; DCM (3 x 60 ml, 1 min), 10% DIEA/DCM (2 x 60 ml, 1 x 1 min, 1 x 10 min), and DCM (3 x 60 ml, 1 min). The neutralized resin was added to Boc-Tyr(2-Br-Cbz)phenylacetic acid (4.43 g; 6.89 mmol), DIPC (1.07 ml; 6.89 mmol), and HOBt (1.05g; 6.89

mmol) in 40 ml of DMF, and the reaction was allowed to proceed overnight. The resin was filtered and washed successively with DMF (3 x 60 ml, 1 min), DCM (3 x 60 ml, 1 min), 5% DIEA/DCM (2 x 60 ml, 1 x 1 min, 1 x 10 min), and DCM (3 x 60 ml, 1 min each). A qualitative Kaiser test was slightly positive for the derivatized resin. Consequently, the above derivatization was repeated using Boc-Tyr(2-Br-Cbz)- phenylacetic acid (643 mg; 1 mmol), DIPC (155 μl; 1 mmol), and HOBt (153 mg; 1 mmol) in 10 ml of DMF, and the reaction was allowed to proceed overnight. At this stage the Kaiser test was still slightly positive, and the above derivatization was repeated using Boc-Tyr(2-Br-Cbz)-phenylacetic acid (321 mg; 0.5 mmol), DIPC (78 μl; 0.5 mmol), and HOBt (77 mg; 0.5 mmol) in 10 ml of DMF, and the reaction was allowed to proceed for 48 h. The Kaiser test was finally negative for the derivatized resin, and the resin was worked-up by washing successively with DMF (3 x 60 ml, 1 min), DCM (3 x 60 ml, 1 min), and Et_2O (4 x 60 ml, 1 min), and dried in a desiccator overnight. Boc-Tyr(2-Br-CBz)-PAM resin (10.1 g; 6.9 mmol; 99% yield) was obtained.

Acetylation of t-Butoxycarbonyl-(L)-tyrosyl(2-Br-Cbz)-PAM Resin (XVIId)

In order to minimize any side-reaction due to the presence of unreacted amino-groups on the resin, the

following procedure was performed (103). Boc-Tyr(2-Br-Cbz)-PAM resin (10.1 g; 6.9 mmol) was dissolved in a solution containing 10 mmol of acetic anhydride (0.944 ml) and 10 mmol of DIEA (1.74 ml) in 30 ml of DMF, and rocked for 30 min. The acetylating mixture was removed by filtration, and washed successively with DMF (3 x 60 ml, 1 min), DCM (3 x 60 ml, 1 min), and Et_2O (5 x 60 ml, 1 min). The acetylated resin was then dried in a desiccator for 24 h under high vacuum over P_2O_5.

Synthesis of

TFA·Trp(For)-His(Tos)-Trp(For)-Leu-Gln-Leu-Lys(N^{ϵ}-FMOC)-Pro-Gly-Gln-Pro-(Nle)-Tyr(2-Br-Cbz)-PAM Resin (XVIII)

a) Syntheses were performed manually, starting with Boc-Tyr(2-Br-Cbz)-PAM resin (10.1 g; 6.9 mmol) in a 100-ml reaction vessel. All residues were double coupled. The Boc group was exclusively used for the N^{α}-protection; the side-chain protecting groups were Trp(For),His(Tos), and Tyr(2-Br-Cbz). Coupling cycles were as previously described except indole was added(0.001 w/v) as a scavenger and DIPC was used in place of DCC. For Glutamine residues the HOBt/DIPC-accelerated active ester coupling procedure was utilized in DMF.

For the cycle immediately following the incorporation of Boc-Gln, 4N HCl/dioxane was used to deprotect the Boc group (see **VIa**). When a third coupling was required, as

revealed by the Kaiser test(99), 1 equiv. of Boc-amino-acid, DIPC, and HOBt in DMF were added, and the reaction was allowed to proceed overnight at room temperature.

Upon completion of the assembly of the tridecapeptide-PAM resin, the resin was washed with DCM (40 ml, 3 x 1 min) and Et_2O (40 ml, 3 x 1 min), and dried to constant weight in a desiccator over P_2O_5 under high vacuum. Boc-tridecapeptide-PAM resin (22.62 g; 6.68 mmol; 97% of theoretical; 0.295 mmol/g) was obtained. A portion of the Boc-decapeptide-PAM resin (720 mg; 0.21 mmol) was treated with TFA/DCM/DMS/Anisole (50:48:2:0.001 v/v/v/w) for 1 x 30 min, and washed with DCM (40 ml, 3 x 1 min) and Et_2O (40 ml, 3 x 1 min). The TFA•resin was dried to constant weight in a desiccator over P_2O_5 under high vacuum, and subjected to High HF cleavage as outlined in Section (C) of this chapter. Crude deprotected peptide was extracted into 6% HOAc solution (6 x 15 ml), the extracts were pooled, and the volume was reduced to 10 ml. Water (25 ml) was added and the resulting solution was lyophilized overnight.Crude HOAc•Trp-His-Trp-Leu-Gln-Leu-(Lys-N^{ϵ}-FMOC)-Pro-Gly-Gln-Pro-Nle-Tyr peptide (359 mg; 0.17 mmol; 90% of theoretical) was obtained, and the FMOC-group was removed from a portion of the HOAc•tridecapeptide salt (102 mg; 0.05 mmol). The deprotected product was one major peak as judged by gradient reversed-phase HPLC as described in Section (D). Crude tridecapeptide was purified on a C_{18}-reversed-phase

(19 x 300 mm) HPLC column, utilizing preparative gradient HPLC as outlined in Section (D). Pure 3TFA·Trp-His-Trp-Leu-Gln-Leu-Lys-Pro-Gly-Gln-Pro-(Nle)-Tyr (40 mg; 40% yield), which was greater than 99% homogeneous as judged by analytical gradient reversed-phase HPLC was obtained.

Synthesis of 2TFA·Trp^{1}(N^{α}-Acetyl)-His-Trp-Leu-Gln-Leu-Lys-Pro-Gly-Gln-Pro-(Nle)-Tyr (XIX)

Boc-tridecapeptide-PAM resin (1.0 g; 0.295 mmol) was treated with TFA as described for (**XVIII**), washed with 10% DIEA/DCM, and DCM (60 ml, 3 x 1 min) and the resulting [Lys^{7}-N^{ϵ}-FMOC,(Nle^{12})]-α-factor resin (866 mg; 0.25 mmol) was added to acetic anhydride (0.235 ml; 2.5 mmol) and DIEA (0.435 ml; 2.5 mmol) in 10 ml of DMF for 30 min. At this stage the Kaiser test was negative, and the derivatized resin was filtered, washed with DMF (40 ml, 4 x 1 min). Then HOBt (153 mg; 1 mmol) in 10 ml of DMF was added for 1 h to remove the tosyl group from any partially deprotected Histidine residue in the crude peptide. The FMOC-group was removed according to procedures outlined for (**XVIII**). Crude acetylated tridecapeptide resin (747 mg) was obtained. A portion thereof (600 mg; 0.204 mmol) was subjected to High HF cleavage as described above. The crude product(305 mg; 81% yield) was purified as outlined above (**XVIII**), and pure material (145 mg; 38% of theoretical) was obtained, which

was greater than 99% homogeneous as judged by analytical gradient reversed-phase HPLC. The peptide was then characterized by amino-acid analysis.

Synthesis of 3TFA·Trp-His-Trp-Leu-Gln-Leu-Lys^7(N^ϵ-Biotinyl)-Pro-Gly-Gln-Pro-(Nle)-Tyr (XX)

The FMOC-group was removed from the Boc-[Lys^7-N^ϵ-FMOC, ($Nleu^{12}$)]-α-factor-Pam resin (1.03 g; 0.29 mmol) with 20% piperidine/DMF for 1 h, and the deprotected peptide resin was washed successively with; DMF (60 ml, 3 x 1 min), MeOH (60 ml, 3 x 1 min), and DMF (60 ml, 3 x 1 min). D-Biotin-ONp (365 mg; 1 mmol) was added to the resin in DMF, and allowed the reaction was allowed to proceed for 24 h. The resin was filtered, washed with DMF (60 ml, 3 x 1 min), and a slightly positive Kaiser test was obtained for the biotinylated-resin. The resin was washed with DCM (60 ml, 3 x 1 min), 10% DIEA/DCM (2 x 60 ml 1 x 1 min, 1 x 10 min), DCM (60 ml, 3 x 1 min), and DMF (60 ml, 3 x 1 min). D-Biotin-ONp (183 mg; 0.5 mmol) was added to the resin and the reaction was allowed to proceed overnight. The resin was filtered, washed with DMF (60 ml, 3 x 1 min), MeOH (60 ml, 3 x 1 min), and DMF (60 ml, 3 x 1 min). The Kaiser test was negative. The Boc group was removed and Lys^7(Biotinyl)-α-factor was then cleaved from the resin by High HF as described for the tridecapeptide (**XVIII**), The crude material (660 mg) was purified as outlined above (**XVIII**), and 99%

pure product (222 mg; 36% of theoretical) was obtained. The peptide was characterized by amino-acid analysis and FAB-MS.

Synthesis of 2TFA·Trp^1(N^{α}-Fluoresceinyl)-His-Trp-Leu-Gln-Leu-Lys-Pro-Gly-Gln-Pro-(Nle)-Tyr (XXI)

The Boc-tridecapeptide-PAM resin (1.0 g; 0.295 mmol) was treated with TFA as described for (**XVII**), and the TFA·tridecapeptide(Lys^7-N^{ϵ}-FMOC) resin was then subjected to High HF cleavage as described above. The crude product(530 mg; 92% yield) was then added to fluorescein disodium salt (435 mg; 1.16 mmol), BOP (358 mg; 0.81 mmol), and DIEA (0.141 ml; 0.81 mmol), and the reaction was allowed to proceed for 48 h. In addition, the reaction was monitored by gradient reversed-phase HPLC, and after 48 h the reaction was determined to be complete. The crude material was then purified as outlined above (**XVIII**), and pure material (88 mg; 15% of theoretical) was obtained, which was greater than 99% homogeneous as judged by analytical gradient reversed-phase HPLC. The peptide was then characterized by amino-acid analysis, FAB-MS, and 200-MHz ^{1}H-NMR spectroscopy.

Synthesis of

3TFA·Lys^{-1}[N$^{\epsilon}$-(β-(4-hydroxyphenyl)propionyl)]-Trp-His-Trp-Leu-Gln-Leu-Lys-Pro-Gly-Gln-Pro-(Nle)-Tyr (XXII)

The Boc-tridecapeptide-PAM resin (**XVIII**)(1.0 g; 0.295 mmol) was extended to the tetradecapeptide stage with FMOC-Lys(N$^{\epsilon}$-Boc) according to procedures outlined for the Boc-tridecapeptide-PAM resin (**XVIII**), the resultant tetradecapeptide-PAM resin was then treated with TFA as described for (**XVIII**), washed with 10% DIEA/DCM, and DCM (60 ml, 3 x 1 min). The tetradecapeptide(Lys^{-1}-N$^{\epsilon}$H$_2$) resin was added to 2 equivalents of β-(4-hydroxyphenyl)propionic acid hydroxysuccinimide ester (155 mg; 0.59 mmol) and 2 equivalents of DIEA (0.102 ml; 0.59 mmol) in 10 ml DMF, and the reaction was allowed to proceed for 2 h. At this stage the Kaiser test was negative; nevertheless, the above derivatization was repeated using an additional 2 equivalents of the succinimide ester (155 mg; 0.59 mmol) and DIEA (0.102 ml; 0.59 mmol) in 10 ml of DMF, and the reaction was allowed to proceed overnight. The Kaiser test was again negative, and the derivatized resin was filtered and washed with DMF (40 ml, 4 x 1 min). Then HOBt (153 mg ; 1 mmol) in 10 ml of DMF were added for 1 h to remove the tosyl group from any partially deprotected Histidine residue in the crude peptide. In addition the FMOC-group was removed,according to procedures outlined for (**XVIII**). The crude Lys ^{1}(N$^{\epsilon}$-HPPA)-tetradecapeptide resin (920 mg; 0.24

mmol) was obtained, and then subjected to High HF cleavage as described above. The crude product(150 mg; 27% yield) was then purified as outlined above (**XVIII**), and pure material (127 mg; 23% of theoretical) was obtained, which was greater than 99% homogeneous as judged by analytical gradient reversed-phase HPLC. The peptide was then characterized by amino-acid analysis and FAB-MS.

C) **HF Cleavage**

Deformylation and Detosylation- The side-chain protecting tosyl-group on histidine has long been considered to be quantitatively removed by HF (104). However several reports from this laboratory have demonstrated that complete removal of these protecting groups for α-factor peptides does not occur (92,59). Based on these results, protected peptide resins are now routinely treated with 5 equiv. HOBt in DMF for 1 h to remove the tosyl-group, and 20% piperidine in DMF (60 ml) for 1 hr, to remove the formyl group. These procedures are performed prior to HF cleavage and have significantly improved the homogeneity of the crude peptides.

HF Cleavage- Before the cleavage of the peptide from the resin, the amino-terminal Boc group was deprotected with 45% trifluoroacetic acid, CH_2Cl_2, 2% DMS for 30 min, and the resin was washed with CH_2Cl_2, MeOH, and CH_2Cl_2 (three times

each) and dried *in vacuo* overnight. One gram of the resin was mixed with 1.5 ml of anisole in a Kel-F HF reaction vessel, and HF was condensed at -78°C under reduced pressure to a total volume of 15 ml (HF + anisole + resin). Cleavage proceeded at 0-2°C for 1.5 h. After evaporation of HF, the residue was washed with precooled ether and then with ethyl acetate (three times each). The crude peptide was extracted into aqueous acetic acid, and the extracts were combined and lyophilized. The yield of the crude product was about 90% for most of the peptides, based on the starting amine content on the resin.

D) Chromatographic Methods

TLC- The following solvent systems were utilized for TLC on silica gel plates (Kieselgel 60 F_{254}) for amino-acid derivatives and peptides: (A) butanol/acetic acid/water (4:1:2), and butanol/acetic acid/water/ pyridine (15:3:12:10), and the R_f values are reported as R_{fA} or R_{fB}, respectively. Spots were detected by UV light and/or visualized by a 1% (wt/v) ninhydrin/n-butanol mixture.

HPLC- A Waters analytical HPLC instrument consisted of a Waters 510 and Waters M6000A pumps, an on-line Waters λ-Max 481 variable-wavelength UV spectrophotometer, and a Waters 680 automated gradient controller attached to an M730 data module. A Waters μ Bondapak C_{18} (300 x 3.90 mm i.d.)

column was used for analytical separations. Sample injections were made with a 25 μl syringe (Hamilton). Sample concentrations were 1 mg/ml and typical volumes of 10-25 μl were injected. Detection was usually at 220 nm, and the sensitivity of the UV detector was generally set at 0.1 AUFS. Normally a 1.5 ml/min flow rate was used, and the recorder chart speed was 0.5 cm/min In general, samples were eluted with a linear gradient of H_2O (0.025% TFA) and acetonitrile (0.025% TFA) from 20 to 40%, or 20 to 60% acetonitrile over 30 min, unless otherwise specified in section (C).

Crude peptides from HF cleavage were purified by reversed-phase, semipreparative HPLC on a Waters μ Bondapak C_{18} column (300 x 30 mm). The cleavage product (250 - 400 mg) was dissolved in about 10 ml of running-solvent, and applied to an equilibrated column at 10% acetonitrile/90% H_2O/0.025% TFA. The product was generally eluted with a linear gradient of H_2O (0.025% TFA) and acetonitrile (0.025% TFA), from 10 to 60% acetonitrile, or 10 to 80% acetonitrile over 60 min at a flow rate of 6 ml/min. Fractions were collected, and normally the desired product eluted sharply within 5-8 fractions. Fractions were analyzed by analytical HPLC as described above. In general, fractions of similar homogeneity were pooled, and then lyophilized overnight. Typically the desired product was greater than 98-99% homogeneous as judged by analytical gradient HPLC methods.

In addition, the purity of the peptides were also checked by TLC on silica gel, and generally one spot in two systems for each peptide was observed with both UV and ninhydrin detection.

Several of the peptides were also purified on a Waters Prep 500 system, utilizing either a C_{18} (50 X 300 mm), or C_{18} (2.54 x 300 mm) reversed-phase column, using a 2% MeOH/H_2O (0.025% TFA) step gradient at a flow rate of 50 ml/min Fractions (25 ml) were collected and then analyzed by analytical HPLC. Fractions with similar homogeneity were pooled, reduced to a low volume, and then lyophilized overnight. Subsequently, the pure material was then reanalyzed by analytical-gradient HPLC as described above, and similar results were obtained.

E) Amino-acid analysis

Amino-acid analyses were performed by Charles Murphy at the Analytical Services Facility of the University of Tennessee, Knoxville. Peptides were hydrolyzed in sealed tubes in 6N HCl at 100° for 24 hours. All peptides synthesized gave acceptable amino-acid ratios.

F) **Fast atom bombardment mass spectrometry**

FAB-mass spectrometry was performed by Dr. Al Tuinmann at the University of Tennessee. FAB-mass spectra were obtained with a VG 2AB EQ mass spectrometer equipped with a flow FAB ion source of an Ion Tech fast atom gun. Approximately 2 μl of a peptide solution (1.0 nmol/μl) dissolved in acetonitrile/water (2:1), 0.1% trifluoroacetic acid was dispersed on the stainless-steel target in a matrix of monothioglycerol. The accelerating voltage of the mass spectrometer was maintained in 8 kV, whereas 8-KeV xenon atoms at a discharge current of 1 mA were used to bombard the sample. Spectra were recorded in the "multichannel acquisition" mode from m/z 800 to 1800 at 20 S/decade by the VG 11-250 J data system. Instrument resolution (m/ΔM) was set at 2000. All peptides gave the expected molecular ion [M'+ H'] as determined by FAB-mass spectrometry.

G) **Bioassays**

S. cerevisiae strains used -The sources and relevant genotype of the strains used for this study are *S. cerevisiae* 2180-1A(MATa) from the Yeast Genetics Stock Center, Berkeley, CA; *S. cerevisiae* RC629 (MATa sst1-2, supersensitive to α-factor by virtue of a mutation in the BAR1 protease (allelic to SST1) which hydrolyzes α-factor) from R. Chan; *S. cerevisiae* RC631(MATa sst2-1,

supersensitive to α-factor because of a mutation in desensitization response) from R. Chan (Hi-Bred International, Johnston, IA); *S. cerevisiae* 4202-15-3(MATa bar1-1, a strain used in binding studies) from D. Jenness (University of Massachusetts, Worchester); and *S. cerevisiae* 50B(MATa ste2^{ts}, temperature sensitive for the α-factor receptor STE2) from Yeast Genetics Stock Center.

Biological Assay for Shmoo Formation- A culture of X2180-1A(MATa) was grown at 30°C with shaking to early log phase (85 Klett units, blue filter with Klett colorimeter) in YNB supplemented with 0.5% ammonium sulfate and 2% glucose. The cells were then harvested by centrifugation at 1000 g, washed twice with sterile distilled water, resuspended to 4.0 x 10^6 cells/ml in YNB, and placed on ice. Dilution series (1:2, 80-1.25 μg/ml) of tridecapeptide and each of the derivatized α-factors were prepared in borosilicate glass tubes with YNB as the diluent. Five hundred microliters of the 4.0 x 10^6 cell suspension was then added to 500 μl of each of the peptide solutions, and the suspensions were incubated at 30°C for 3.5 h in a rotary water bath shaker. At the completion of the incubation period, the cells were placed on ice, and then 10 μl portions were placed in a hemocytometer and observed microscopically to quantitate the total number of cells, shmoos, and unbudded cells.

Growth Arrest (Halo Assay)- YEPD plates were overlayed with 4 ml of MATa cells (2.5 x 10^5 cells/ml) in noble agar (0.825%). Filter disks (Whatman No. 1 or Whatman 3MM) were then placed on the overlay, and 10-µl portions of peptide solutions at various concentrations were pipetted onto the disks. The plates were incubated at 30°C for 48 h and then observed for clear zones (halos) around the disks, an indication of the arrest of cell growth. The diameter of the clear zone was determined by subtracting the diameter of the disk from the diameter of the zone of inhibition.

Competition Assay- Ten microliters of 1 mg/ml des-Trp^1, Ala^3-α-factor, a dodecapeptide with the sequence His-Ala-Leu-Gln-Leu-Lys-Pro-Gly-Gln-Pro-Met-Tyr, was added to 10-µl portions of 0.1 mg/ml solutions of α-factor or each of the peptides. Ten-microliter portions of these mixtures were then tested in the halo assay. Controls without des-Trp^1, Ala^3-dodecapeptide were tested concurrently.

H) NMR Methods

All spectra were recorded in 100% DMSO-d_6 from Aldrich, at an approximate concentration of 5 mg/0.5 ml (w/v) in 5 mm Wilmad 528 NMR tubes, corresponding to a peptide concentration of 5-12 mM. The chemical shifts and line-widths of the peptides did not change upon dilution to 0.1 mM, which indicated that aggregation was not occurring

at the concentrations used. Most samples were dried in an Abderhalden drying-pistol under high-vacuum for 24 h, while refluxing methanol, to remove loosely bound water carried over from the lyophilization. All spectra were accumulated at 27°C, unless otherwise noted.

The proton NMR spectra were either acquired on a Brucker 200-MHz spectrometer equipped with an Aspect 2000A computer, or on a JEOL GX-400 400-MHz spectrometer. Most of the raw data were then processed on an offline SUN 3/110 workstation, utilizing an NMRI 3.95 software package, or on a μ-VAX using the FTNMR-51 package available from Hare Research. Spectra were either referenced against tetramethylsilane as 0 ppm, or are reported relative to the residual proton resonance of DMSO at 2.49 ppm.

One-dimensional spectra were acquired with 8K data points and a spectral width of 10-12 ppm, then zero-filled to 32K. In addition the spectra were apodized by application of a $\pi/16$ phase-shifted sine-bell multiplication, prior to the zero-filling and Fourier transformation. Vicinal proton coupling constants were also calculated from spectra utilizing a Gated-Homonuclear decoupling scheme. These coupling constants were then corrected for electronegativity effects(166), and used in a Karplus type equation to generate possible ϕ and χ^1 angles(158). For the Substance P analog, the rotamer populations for the aromatic side-chains

were also calculated(105). For example, the following equations were utilized to calculate the rotamer populations for the Phe^{7} *cis*-diastereomer of [pGlu^{6}, NMePhe^{8}, Aib^{9}]-SP$^{6-11}$.

Eq.(1) $$P_I = \frac{J_{\alpha\beta 2} - J_g}{J_t - J_g}$$

Eq.(2) $$P_{II} = \frac{J_{\alpha\beta 1} - J_g}{J_t - J_g}$$

Eq.(3) $$P_{III} = 1 - (P_I + P_{II})$$

We obtained coupling constants of 3.87 Hz and 9.92 Hz for $J_{\alpha\beta 2}$ and $J_{\alpha\beta 1}$. These were corrected for electronegativity effects by multiplying these values by a factor of 1.03(166). This yielded values of 3.99 and 10.22 Hz for $J_{\alpha\beta 2}$ and $J_{\alpha\beta 1}$, respectively. To calculate the rotamer I state population for the Phe^{7}-cis isomer, the value of 3.99 Hz was used in equation 1, and by utilizing the average J_{gauche} coupling constant for rotamer I = 3.95 Hz and the average J_{trans} = 12.2 Hz(159), we calculated that the Phe^{7}-*cis* isomer's population in rotamer-state I was approximately 0.5% of the mole fraction present. Identical approaches were applied to calculate the various contributors to the averaged observed coupling constants for

the Phe^7 *cis*-isomer, as well as for the remaining aromatic side-chains in this SUBP analog.

200-MHz Double-Quantum-Filtered-Phase sensitive-COSY and Relayed-COSY spectra were acquired employing pulse sequences of [90-t_1-90-T-90+φ-FID(t_2)](Time Proportional Phase Incrementation routines, TPPI)(106,107) and [90-t_1-90-0.25/J-180-0.25/J-90-FID(t_2)](108,109), respectively. For the Substance P analog, the average J-value was 7.5 Hz, whereas the cyclic-α-factor utilized J-values of 3, 5, 6, 7, 8.3, 10, 12.5, 16.5, and 25 Hz. Data matrices of 2K x 256 were recorded, and the spectral width in each dimension was 10-12 ppm. Spectra were accumulated with four dummy-transients and 128-160 acquisitions per t_1-value, with post-acquisition delays of 1 s. A final 1K x 1K real data matrix was obtained by zero-filling the t_1-dimension prior to the Fourier transformation. Apodization of the COSY data was accomplished by application of a phase-shifted exponential sine-bell multiplication in both dimensions. Furthermore, the first data point in the t_1-interferogram was multiplied by 0.5 prior to the Fourier transformation in order to reduce t_1-noise ridges. In the cases where severe t_1-noise ridges were observed, a noise profile was generated from a signal-free region of the 2D-spectrum, and this noise-spectrum was then subtracted from the t_1-spectra. This noise-ridge subtraction routine dramatically improved the appearance of the 2D-data; however

careful inspection of extremely weak signals which were the result of spurious noise was mandatory in these cases.

400-MHz NOESY and ROESY experiments were obtained utilizing pulse sequences of [90-t_1-90-t_m-90-FID(t_2)] and [90-t_1-isotropic mixing pulse-FID(t_2)], respectively. All other acquisition and processing parameters were similar to those used for the COSY type data. For the Substance P analog, a 300-millisecond mixing-time and a 250-millisecond isotropic mixing pulse were applied for the NOESY and ROESY experiments, respectively, and data matrices of 2K x 256 were recorded. For the cyclic-α-factor, a 400 millisecond NOESY and a 300-millisecond ROESY were obtained, and data matrices of 2K x 256 were recorded. No attempt was made to monitor spin-diffusion for these peptides; however, future analyses can address this point.

In order to determine the presence of hydrogen-bond interactions within the peptide, temperature-dependent chemical shift coefficients for the peptide amino groups were obtained utilizing six experiments(110,111). These experiments ranged from 300 K to 325 K, and the temperature was increased in 5° C increments. The standard deviation for each slope was then calculated. For the Substance P analog, one-dimensional spectra were utilized for this analysis, whereas the cyclic-α-factor required six 2D-absolute value-COSY experiments, due to severe mutually overlapping

peaks. Acquisition and processing parameters were similar to those used above.

I) Rabbit Antibody Production

Four-month-old, female, New Zealand white rabbits were purchased from Myrtle Rabbitry, Thompson Station, TN. For the pre-immune serum approximately 50 ml of blood was collected from pinna(ear) punctures and the serum was stored at -20 C.

Immunogen was prepared by suspending 0.5 mg peptide, or 1.0 mg of carrier-conjugated peptide, in 1.0 ml phosphate-buffered saline, pH 7.4. For the initial injection, the suspension was combined with 1.0 ml Freunds Complete Adjuvant (Sigma Chemical Co., St. Louis, MO.) and repeatedly passed through interlocked syringes until an emulsion was formed. All subsequent booster injections were prepared as described except Freunds incomplete Adjuvant (Sigma Chemical Co.) was used. Injections (0.25 ml/site) were delivered intradermally across the surface of the back at eight sites. Injections were administered at three week intervals for peptide immunogens and at monthly intervals for conjugated-peptide immunogens, with periodic bleeds to determine titers. The potent antisera generated after at least three booster injections; were receptor C-terminal region 23-mer, 1:1,300; receptor C-terminal region

(23-mer)-conjugated to BSA, 1:2,500; receptor extracellular loop 19-mer, 1:10,000; and receptor 19-mer conjugated to KLH, 1:1,800.

H) **Polarimetry**

The optical rotation of compounds was determined on a Perkin-Elmer 141 polarimeter at 25°C, with a 1 dm path length. The light source was also set at the sodium D-line.

III) Probes for the α-factor binding site within the STE-2 receptor of *Saccharomyces cerevisiae*

A) Topological probes for the α-factor receptor

Introduction:

The STE-2 gene product, which has been demonstrated to be the ligand binding component of the α-factor receptor (57), has been cloned and sequenced(21,22). Based on the hydropathy profile for the primary translation product of the STE-2 gene product, a model for the possible folding pattern of this 431 residue long receptor has been generated. This model is similar to that for the rhodopsin/β-adrenergic receptor family, and indicates that the predicted STE-2 gene product contains seven transmembrane helices connected by short hydrophilic loops. The receptor ends in a cytoplasmic domain containing a 135 residue long hydrophilic C-terminal region.(61-63)

Immunological, biochemical, and genetic analyses have demonstrated that the STE-2 gene product is a membrane-bound glycoprotein, and that its C-terminal tail region is located on the cytosolic side of the membrane(57).

In addition, the C-terminal region of 135 residues are not required for pheromone binding and subsequent signal transduction, but mediates an adaptive response upon prolonged exposure to the pheromone(57,61-63). This desensitization to the α-factor is believed to be the result of phosphorylation of the C-terminus (57). Hence, all the information required for ligand binding and signal transduction is contained within the amino-terminal 305 residues.

In contrast, a shorter fragment of the STE-2 gene product containing only the amino terminal 261 residues, was inactive in mating. Hence, removal of the seventh transmembrane helix resulted in an inactive receptor(61). However it is still unclear if this was due to the loss of pheromone binding or due to the receptor's inability to interact with its effector.

The recently introduced use of antibodies directed against synthetic peptides of the primary sequence of a protein has proven to be a powerful tool in the spatial analysis of membrane embedded proteins (112-114). This approach has been successfully applied to the topological study of the ADP/ATP carrier (115), the entire human cytochrome C oxidase complex(116), the lactose/H^+ transporter of E. coli (117), the glucose transporter protein (118), and the nicotinic acetylcholine receptor

(119). Furthermore, mapping of the α-bungarotoxin binding site within the α-subunit of the acetylcholine receptor (120), and mapping of the binding site of the receptor for leutinizing hormone-releasing hormone (LHRH) (121), have also been reported utilizing anti-peptide antibodies. Moreover, assignment of secondary structures by anti-peptide antibodies has also been proposed (122).

The results of the above studies indicate that antibodies against the α-factor receptor may be used to gain information on the topology of the **STE-2** receptor, and also to generate screening-reagents for **STE-2** mutants. In addition, it is possible that one may obtain the fortuitous result of obtaining an antisera that can competitively inhibit pheromone binding to the **STE-2** receptor. This result would begin to localize the binding-site for the α-factor pheromone within the **STE-2** gene product.

In order to gain further insight on the structural features that the STE-2 gene product exhibits in its membrane-associated state, a series of topological probes were generated against two of the hydrophilic loop regions, and a portion of the C-terminal tail. The short term goal of this study was to determine the location of these regions within the STE-2 receptor, as residing intracellularly or extracellularly. These results would not only further support the existing model for the receptor, but more

importantly, they would provide direct immunological evidence on the topology of specific regions within the receptor, as well as form a basis for detailed investigation of the receptor in its membrane-bound state.

To generate these specific immunological probes for topology, rabbit polyclonal antiseras were obtained against synthetic peptides corresponding to the hydrophilic loops between helix 2 and helix 3, and between helix 4 to helix 5, and are depicted in Figure 3. A region of the C-terminus was also synthesized, and utilized as a synthetic antigen as well. The antisera were then isolated and utilized to test for recognition of that particular sequence within the whole STE-2 receptor. If the antisera preferentially recognized whole **MATa**-cells and not **MAT**α-cells, then the sequence would most likely be on the exterior. If the antisera failed to bind to the exterior of the whole cell, but adhered to lysed-cells, then that particular sequence was most probably located intracellularly. To insure that the cell-wall was not hindering accessibility of the antisera to its epitope, the antisera could be also incubated with spheroplasts. ELISA techniques were to be utilized to visualize the antisera binding.

Results and Discussion:

Synthesis of the peptide antigens was achieved by the solid-phase approach introduced by Merrifield (123,124). The 23 residue peptide antigen, corresponding to region 350-372 in the C-terminus of **STE-2**, was assembled on a phenylacetamidomethyl resin. This resin was introduced to increase both the yield and homogeneity of crude peptides utilizing the solid-phase methodology (102). The presence of the electron-withdrawing acetamido bridge in this resin increases the stability of the peptide-resin linkage. Since this linkage is more resistant to cleavage during the repetitive acidolytic steps used to remove the Boc protecting group, fewer peptide chains are lost for each synthetic cycle, resulting in higher yields and increased homogeneity.

Intermediates in the synthesis of the Boc-Ile-PAM resin were carefully scrutinized prior to the use of the resin in generating the peptide antigen. These precursors were analyzed by TLC, melting piont, optical rotation, and 200-MHz ^{1}H-NMR spectroscopy. The results of these analyses indicated the proposed structure for these intermediates.

Once the Boc-Ile-PAM resin was assembled, the resin was acetylated to "cap" any unreacted amino groups present on the resin. This "capping" procedure minimizes side reactions that can occur during the synthetic cycling (103). The Boc group was exclusively used for the N^{α}-protection, and the scavenger DMS was routinely included in the TFA deprotection mixture. The presence of a scavenger reduces alkylating side reactions to aromatic-residues during removal of the Boc-group. Proper side-chain protecting groups for polyfunctional amino acids were also carefully chosen to minimize side reactions, as well as for ease in removal during the final HF cleavage step. In addition, all residues were routinely double-coupled regardless of a negative Kaiser test in the first coupling step, to ensure completeness of the coupling reaction and minimize deletion peptides(125). The Kaiser test was always performed prior to and after each coupling cycle.

Once the peptide was assembled on the PAM resin, the Boc group was removed prior to High HF cleavage of the peptide from the resin. In general, the crude peptide was obtained in approximately 95% yield and was one major peak on gradient C_{18}-reversed-phase HPLC. After purification of these peptides using HPLC, peptides of at least 99% purity were isolated in yields of 81, 49, and 41% for the decapeptide, pentadecapeptide, and the 23-residue peptide antigen, respectively.

The peptide antigen was then characterized by TLC, HPLC, amino-acid analysis, optical rotation, and 200-MHz or 400-MHz ^{1}H-NMR spectroscopy. TLC and HPLC indicated the peptide antigen was at least 99% homogeneous (see Fig. 4) and amino acid analysis supported the presence of all residues (Table 1). Displayed in Fig. 5 is a 400-MHz ^{1}H-NMR spectrum for the antigen 10 peptide, which further supported the proper structure for the peptide. Characteristic resonances were observed such as the ring protons for Phe^{364} at 7.23 ppm; the methyls of Val^{365} and Ile^{372} at 0.83 ppm; the methyls of Thr^{363}, Thr^{368}, and Ala^{369} at 1.15, 1.02, and 1.22 ppm, respectively; the side-chain OH groups of Ser^{366}, Thr^{363}, and Thr^{368} at 5.56, 5.11, and 4.65 ppm; the γCH_2 of Glu^{367} at 2.26 ppm; and the βCH_2 of Asp^{370,371} at 2.69-2.47 ppm. These assignments were confirmed by DQF-phase sensitive COSY and 400 msec NOESY analyses.(data not shown).

Figure 4. C_{18}-Gradient reversed phase HPLC of STE-2 receptor peptides after purification. For peptides A-C, and E, the gradient used was from 10-30% acetonitrile (0.025% trifluoracetic acid) over 30 mins. For peptide D, a 30-50% acetonitrile(0.025% trifluoracetic acid) gradient over 30 mins was utilized.

Peptide A; Thr-Phe-Val-Ser-Glu-Thr-Ala-Asp-Asp-Ile corresponding to region 363-372;

Peptide B; Lys-His-Ser-Glu-Arg-Thr-Phe-Val-Ser-Glu-Thr-Ala- Asp-Asp-Ile corresponding to region 358-372;

Peptide C; Arg-Arg-Lys-Glu-Thr-Thr-Ser-Asp-Lys-His-Ser-Glu-Arg-Thr-Phe-Val-Ser-Glu-Thr-Ala- Asp-Asp-Ile corresponding to region 350-372;

Peptide D; Ser-Ser-Val-Thr-Thr-Ala-Leu-Thr-Gly-Phe-Pro-Gln-Phe-Ile-Ser-Arg-Gly-Asp-Val-amide corresponding to STE-2 region 107-125, and is depicted as E1 in Figure 3;

Peptide E; Val-Thr-Tyr-Asn-Asp-Val-Ser-Ala-Thr-Gln-Asp-Lys-Thr-Phe-Asn-Ala-amide corresponding to STE-2 region 191-206, and is depicted as E2 in Figure 3.

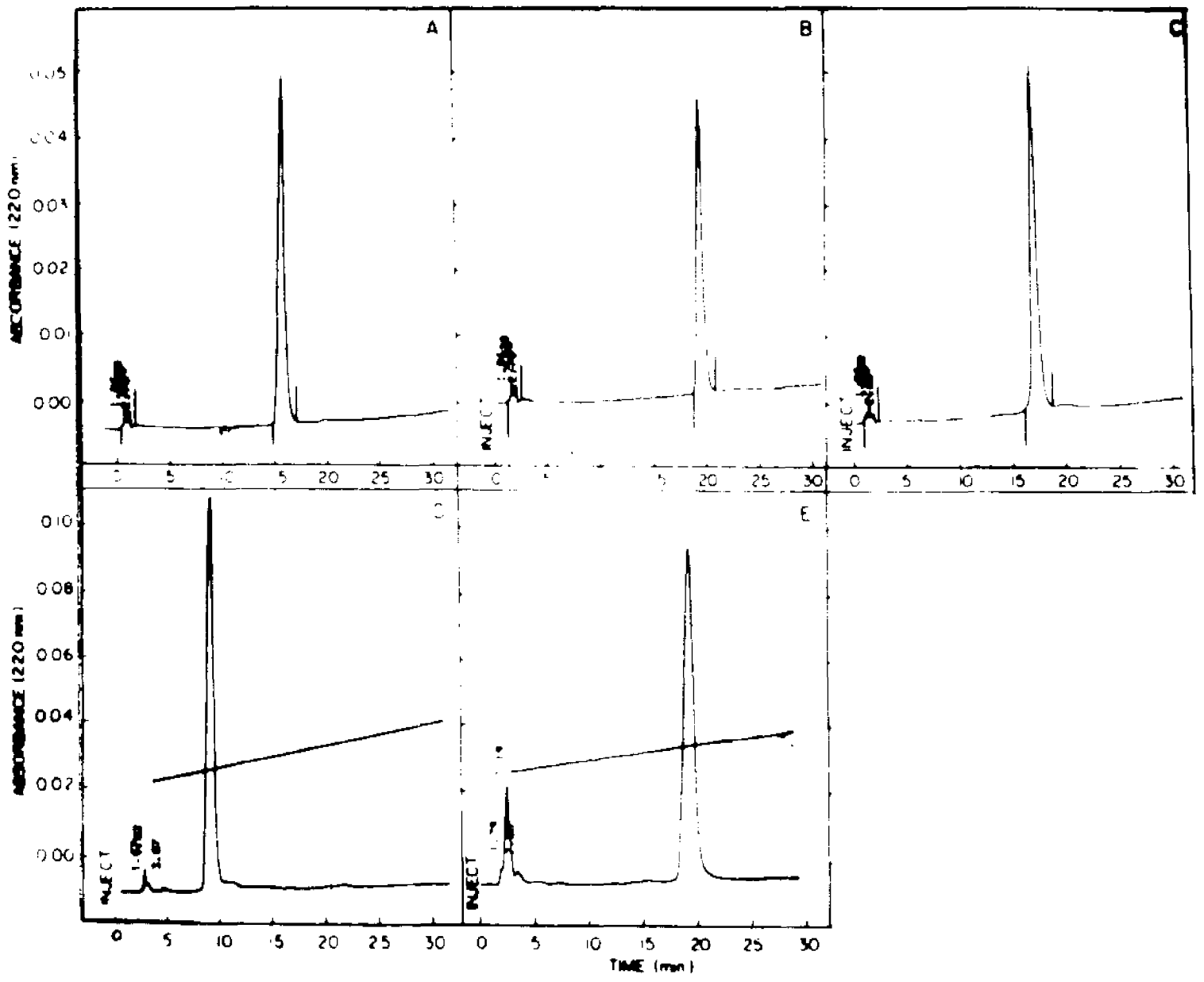
A
B
C
D
E
ABSORBANCE (220 nm)
0.05
0.04
0.03
0.02
0.01
0.00
0.10
0.08
0.06
0.04
0.02
0.00
INJECT
0 5 10 15 20 25 30
TIME (min)

Table 1. Chemical and physical properties of STE-2 receptor peptides.

Peptide I; Thr-Phe-Val-Ser-Glu-Thr-Ala-Asp-Asp-Ile; (corresponding to STE-2 region 363-372);

II, Lys-His-Ser-Glu-Arg-Thr-Phe-Val-Ser-Glu-Thr-Ala-Asp-Asp-Ile; (corresponding to STE-2 region 358-372);

III, Arg-Arg-Lys-Glu-Thr-Thr-Ser-Asp-Lys-His-Ser-Glu-Arg-Thr-Phe-Val-Ser-Glu-Thr-Ala-Asp-Asp-Ile; corresponding to STE-2 region 350-372);

IV, Ser-Ser-Val-Thr-Thr-Ala-Leu-Thr-Gly-Phe-Pro-Gln-Phe-Ile-Ser-Arg-Gly-Asp-Val-amide; corresponding to STE-2 region 107-125, and is depicted as E1 in figure 3.);

V, Val-Thr-Tyr-Asn-Asp-Val-Ser-Ala-Thr-Gln-Asp-Lys-Tyr-Phe-Asn-Ala-amide.(corresponding to STE-2 region 191-206, and is depicted as E2 in figure 3.)

Table 1.

Chemical and physical properties of STE-2 receptor peptides

Analysis	I	II	III	IV	V
Amino-acid					
Asp	2.02	2.00	2.89	0.87	4.14
Glu	1.06	1.97	2.98	1.06	1.13
Ser	1.04	2.01	3.06	3.11	0.96
Gly	----	----	----	2.27	----
His	----	1.04	1.00	----	----
Arg	----	0.97	3.06	0.96	----
Thr	1.89	1.98	3.96	2.01	1.66
Ala	1.08	1.12	1.10	1.09	2.14
Pro	----	----	----	1.11	----
Tyr	----	----	----	1.07	2.03
Val	0.98	0.96	1.07	2.14	1.88
Met	----	----	----	----	----
Ile	1.01	1.00	1.02	1.03	----
Leu	----	----	----	----	----
Phe	0.99	0.99	0.99	2.20	0.96
Lys	----	0.97	1.95	----	0.96
Total	10	15	23	19	16
Yield(%)	81%	49%	44%	14%	37%
R_f [illegible] A[a]	0.33	0.02	0.00	0.35	0.22
R_f [illegible] B[a]	0.75	0.03	0.00	0.70	0.68
p' value[b]	8.99	7.46	6.85	3.68	7.90
$[\alpha]^{25}D$	-34.7	-40.6	-42.1	-48.6	-26.4

[illegible]

Figure 5. 400 MHz proton NMR spectrum of STE-2 receptor peptide, Thr-Phe-Val-Ser-Glu-Thr-Ala-Asp-Asp-Ile, in DMSO-d, at 25 °C,(corresponding to STE-2 region 363-372).

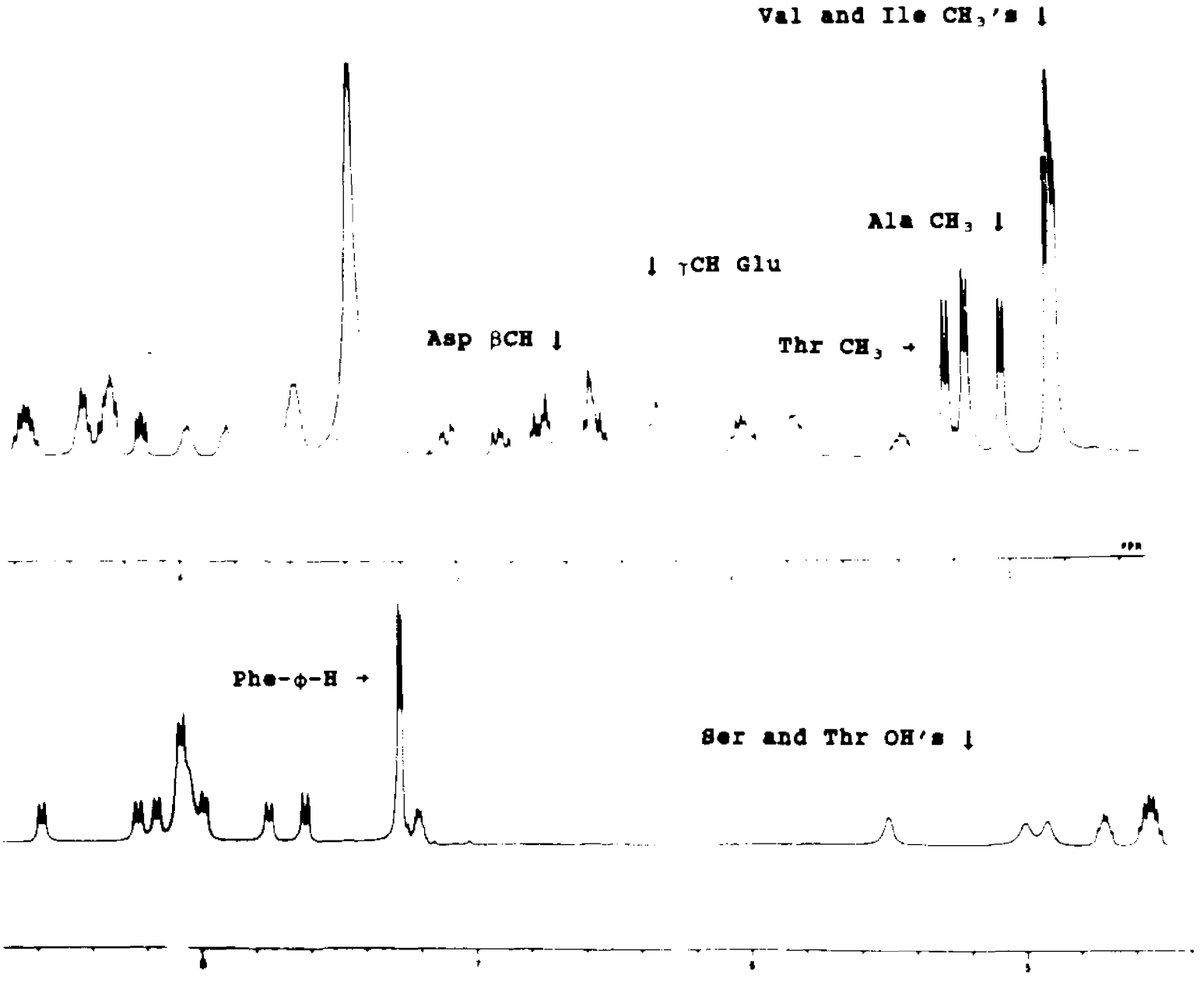
Val and Ile CH3's
Ala CH3
γCH Glu
Asp βCH
Thr CH3
ppm
Phe-ϕ-H
Ser and Thr OH's

The two hydrophilic loop peptides corresponding to regions 107-125 and 191-206 within the **STE-2** gene (depicted as loops E1 and E2 in Figure 3) were generated on a benzhydrylamine or 4-methylbenzhydrylamine resin, respectively. Upon final cleavage with HF, these peptides would then be obtained as their C-terminal amides(126,127). It was decided to generate these peptide antigens as their amides to better mimic those corresponding regions within the **STE-2** gene product. Since these regions are located internally in the primary sequence of the receptor, both the N-terminus and C-terminus of these peptides should not carry a charge. Synthesis of a peptide on a PAM resin would yield a peptide with a free amino and carboxyl termini. Antibodies generated against such peptides may recognize an epitope containing a charged species. This could result in failure of antibody to recognize the sequence within the protein, due to the fact that these charged termini are absent(128).

Synthesis of the hexadecapeptide corresponding to region 191-206 within the **STE-2** receptor, was carried out on a 4-methylbenzhydrylamine resin after obtaining a relatively poor yield for the nonadecapeptide antigen corresponding to region 107-125(see Table 1). The poor yield of the nonadecapeptide was probably due to the inherent stability of the peptide-benzhydrylamine resin linkage and the inherent problem of cleaving this linkage when bulky amino

acids such as the valine residue in the nonadecapeptide are attached to the resin. The more acid labile 4-methylbenzhydrylamine resin was introduced to circumvent this problem(103). The yield of pure hexadecapeptide amide was 37% when the 4-methylbenzhydrylamine resin was utilized. This represented significant improvement compared to the 13% yield obtained for the nonadecapeptide amide synthesized on the standard benzhydrylamine resin.

The synthetic protocol for generating these peptide resins was basically similar to those procedures utilized for the synthesis of the 23 residue peptide of the C-terminus, with the exception that 4N HCl in dioxane was used to remove the Boc-protecting group for glutamine residues, rather than the typical TFA deprotection mixture. DMS was also added as a scavenger to this HCl mixture to prevent side reactions. The use of a strong acid such as HCl to deprotect glutamine residues reduces the chain terminating formation of pyroglutamyl peptides during the neutralization step (129). This side reaction in which the N-terminal glutamine residue intramolecularly cyclizes to generate a pyroglutamyl residue is catalyzed by weak acids, such as TFA, and even Boc-amino acids (103). This cyclization side reaction is most prevalent during the neutralization step, and replacement of HCl for TFA results in a marked improvement in the yield and homogeneity of the crude peptide. Furthermore, since this side reaction is

catalyzed by weak acids such as Boc-amino acids or HOBt, we employed reverse addition of DIPC and the Boc-amino acid (103), in the coupling step following the Gln residue. To reduce the dehydration side reaction in which the side chain amide forms the nitrile, glutamine and asparagine residues were incorporated by the HOBt/DIPC-accelerated active ester coupling procedure in DMF.

The peptide amides were cleaved, purified, and characterized as outlined for the 23 residue peptide, and were obtained in yields of 14% and 37 % for the nonadecapeptide amide and hexadecapeptide amide, respectively. Both peptide amides were at least 98 and 99% homogeneous as judged by gradient HPLC.

Once all the synthetic antigen peptides were characterized, a rabbit polyclonal antisera was generated against each of the peptides,(see experimental methods). The antisera for each of the peptides are currently being purified, and in the near future these antibodies will be utilized as site specific topological probes for the STE-2 receptor. The results of these studies should provide new insight into the spacial arrangement of these regions within the STE-2 receptor in its membrane-bound state.

B) Synthetic probes of the α-factor receptor

Introduction:

Sexual conjugation of haploid *a* and α cells in the yeast Saccharomyces cerevisiae is initiated through the reciprocal exchange of diffusible peptide pheromones. α-cells secrete an α-factor pheromone which targets *a*-cells, whereas *a*-cells secrete an *a*-factor pheromone which targets α-cells (35). The α-factor is a tridecapeptide, Trp-His-Trp-Leu-Gln-Leu- Lys-Pro-Gly-Gln-Pro-Met-Tyr, which specifically binds to the STE-2 receptor located on the surface of MAT*a* cells (57,58). The *a*-factor is a post-translationally modified dodecapeptide, Tyr-Ile-Ile-Lys-Gly-Val-Phe-Trp-Asp-Pro-Ala--Cys(S-farnesyl)OCH_3, which interacts with its STE-3 receptor found on the surface of Matα cells (92). Both pheromones trigger a similar set of physiological responses in their target cell, which ultimately results in sexual mating (39). Several studies have demonstrated quite elegantly that the mating process in S. cerevisiae represents an excellent model system to understand the mode of action of peptide hormones (21-29).

Both pheromones interact with cell surface receptors whose genes have been cloned and sequenced(21,22). The predicted protein sequences indicate that both receptors are

likely to span the membrane seven times(60). This similar structural motif closely resembles that of several mammalian hormone receptors(61-63). In addition, both receptors are thought to interact with G-proteins, which mediate signal transduction from receptor to effector. The genes coding for these G-proteins have also been cloned and sequenced, and the deduced protein sequences indicate that they are highly homologous to mammalian G-proteins(26,27). Given the wealth of biological, biochemical, genetic, and immunological information available on this yeast, significant insights on receptor-hormone interactions may soon be elucidated from this model system.

A primary goal in Dr. Naider's laboratory has been to localize the binding site of the α-factor receptor, and to discern the relationship between the structure of the α-factor and its activity. Important aspects of our approach are the synthesis of analogues that can be used to tag the receptor binding site, and the study of the active conformation of the pheromone. In the following section, we discuss synthetic strategies that are being developed to prepare probes of the **STE-2** receptor binding site, and to extend previous structure-activity relationships (SAR) for the α-factor (31,66). These studies provide insights into the structural requirements for binding of α-factor to its receptor, and form a basis for detailed investigation of the receptor utilizing biochemical procedures.

The short-term goal of this study was to determine the optimal placement of either a fluorescent, affinity, or "potentially radioactivatible tag" on the α-factor molecule, without significant loss of activity. The results of this study will aid in the long-term goal of designing an α-factor analog which can be crosslinked into the **STE-2** receptor by a photoactivatable group, and isolated through the use of one the above mentioned tags. In addition, these tagged α-factors can be used as screening reagents for **STE**-2 receptor mutants. Furthermore, the accessibility of the tagging group on the pheromone when α-factor is bound to its receptor can also be assessed, by using a probe which specifically recognizes the tagging group. This approach has been successfully applied to determine the size of the binding pocket for the formyl peptide receptor(130).

Previous results from this laboratory have indicated that both the *N*-terminal amino group of Trp^1, or the epsilon amino group of Lys^7 can be extended with rather large bulky groups, without dramatic loss in activity (45,66). Derivatization of the α- or ϵ-amino groups of the α-factor affords the biochemist direct routes for insertion of either a fluorescent group (fluorescein), an affinity group (biotin), or a potentially radioactivatible group such as β-(4-hydroxymethyl)propionate which can be subsequently radioiodinated with IODOBEADS to generate the Bolton-Hunter

group. Furthermore, the α-factor can be extended on the *N*-terminus by an additional lysine residue to generate a tetradecapeptide analog, without abolition of its activity (92). The epsilon amino group of this [Lys^{-1}]-α-factor can then be reacted as well with the above mentioned groups. The synthesis and biological activity for a series of α-factors modified at positions Lys^{-1}, or Trp^{1}, or Lys^{7} with either fluorescein, biotin, or β-(4-hydroxymethyl)propionate are reported.

Results:

Solid-phase peptide synthesis of these α-factor analogs was accomplished by using either a standard chloromethyl resin or the phenylacetamidomethyl(PAM) resin. The synthetic protocol for generating these α-factor analogs followed procedures similar to those described for the antigen peptides in the previous section.

Previously reported yields of 17% for the native α-factor and 3-11% for several of the extended analogs from this laboratory indicated that the synthetic protocol was less than optimal for generating these types of peptides (45). In order to improve upon the yield and homogeneity of the crude peptides, several significant changes in the synthetic protocol were made. Replacement of the methionine residue in position 12 of the pheromone with isosteric

norleucine not only resulted in a peptide with identical activity as the native pheromone, but also reduced side reactions, and improved the yield and homogeneity of the crude peptides. Furthermore, a marked improvement in the yield and homogeneity of the crude product was obtained, when 4N HCl in dioxane was utilized to remove the N^{α}-protecting Boc groups for glutamine residues (92). This deprotecting reagent minimizes the chain terminating side reaction which generates pyroglutamyl peptides. In fact, this inorganic acid is probably a better choice for deprotecting Boc-peptide resins due to its inability to acylate peptide chains. In contrast, TFA can acylate the growing peptide chain resulting in chain termination(131).

However, the current cost for HCl in dioxane is rather high. In addition, the DIEA•HCl formed during the neutralization step is insoluble in methylene chloride and requires that highly toxic solvents such as chloroform be used during the neutralization and subsequent washes to remove it. Due to these features, this deprotecting reagent becomes less attractive to be used in all the deprotection steps.

Another significant change in our synthetic protocol was the removal of the side-chain tosyl protecting group for histidine prior to High HF cleavage. Although Tam and Merrifield claimed this group to be quantitatively removed

in HF(104), our laboratory found incomplete deprotection for this residue in a number our peptides(92). Treatment of the peptide with HOBt in DMF prior to HF cleavage resulted in better yields and increased the homogeneity for the crude peptides. As a result of these changes in our synthetic protocol, we routinely obtain yields of 40-50% for pure α-factor. The presence of problematic residues such as tryptophan, histidine, and tyrosine in this peptide is probably a reason why even higher yields are not obtained. Displayed in Figure 6 are the gradient C_{18}-reversed phase HPLC for the tagged α-factor analogs, indicating that these peptides are highly homogeneous.

Since biotin has been shown to survive anhydrous HF(59), [Nle^{12}]-α-factor biotinylated on the α-amine or [Lys^{-1}, Nle^{12}]-α-factor biotinylated on the ε-amine of the N-terminal Lys were prepared by assembling the desired peptide on a chloromethylpolystyrene resin, and then reacting the appropriate amine group with biotin p-nitrophenyl ester. The side chain of the N-terminal Lys was protected with the FMOC group and deprotected with piperidine in DMF. Derivatized peptides were cleaved from the resin by anhydrous HF and the desired products were isolated by HPLC. Both the [N^{α}-Biotin-Trp^{1}, Nle^{12}] and [N^{ϵ}-Biotin-Lys^{-1},Nle^{12}] pheromones had the appropriate amino acid analyses and gave correct FAB-MS values(Table 2)

[N^{ϵ}-Biotinyl-Lys^{7}, Nle^{12}]-α-factor was prepared by assembling Boc-Trp(For)-His(Tos)-Trp(For)-Leu-Gln-Leu-Lys(FMOC)-Pro-Gly-Gln-Nle-Tyr(2-Br-Cbz)-PAM resin. The FMOC group was removed with piperidine in DMF, and biotin was incorporated via its *p*-nitrophenyl ester using 1-hydroxbenzotriazole as a catalyst. The formyl groups were removed from the derivatized resin with piperidine, and the Boc group removed by acidolysis. The biotinylated-peptide resin was cleaved by anhydrous HF, and purified by HPLC. For [N^{α}-Acetyl-Trp^{1}, Nle^{12}]-α-factor, the Boc group was removed from the above protected [Nle^{12}]-α-factor resin, the resin was treated with acetic anhydride, the FMOC and formyl groups were removed by piperidine, the Tos group was removed by HOBt, and the derivatized resin was subjected to High HF cleavage. The crude acetylated peptide was then purified by HPLC.

[N^{ϵ}-HPPA-Lys^{1}, Nle^{12}]-α-factor was prepared by first synthesizing FMOC-Lys(Boc)-Trp(For)-His(Tos)-Trp(For)-Leu-Gln-Leu-Lys(FMOC)-Pro-Gly-Gln-Nle-Tyr(2-Br-Cbz)-PAM resin. The Boc group was removed, and β-(4-hydroxyphenyl)propionyl incorporated via its succinimide ester. The protecting groups were removed and the derivatized peptide resin was cleaved by HF. Crude [N^{ϵ}-HPPA-Lys^{1}, Nle^{12}]-α-factor was then purified by HPLC. All of the above peptides gave correct FAB-MS values.

In contrast to both biotin and HPPA, fluorescein would not survive anhydrous HF. This molecule was incorporated into the α-factor by assembling the following reagent peptide,Trp(For)-His-Trp(For)-Leu-Gln-Leu-Lys(FMOC)-Pro-Gly-Gln-Nle-Tyr, in 90% yield. Both the FMOC and formyl groups survive High HF and the protected pheromone was derivatized with fluorescein on the α-amine subsequent to its removal from the resin(132). The N^{α}-fluoresceinated-peptide was then deprotected with piperidine. Although this method resulted in the desired product, incomplete removal of the formyl protecting group from one of the tryptophan residues occurred, as deduced from the FAB-mass spectra. It is believed that probably the formyl group on Trp^{1} was not completely removed. Hence two products were obtained after purification by HPLC, the desired [N^{α}-Fluorescein-Trp^{1}, Nle^{12}]-α-factor and the [N^{α}-Fluorescein-Trp^{1}(N^{1}-formyl), Nle^{12}]-α-factor. This resulted in a combined yield of 15%. All final peptides were >98% homogeneous as judged by reversed phase HPLC and gave one ninhydrin-positive spot on silica TLC plates(Table 2.).

The isolated acylated pheromones were assayed using a growth arrest assay on MATa cells (Table 3). Both a wild-type *S. cerevisiae* 2180a and two supersensitive strains *S. cerevisiae* RC629(*sst*1) and *S. cerevisiae* RC631(*sst*2) were used in the assays. The supersensitive strain (*sst*1) is highly responsive because it lacks a peptidase that

inactivates the pheromone(50). Furthermore, to measure directly whether these tagged-pheromones are interacting with the α-factor receptor, a temperature-sensitive mutant *S. cerevisiae* 50B(*ste2*^{ts}) was used to measure growth arrest at the permissive and the restrictive temperatures. At 24 °C, α-factor and the acylated pheromones arrested growth, but at the restrictive temperature of 34 °C, none of these peptides arrested growth(data not shown). As controls, the activities of [Nle^{12}]-α-factor and [Lys^{-1}, Nle^{12}]-α-factor were also measured. The activity of the pheromone with the additional Lys residue at the amine terminus was five-fold less active than that of the tridecapeptide when tested against the wild type *S. cerevisiae* 2180a, and is ten-fold less active against the *sst1* mutant. The [N$^{\alpha}$-Acetyl-Trp^{1}, Nle^{12}]-α-factor was identical to the tridecapeptide with both strains. The [N$^{\epsilon}$-HPPA-Lys^{-1}, Nle^{12}]-α-factor gave comparable activity to the [Lys^{-1}, Nle^{12}]-α-factor with wild type and the *sst1* strain. The [N$^{\alpha}$-Biotin-Trp^{1}, Nle^{12}] and [N$^{\epsilon}$-Biotin-Lys^{-1}, Nle^{12}] pheromones were five-fold less active than the α-factor with both above strains. In contrast, the [N$^{\epsilon}$-Biotin-Lys^{7}, Nle^{12}]-α-factor was ten-fold less active against the *sst1* mutant. This same trend was observed for the fluoresceinated probes, where [N$^{\alpha}$-Fluorescein-Trp^{1},Nle^{12}]- -α-factor was five fold less active than the α-factor with wild type and the *sst1* strain, where [N$^{\alpha}$-fluorescein-Trp^{1}(N^{1}-formyl),Nle^{12}] and [N$^{\epsilon}$-fluorescein-Lys^{7},Nle^{12}]-α-factor pheromones were

ten-fold less active against the *sst1* mutant. The [N^{ϵ}-Acetyl-Lys^{7}, Nle^{12}]-α-factor was five-fold less active than the α-factor against the wild type and the *sst1* strains.

Discussion:

This study shows that fluorescent, affinity, and potentially radioactive groups can be incorporated into the α-factor. Utilization of the proper side-chain protecting groups has also demonstrated that preferential acylation of either the α-amine of Trp^{1} or the ε-amine of Lys^{7} of the pheromone is readily achievable. In particular, the reagent peptide, Trp(For)-His-Trp(For)-Leu-Gln-Leu-Lys(FMOC)--Pro-Gly-Gln-Nle-Tyr, was most useful in synthesizing the fluoresceinated pheromone. This synthesis demonstrates that groups that are sensitive to solid-phase techniques, particularly the anhydrous HF cleavage step, can be readily incorporated into a peptide. Although the yield for this fluoresceinated peptide was low (5-15%), it is believed that this was probably due to steric hindrance by the bulky *N*-terminus of this sequence, as well as side reactions inherent with the phenolic OH in unprotected fluorescein.

Table 2. Chemical and physical properties of "tagged" α-factor analogs.

Peptide I, [Nle^{12}]-α-factor;

Peptide II, [N$^{\alpha}$-Acetyl-Trp^{1}, Nle^{12}]-α-factor;

Peptide III, [N$^{\alpha}$-Biotinyl-Trp^{1}, Nle^{12}]-α-factor;

Peptide IV, [N$^{\alpha}$-Fluoresceinyl-Trp^{1}, Nle^{12}]-α-factor;

Peptide V, [(N$^{\alpha}$-Fluoresceinyl, N^{1}-formyl)-Trp^{1}, Nle^{12}]-α-factor;

Peptide VI, [N$^{\epsilon}$-Biotinyl-Lys^{7}, Nle^{12}]-α-factor;

Peptide VII, [N$^{\epsilon}$-Biotionyl-Lys ^{7}, Nle^{12}]-α-factor;

Peptide VIII, [N$^{\epsilon}$-β(4-Hydroxyphenyl)propionyl-Lys ^{7}, Nle^{12}]-α-factor.

Table 2.

Chemical and physical properties of tagged α-factor analogs

Analysis	I	II	III	IV	V	VI	VII	VII
Amino-acid	----	----	1.81	----	----	----	1.88	
Gly	----	----	1.09	----	----	----	1.07	
His	----	----	0.79	----	----	----	0.88	
Leu	----	----	1.81	----	----	----	1.78	
Lys	----	----	0.89	----	----	----	1.67	
Nle	----	----	0.67	----	----	----	0.69	
Pro	----	----	2.01	----	----	----	2.01	
Tyr	----	----	1.00	----	----	----	1.00	
Yield(%)	40%	38%	16%	5%	10%	36%	18%	23%
R_f [illegible]	0.35	0.35	0.33	0.41	0.47	0.33	0.26	0.29
R_f [illegible]	0.53	0.55	0.52	0.78	0.76	0.55	0.47	0.53
K value[c]	7.69	11.2	9.71	11.66	18.12	10.28	7.65	9.71
[illegible]	-30.0	-43.0	-27.1	-31.7	-38.8	-17.5	-25.4	-41.2
[illegible]			[illegible]	[illegible]	[illegible]	[illegible]	[illegible]	[illegible]
[illegible]			[illegible]	[illegible]	[illegible]	[illegible]	[illegible]	[illegible]

[a] [illegible] system A [illegible] acetic acid-water-ethanol [illegible] [illegible] system B [illegible] acetic acid-water-pyridine [illegible]. [b] [illegible] values were determined using [illegible] on silica [illegible]. [c] K' values were determined on a µBondapak C18 column using a [illegible]% acetonitrile gradient over a [illegible] [illegible] buffer [illegible] and [illegible] gradient acetonitrile

Table 3. Biological activity for "tagged" α-factor analogs, utilizing Wild type strain *S. cerevisiae* 2180a, supersenstitive strain *S. cerevisiae* RC629 ( ) and RC631( ), and temperature sensitive strain *S. cerevisiae* 50B( ). The values listed are halo diameters in mm. The assay for 50B( ) was carried out at 24 °C. Control on 50B( ) at 37 °C was carried out, and all peptides were inactive under these conditions.

Peptide 1; [Nle]-α-factor;

Peptide 2; [N'-Fluoresceinyl-Trp , Nle]-α-factor;

Peptide 3; [N'-Fluoresceinyl-Trp , N -formyl, Nle]-α-factor;

Peptide 4; [N'-Biotinyl-Trp , Nle]-α-factor;

Peptide 5; [N'-Acetyl-Trp , Nle]-α-factor;

Peptide 6; [N'-Fluoresceinyl-Lys , Nle]-α-factor;

Peptide 7; [N'-Biotinyl-Lys , Nle]-α-factor;

Peptide 8; [N'-Acetyl-Lys , Nle]-α-factor;

Peptide 9; [Lys ,Nle]-α-factor;

Peptide 10; [N'-Biotinyl-Lys , Nle]-α-factor;

Peptide 11; [N'-3-(4-hydroxyphenyl)propionyl-Lys , Nle]-α-factor.

Table 3.

Halo assay using the wild type 2180a strain.

Peptide (µg/disk)	#1	#2	#3	#4	#5	#6	#7	#8	#9	#10	#11
10	18	11	11	13	18	12	15	15	13	12	13
5	16	12	10	12	14	12	12	12	10	9	10
1	12	0	0	0	11	0	0	0	0	0	0
0.5	0	0	0	0	0	0	0	0	0	0	0
0.1	0	0	0	0	0	0	0	0	0	0	0
0.05	0	0	0	0	0	0	0	0	0	0	0
0.01	0	0	0	0	0	0	0	0	0	0	0

Halo assay using the RC629( ) strain.

Peptide (mg disk)	#1	#2	#3	#4	#5	#6	#7	#8	#9	#10	#11
10	32	22	20	32	32	19	23	28	21	19	19
5	31	18	16	26	29	17	18	26	18	16	17
1	23	15	14	19	24	13	13	20	14	13	14
0.5	21	12	11	15	21	10	10	17	10	10	10
0.1	14	9	0	10	15	0	0	9	0	0	0
0.05	11	0	0	0	11	0	0	0	0	0	0
0.01	0	0	0	0	0	0	0	0	0	0	0

Halo assay using the RC611( ) strain.

Peptide (mg/disk)	#1	#2	#3	#4	#5	#6	#7	#8	#9	#10	#11
10	31	26	24	30	30	27	26	30	27	25	25
5	30	20	22	27	28	23	23	28	24	21	19
1	24	18	18	20	21	19	15	22	20	17	13
0.5	19	14	17	18	20	11	11	19	17	15	11
0.1	14	10	14	11	13	0	0	11	12	11	10
0.05	11	10	10	10	11	0	0	10	10	10	0
0.01	0	0	0	0	0	0	0	0	0	0	0

Halo assay using the 50R( ) strain.

Peptide (µg disk)	#1	#2	#3	#4	#5	#6	#7	#8	#9	#10	#11
10	22	14	13	15	22	17	16	19	15	15	18
5	19	12	11	11	17	13	14	16	12	12	14
1	12	10	11	11	14	10	10	11	0	10	10
0.5	10	0	10	0	10	0	0	0	0	0	0
0.1	0	0	0	0	0	0	0	0	0	0	0
0.05	0	0	0	0	0	0	0	0	0	0	0
0.01	0	0	0	0	0	0	0	0	0	0	0

Figure 6. Gradient C_{18}-reversed phase HPLC for "tagged" α-factor analogs after purification.

Peptide A; [Nle^{12}]-α-factor;

Peptide B; [N$^{\alpha}$-Acetyl-Trp^{1}, Nle^{12}]-α-factor;

Peptide C; [N$^{\alpha}$-Biotinyl-Trp^{1}, Nle^{12}]-α-factor;

Peptide D; [N$^{\alpha}$-Fluoresceinyl-Trp^{1}, Nle^{12}]-α-factor;

Peptide E; [N$^{\alpha}$-Fluoresceinyl-Trp^{1}, N$^{\alpha}$-formyl,
Nle^{12}]-α-factor;

Peptide F; [N$^{\alpha}$-Biotinyl-Lys^{7}, Nle^{12}]-α-factor;

Peptide G; [N$^{\alpha}$-Biotinyl-Lys^{7}, Nle^{12}]-α-factor;

Peptide H; [N$^{\alpha}$-3(4-hydroxyphenyl)propionyl-Lys^{7},
Nle^{12}]-α-factor.

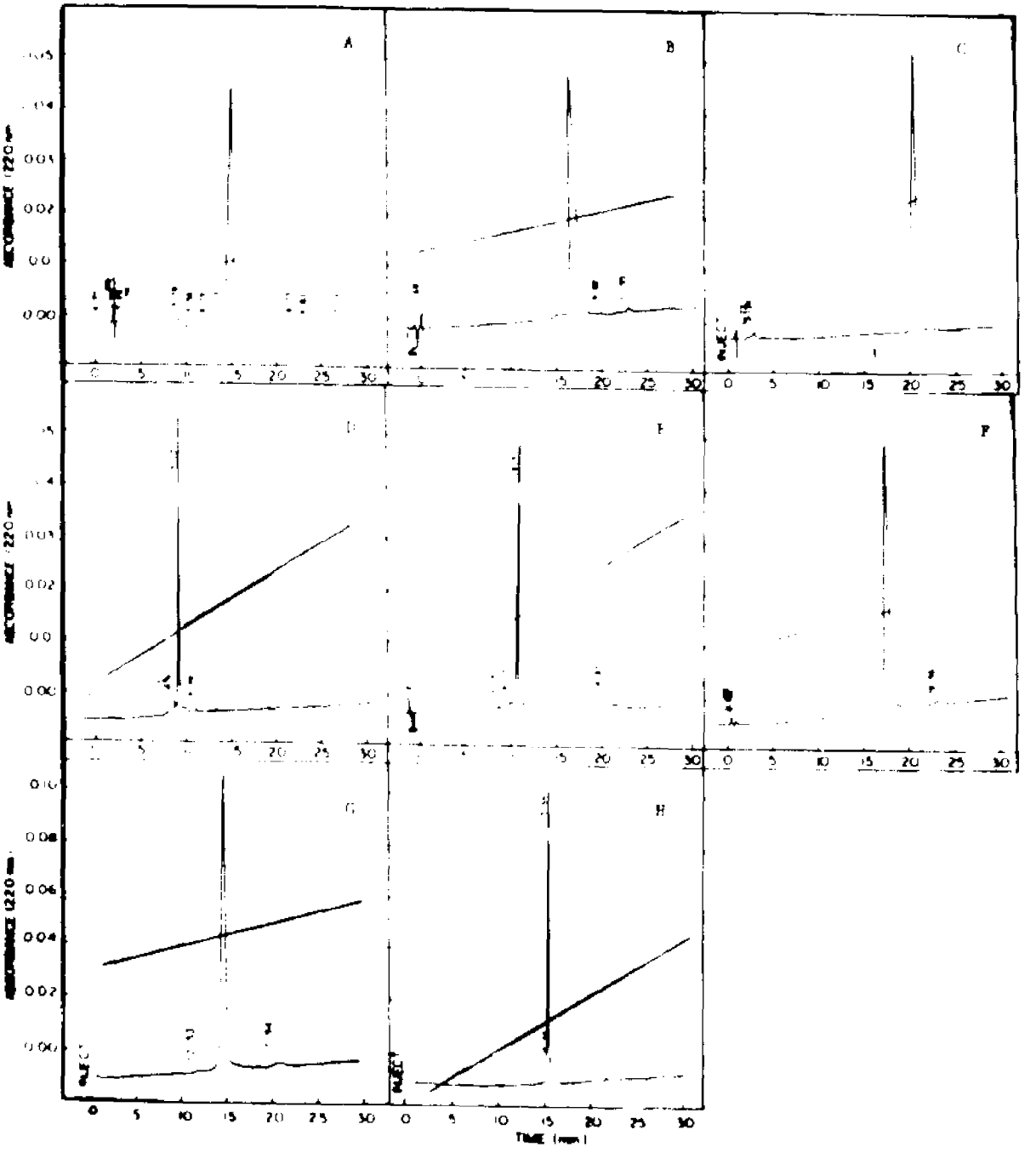
A
B
C
D
E
F
G
H
TIME (min)

Figure 7. 200 MHz proton NMR of
{N$^{\alpha}$-Biotinyl-Trp^{7}, Nle^{8}}-α-factor in DMSO-d_6 at 25 °C.

Biotin =

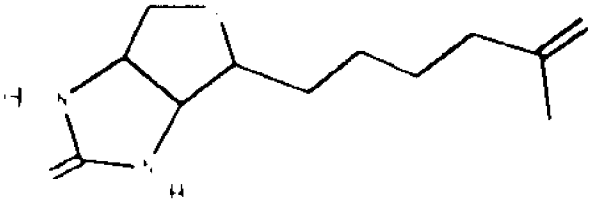

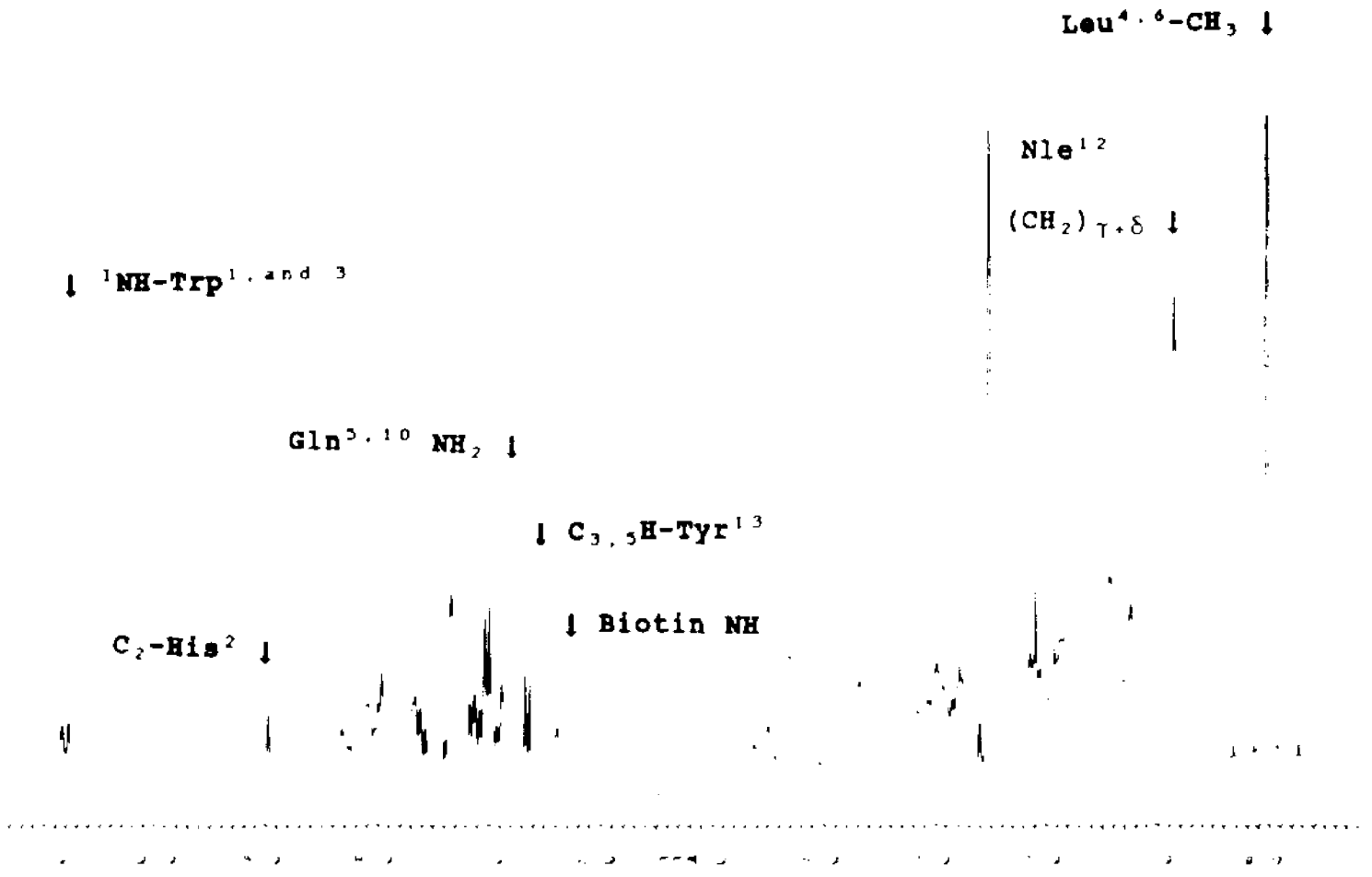
Leu4,6-CH3
Nle12
(CH2)γ,δ
1NH-Trp1,and 3
Gln5,10 NH2
C3,5H-Tyr13
Biotin NH
C2-His2

Figure 8. 200 MHz proton NMR of [N'-Biotinyl-Lys [5], Nle[13]]-α-factor in DMSO-d_6 at 25 °C.

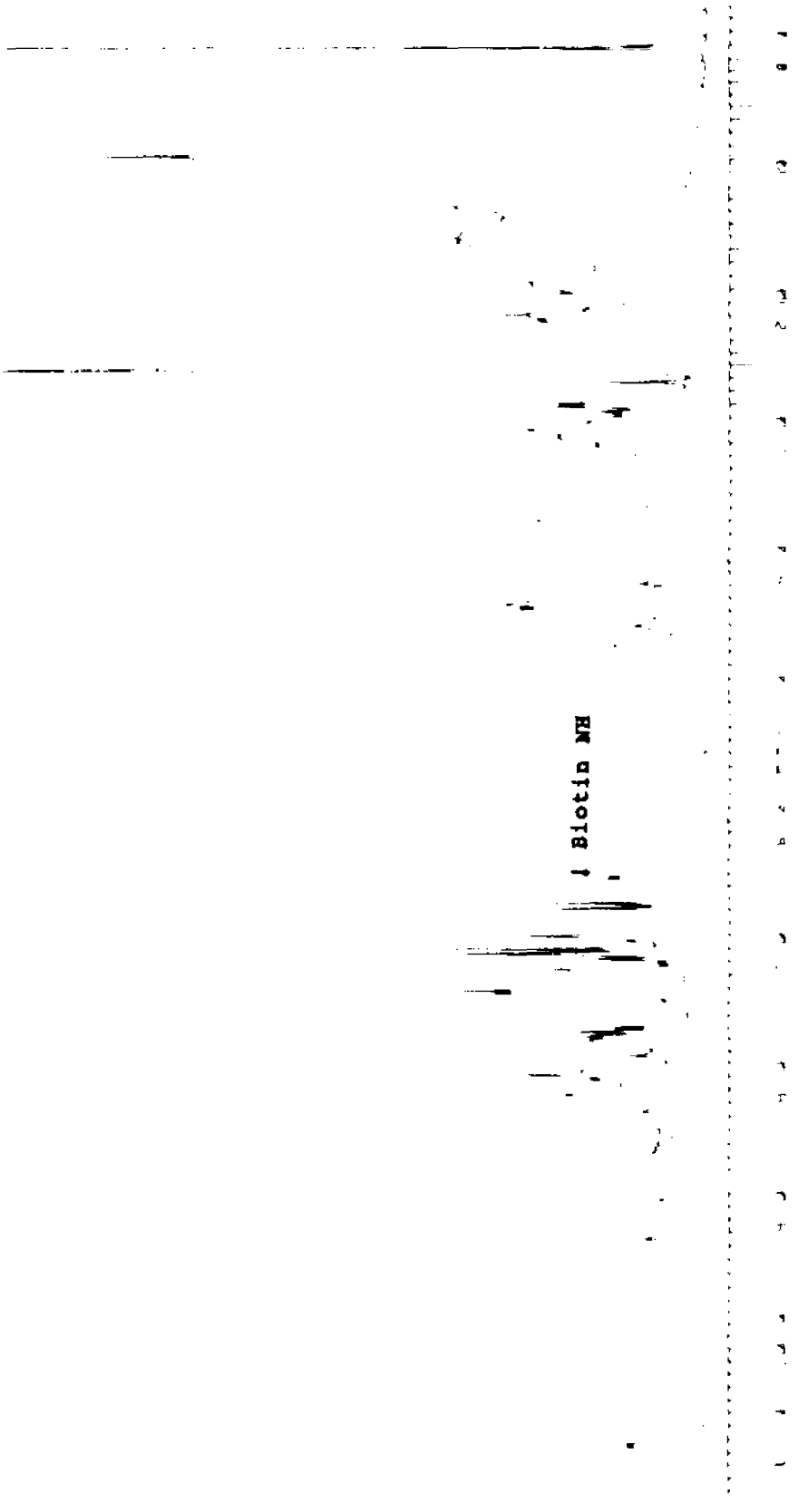
Biotin MM

Figure 9. 200 MHz proton NMR of [N^{α}-Fluoresceinyl-Trp^{1}, Nle^{12}]-α-factor in DMSO-d_6 at 25 °C.

Fluoresceinyl =

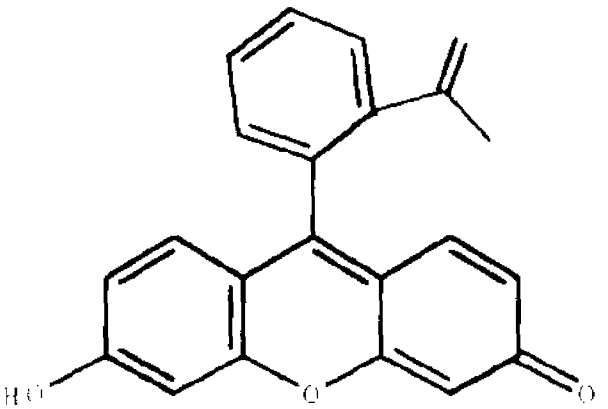

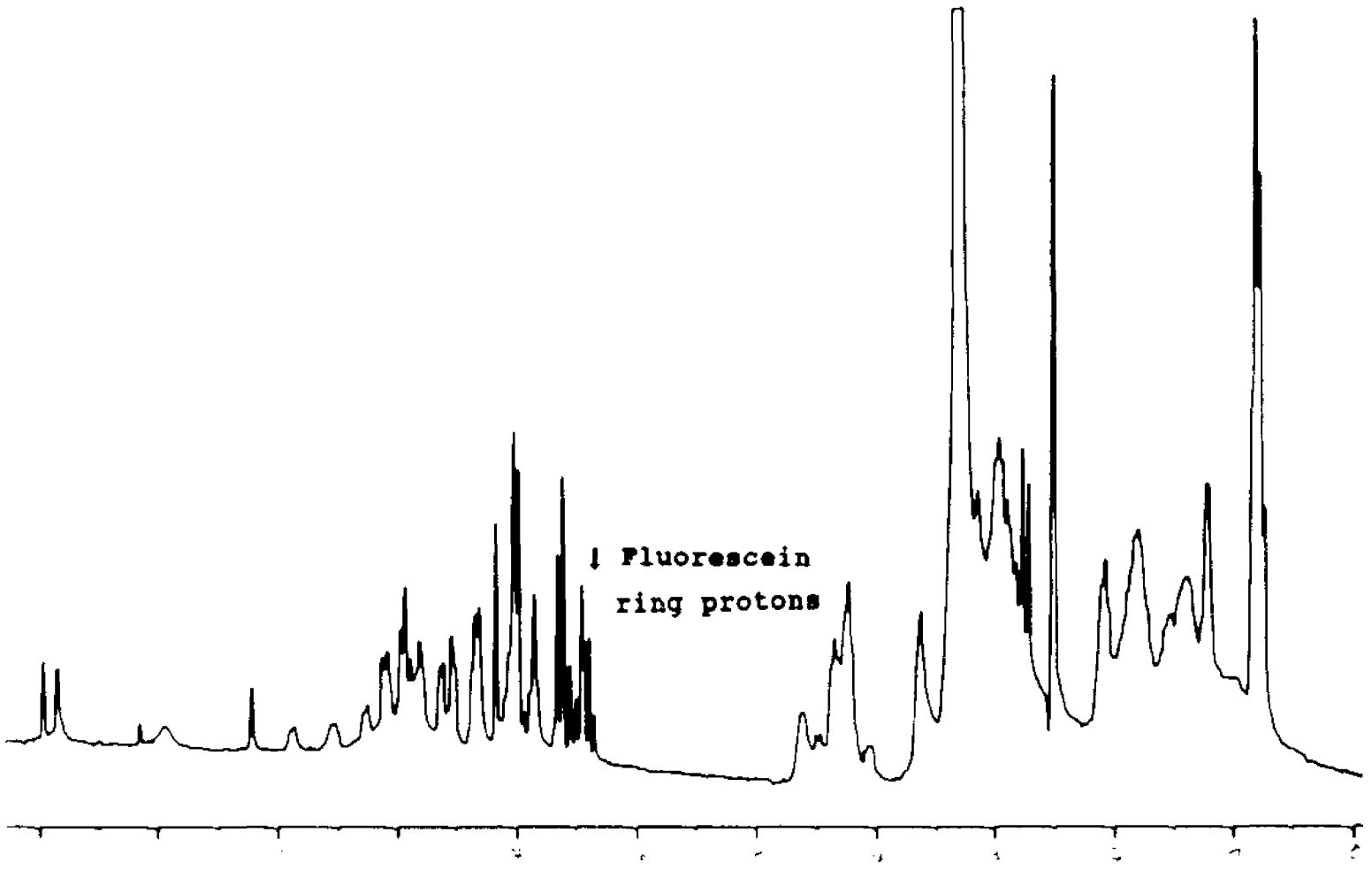
Fluorescein
ring protons

In the present study, yields of 40% for the α-factor and 23-38% for derivatives synthesized on the PAM resin are reported. In contrast, derivatives generated on the standard chloromethyl resin resulted in yields of 16-18%. Even the lowest of these yields represents a significant improvement to those achieved in earlier syntheses of the α-factor(45).

As shown in Table 2, all of the tagged α-factor analogs gave excellent FAB-MS values, which supported their structure. In addition, the results of the amino-acid analysis for the [N^{α}-Biotin-Trp^{1}, Nle^{12}] and [N^{ϵ}-Biotin-Lys^{1}, Nle^{12}] pheromones further supported the proper structure for these peptides. Although low values were obtained in the amino acid analysis for the norleucine residue in these peptides, it is believed these values do not truly reflect the norleucine content in these analogs. This is supported by the excellent FAB-MS values obtained, as well as 200-MHz ^{1}H-NMR spectroscopy performed on these peptides. The high resolution one dimensional spectra for two of the biotinylated-α-factor peptides are shown in Figures 7 and 8. These spectra not only indicated the proper structure for these peptides, but also confirmed the presence of tryptophan. The characteristic resonances for the indole NH's of Trp^{1} and Trp^{3}(10.7-10.9 ppm) gave the expected intergration ratios when compared with the $C_{2,4}$H-protons of Tyr^{13}(6.6-6.7 ppm). Support for the presence of biotin in Figure 7 and 8 is derived by its amide

signal at 6.4 ppm. Other characteristic resonances observed are the methyls of $Leu^{4,6}$ at 0.85 ppm; the side-chain protons of Nle^{12} at 1.25 ppm; the C_2-proton of His^2at 8.98 ppm; and the side-chain amides of $Gln^{5,10}$ at 6.89 ppm.

Characterization of the purified peptides by HPLC and TLC indicated that most of the peptides were greater than 99% homogeneous(Figure 6). Displayed in Figure 9 is the proton NMR spectrum for the fluoresceinated pheromone. This spectrum also supported the proposed structure for the fluoresceinated analog. Similar chemical shifts were observed for the characteristic resonances for the indole NH's of Trp^1 and Trp^3(10.7-10.9 ppm) which gave the expected intergration ratios when compared with the $C_{2,4}$H-protons of Tyr^{13}(6.6-6.7 ppm). Support for the presence of fluorescein in Figure 9 is derived by its ring proton signals at 6.55-6.30 ppm. Other characteristic resonances observed are the methyls of $Leu^{4,6}$ at 0.85 ppm; the side-chain protons of Nle^{12} at 1.25 ppm; the C_2-proton of His^2at 9.2 ppm; and the side-chain amides of $Gln^{5,10}$ at 7.91 ppm.

The biological data on these tagged α-factor analogs are extremely interesting. All of the peptides retained significant activity toward the wild type strain 2180a. In addition all of the peptides directly interact with the α-factor receptor, as judged by the results with the temperature sensitive mutant 50B(*ste2*^{ts}). In order to judge

the relative efficacy of these modified α-factor analogs towards the STE-2 receptor, comparisons were made between the activity of one analog versus the activity of all other modified peptides in the *sst1* strain. To determine the relative affinity of a particular analog towards the BAR1 protease, the activity of one particular analog was compared against the wild type and the activity of the same peptide against the *sst1* strain. As shown in Table 3, the [N^{α}-Acetyl-Trp^{1}, Nle^{12}]-α-factor was consistently as active as the tridecapeptide against all strains tested. These results clearly indicate that the charged ammonium group on the *N*-terminal tryptophan is not required for activity. Furthermore, the *N*-terminus of the pheromone can be extended with even larger groups without significant loss in activity. This is supported by fact that the [N^{α}-fluorescein-Trp^{1}, Nle^{12}] and the [N^{α}-fluorescein-Trp^{1}(N^{1}-formyl), Nle^{12}]-α-factors, as well as the [N^{α}-biotin-Trp^{1}, Nle^{12}] pheromone were only five-fold less active than the [Nle^{12}]-α-factor when tested against wild type 2180a, supersensitive RC629(*sst1*), and temperature sensitive 50B(*ste2*^{ts}) strains, whereas these analogs were equally active against the supersensitive RC631(*sst2*). This conclusion is further supported by the five-fold reduction in activity of [N^{ϵ}-HPPA-Lys^{-1}, Nle^{12}], [Lys^{-1}, Nle^{12}] and [N^{ϵ}-Biotin-Lys^{-1}, Nle^{12}] pheromones when tested against wild type 2180a, and 50B(*ste2*^{ts}) strains. These pheromones were equally active when tested against RC631(*sst2*). In contrast,

all of the tetradecapeptides were approximately 10-fold less active against RC629(*sst1*). These results further support previous studies which indicate that the α-factor receptor may have an extended binding site since N^{α}-terminally extended analogs are still significantly active. Furthermore, the ε-amine of the *N*-terminal lysine^{-1} analog can also be derivatized without any further loss in activity, since the Lys^{-1} analog is equally active as the acylated-Lys^{-1}-analogs in the *sst1* strain. Moreover, the ammonium groups of the *N*-terminal lysine^{-1} reduce the activity 5 fold in the *sst1* mutant, when compared against the acylated-Trp^{1} analogs. These results suggest that a large bulky group on the N^{α}-terminus of the pheromone is not responsible for the observed five-fold drop in activity exhibited by the Lys^{-1} analog , but that the charges on the N-terminal lysine may be involved. However, activity does not necessarily correlate with binding, and direct binding assays should be performed before a valid assessment can be made. All of the tetradecapeptide analogs are as active as the acylated Trp^{1} analogs against the wild type strain, but are less active in the *sst1* strain. This suggests that the tetradecapeptide(Lys^{-1}) analogs are not degraded as well as the tridecapeptide analogs by the BAR1 protease responsible for the *sst1* mutation. If the tridecapeptides were cleaved more readily than the tetradecapeptides, this would result in a higher activity for the tetradecapeptide analogs in the wild type 2180a strain. When the BAR1 protease is absent,

the actual relative efficacy towards STE-2 may be exhibited by peptides. Hence, a lower activity should be observed for the tetradecapeptides in this strain.

In conclusion, this study has demonstrated the successful incorporation of either a fluorescent, affinity, or a potential radioactive tag into the α-factor on either the α-amine of Trp^1 or the ε-amine of Lys^7. All of these tagged pheromones are approximately five to ten fold less active than the tridecapeptide when tested against RC629(*sst1*), suggesting these analogs have comparable affinity toward the α-factor receptor. From a synthetic standpoint, the [N^{α}-Biotin-Trp^1, Nle^{12}]-α-factor appears the best candidate for tagging the pheromone, since this analog is one of the better agonists when tested against the *sst1* mutant, and that this group can be easily incorporated into the α-factor. However, until the accessibility of the biotin group can be determined through the binding of the protein avidin to it, no definitive decision can be made. The [N^{α}-fluorescein-Trp^1, Nle^{12}]-α-factor is also a good candidate for tagging the α-factor; however, incorporation of this group into the α-factor is significantly more difficult.

Since both the α-amine of Trp^1 or the ε-amine of Lys^7 can be modified without significant loss of activity, it would appear that these groups can be used to incorporate

both a photoactivatable group and a tag for detection. However, a dibiotinylated pheromone should be synthesized to test the validity of this approach. It is reasonable to conclude that our results suggest that the *N*-terminus and the side-chain ϵ-amine of Lys^{7} may be pointing away from the contact points between the pheromone and the receptor.

Extension of the *N*-terminus of the pheromone by an additional lysine residue results in a ten-fold reduction in activity, further modification of the ϵ-amine of this *N*-terminal $lysine^{-1}$ analog results in no further decrease in activity. Hence it appears that incorporation of a lysine residue on the *N*-terminus is not advantageous for pheromone binding. In contrast, neutral additions appear to be better tolerated at this position in the pheromone since the acetyl(V), biotin(IV), and fluoresceinated peptides(III) are all ten-fold more active in the *sst1* strain than the Lys^{-1} analogs(see Table 3).

The successful synthesis of fluoresceinated and biotinylated pheromones with high biological activity indicates that biochemical procedures may now be readily applied to begin to elucidate structural requirements for binding of α-factor to its receptor, and forms a basis for detailed investigation of the receptor binding site.

IV) Conformational analysis on cyclo^{7,10}[Nle^{12}]-α-factor in DMSO at 25 °C.

Conformational analysis of cyclo^{7,10}[Nle^{12}]-α-factor in DMSO.

Introduction:

The tridecapeptide α-factor, a yeast pheromone of *Saccharomyces cerevisiae*, is a member of a larger family of compounds classified as linear peptide hormones. The chemical structure of these molecules contains the information necessary for interaction with their cognate receptors. Although the relatively small size of these peptides suggest significant conformational flexibility in solution, a number of conformational analyses have been performed on these messengers with the goal of elucidating biologically significant structural features. The aim of these studies has been to relate the solution state conformation of these molecules to their biologically active state. The results of these types of studies will not only lead to a better understanding on how the peptide hormone elicits its biological activity, but also aid in the design of analogs which have antagonistic or agonistic properties.

This approach has been successfully applied to leutinizing hormone releasing hormone(LHRH), which may be an evolutionary ancestor to the α-factor(80), as well as human growth hormone(2),the enkephalins(4), the tachykinins(30),

somatostatin(3), bombesin(133), gramicidin A(134), peptide T(135), as well as a plethora of other molecules.

Two techniques have been applied to determine the conformation of a peptide hormone. These are circular dichroism (CD) and nuclear magnetic resonance (NMR). Both spectroscopic approaches take advantage of the interaction of energy with matter. In circular dichroism, the interaction of a peptide hormone with circularly polarized light can elucidate structural features that are present in the molecule. These structural features are usually detected as characteristic bands in a CD profile. For example, strong negative absorption bands at 210-215 nm are usually indicative of an α-helical and/or β-sheet type structure, whereas in a random-coiled structure, a positive absorption band is observed at these wavelengths. Furthermore, positive absorption bands at 190-195 nm are characteristic of helical and sheet structures. In contrast, flexible random-coiled structures have negative bands at these wavelengths(136). Most significantly, pure α, β and coiled structures may be discriminated, and methods exist to calculate the % helix, coil, and sheet based on the CD pattern(137).

Although CD is a powerful tool in determining structural characteristics for a peptide, one major drawback of this technique results from the inability to determine where in the primary sequence the structural element is located. In general, Chou-Fasman rules are applied to find the most probable position that a predetermined structural feature may be located within the primary sequence(76). This approach is most correctly applied to globular proteins and long polypeptide chains. In contrast, not only can certain NMR parameters elucidate structural characteristics for the molecule under investigation, but also where in the primary sequence this structural feature is located. Notably, the angular dependence of the vicinal coupling constant can elucidate a relative angle between the two nuclei involved(138). Secondary structure dependent chemical shifts can help refine an existing model(139). Temperature-dependent amide chemical shift coefficients can elucidate groups involved in stabilizing hydrogen-bond interactions(158). Most importantly, the NOE can yield a qualitative description on the spatial proximity of groups relative to one another(140,141), and also be quantitatively analyzed to determine relative distances between the interacting nuclei(142-144).

With the advent of affordable high field FT-NMR spectrometers, as well as recent advances in two-dimensional and multidimensional techniques, NMR has now appeared to

become a popular technique to elucidate structural characteristics for a molecule. This is evidenced by the increasing number of published reports using NMR for structural characterization that appear in the literature almost daily.

Focusing our attention on the α-factor, a number of NMR studies have been performed on this tridecapeptide and several analogs in either DMSO, H_2O, or lipid vesicles. Miyazawa and Higashijima proposed that the α-factor folds in such a manner as to form 3 β-turns in aqueous solution (87). Several years later, the same group refined their model and suggested that the *N*-terminus forms an α-helical structure, and that the central and *C*-terminal end form β-turns in aqueous solution (84). A year later, Wakamatsu and the above group postulated that the α-factor forms an *N*-terminal α-helical structure and extended structure throughout the remainder of the peptide, when α-factor is bound to lipid vesicles (88). In 1987, all of the above reseachers refined their model, and suggested a 3_{10}-helical structure for the *N*-terminus and an extended structure for the central and *C*-terminal portions of this peptide in lipid (86). In 1989, Jelicks et al.(89) proposed a compact *N*-terminal structure and a centrally located βII turn for α-factor in lipid vesicles. In the same year, Naider et al.(91), proposed

that the most prominent structural feature for this peptide is a centrally located βII turn spanning residues 7-10 in both aqueous and lipid environments.

One major shortcoming in all of the above reports appears to be the flexible nature of the α-factor peptide. This conformational flexibility leads to a wide distribution of allowable conformers and it makes it quite difficult to extend biophysical analyses to the biologically active state. Interestingly, the most common structural feature in all the above reports appears to be a centrally located β-turn.

In order to determine the biological significance for a centrally located turn, Xue et al.(92) synthesized a cyclic analog of the α-factor. This cyclic analog was generated by forming a covalent amide bond linkage between the side-chains of the Lys^{7} and the Glu^{10} residues in this peptide causing a bend to be maintained in the center of the pheromone spanning residues 7-10. Only a modest reduction in biological activity was observed for the cyclic analog, which was one-fourth to one-twentieth as active as the linear α-factor depending upon the tester strain used.

The above report provides a major step forward in understanding the molecular basis for activity elicited by the α-factor molecule. As stated earlier, the results of

the structure/activity(SAR) type studies indicated that both the His^{2} and Tyr^{13} residues are critically important for activity in the α-factor. Cyclization may bring the ends of this peptide closer together and may aid the formation of the bioactive structure. Furthermore, the proposed turn has been correlated with biological activity; substitution in position 9 by amino-acids which would stabilize a type II β-turn are active, whereas destabilizing amino-acids are inactive. (Jelicks et al.(90). Moreover, the relatively high activity of this cyclic agonist supports a turn structure spanning residues Lys^{7}-Pro^{8}-Gly^{9}-Gln^{10} in the α-factor, as deduced from the earlier NMR studies.

The most pertinent consequence of the cyclic α-factor analog for the present study is that the conformational flexibility of this agonist has been significantly restricted. This should reduce the distribution of allowable conformations that this peptide can assume. Since the activity of this cyclic agonist is in the same range as the native pheromone, the $cyclo^{7,10}$ [Nle^{12}] α-factor should be an excellent model to determine structural characteristics that may be present in the more flexible native α-factor. In the following section, a detailed conformational analysis on the $cyclo^{7,10}$ [Nle^{12}] α-factor is presented. The goal of this study is to elucidate structural characteristics for the solution-state

conformation of this agonist in DMSO, which hopefully may be extendable to the biologically active state for this pheromone.

Results:

Displayed in Figure 10 is the high-resolution spectrum of cyclo^{7,10},[Nle^{12}]-α-factor in DMSO-d_6. Peak assignment of the proton NMR spectrum for cyclo^{7,10} [Nle^{12}] α-factor was accomplished by a combination of two-dimensional homonuclear DQF-phase sensitive-COSY, nine Relayed-COSY's, NOESY, and ROESY experiments. In a typical 2D-COSY experiment, diagonal peaks correspond to resonances found in the 1-D spectrum. In contrast, any off-diagonal peak correlates the two perpendicularly related diagonal peaks as neighbors which are separated by either two or three bonds. The results of this type of experiment allows one to assign protons in a spin-system to a particular residue. The choice of a double quantum filter for the COSY experiment not only reduces the intensity of cross-peaks from geminally coupled-protons, allowing smaller peaks to be observed near the diagonal, but also removes the large dispersive tails of diagonal peaks since both the cross-peak and diagonal peaks are in-phase absorptive(145,158,159). In addition,

Figure 10. 400 MHz proton spectrum of cyclo^{1,5}[Nle^{12}]-α-factor in DMSO-d_6 at 25 °C. Peptide concentration was 5 mg/ 0.5 ml. Illustrated below is cyclo^{1,5}[Nle^{12}]-α-factor.

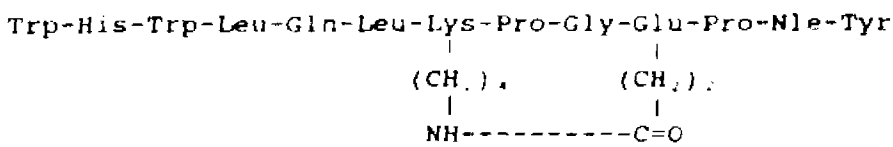

acquisition of the COSY experiment in the phase-sensitive mode allows the multiplicity of the cross-peak to be determined. The multiplicity of the cross-peak reflects the number of coupling partners involved in the spin-system under investigation. In general, the greater the number of coupling partners involved, the more complex is the multiplicity pattern observed for the cross-peak. This aids in making peak assignments for particular residues found within the primary sequence (146). For example, in an ABX spin-system such as a glycine residue, one observes two "square" arrays in which the upper-left corner and lower-right corner of each array appear as negative crosspeaks, whereas the lower-left and upper-right corners of each array appear as positive crosspeaks, for each of the α-protons. This multiplicity pattern provides a "finger print" for glycine-residues within a peptide or protein. Different multiplicity patterns are observed for other types of residues in the same molecule. This type of experiment is most useful in highly crowded regions of the spectrum. However DQF COSY experiment also has drawbacks. Due to the antiphase nature of the crosspeaks, cancellation of crosspeak signals can result when two crosspeaks overlap, or when the line widths of diagonal peaks equal their coupling constants. In such cases, a TOCSY (total correlation spectroscopy) experiment can be far superior(147,148).

The 400-MHz one-dimensional proton spectrum for the amide region of cyclo ^{7,10} [Nle^{12}] α-factor is displayed in Figure 11, and the corresponding 400-MHz DQF-phase sensitive COSY in Figure 12. Two characteristic triplets can be observed in Figure 11, which are attributable to the amide proton of Gly^{9} (7.73 ppm), and to the side chain cyclic amide linkage between the Lys^{7} and Glu^{10} residues (7.57 ppm).

As can be seen in Figure 12, the NH-αCH,(7.73, 3.66),(7.73, 3.60) crosspeaks for the Gly^{9} residue exhibit a typical AA'X multiplicity pattern. The Lys^{7}ε-NH to Lys^{7}ε-CH_2 crosspeaks (7.54, 3.23),(7.54, 2.93) assign the ε-protons of Lys^{7} to a region where only the β-protons of aromatic residues are located. If these two triplets were due to aromatic residues one should not observe any other crosspeak from this region. However, as depicted in Figure 13, a very weak crosspeak (2.93, 1.43) which correlates an $^{\epsilon}$CH-proton of Lys^{7} to its δ-protons was observed. This crosspeak is symmetrical about the diagonal at lower contours, and is consistent with the expected multiplicity patterns for these residues. Moreover, the results of the 400-MHz NOESY experiment are consistent with the above assignments. Specifically, strong sequential connectivities αCH_i-NH_{i+1} were observed for both of these triplets. As illustrated in Figure 14, both the α and δ protons of the

Figure 11. Amide region of 400-MHz proton spectrum of cyclo^{1,6}[Nle^{12}]-α-factor in DMSO-$_{d_6}$ at 25 °C. Peptide concentration was 5 mg/ 0.5 ml. Characteristic triplets of Gly^{9} and Lys^{7} are indicated by arrows.

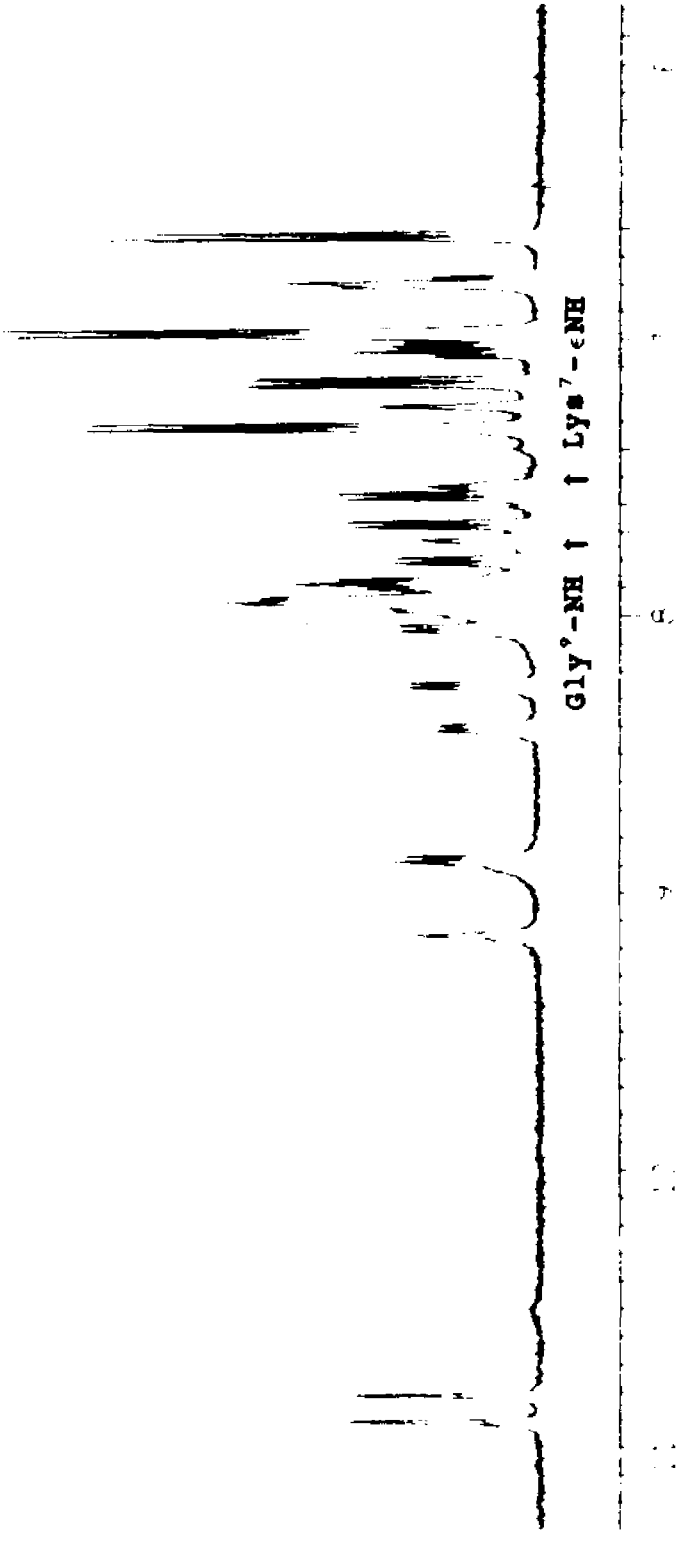
Gly⁹-NH
Lys⁷-εNH

Figure 12. 400 MHz DQF-phase sensitive COSY of cyclo^{7,10}[Nle^{12}]-α-factor in DMSO-d_6 at 25 °C. Peptide concentration was 5 mg/ 0.5 ml. Displayed is characteristic AA'X multiplicity pattern for Gly^{9}.

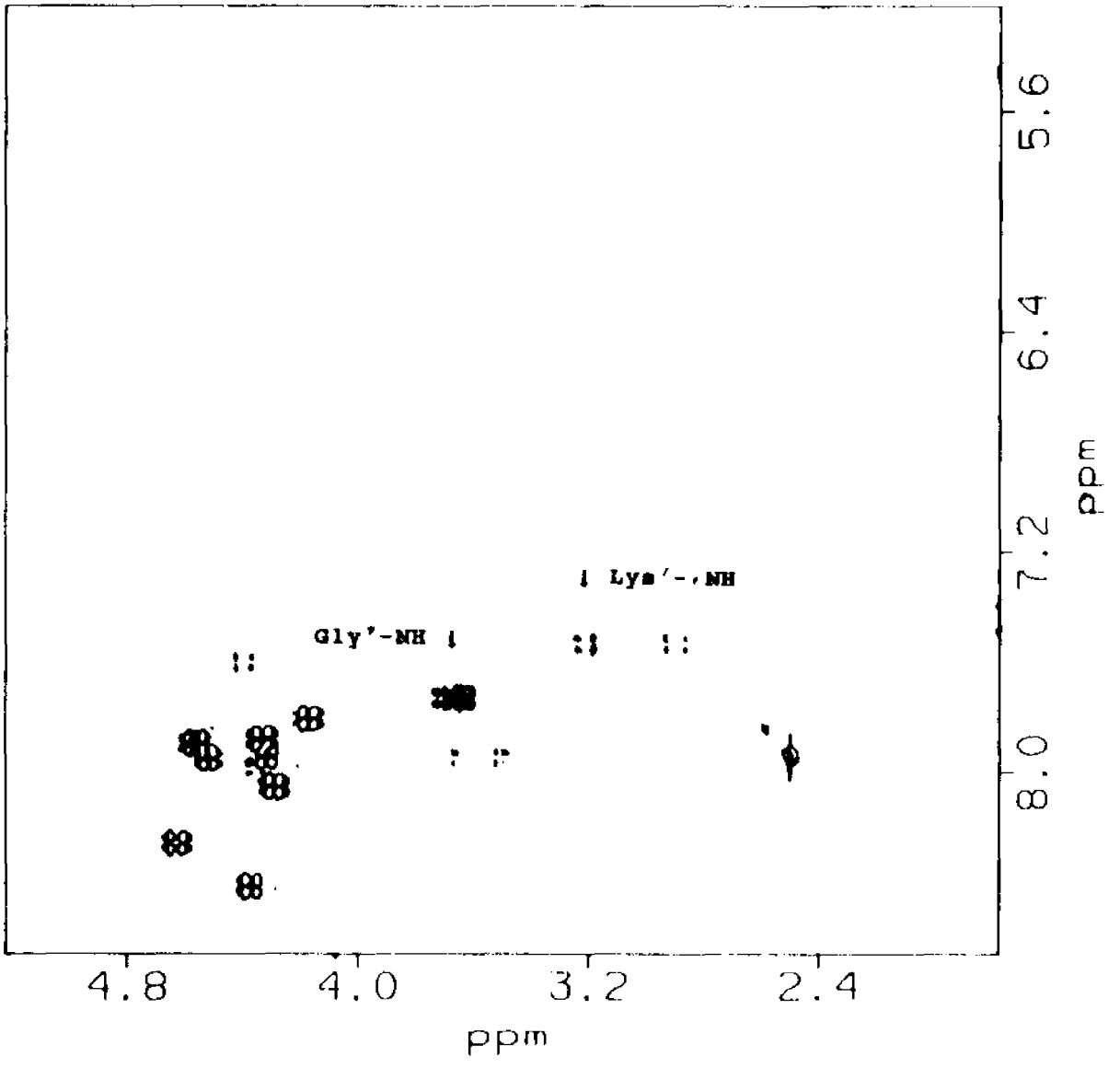
Lysε'-NH
Gly'-NH
4.8
4.0
3.2
2.4
ppm
5.6
6.4
7.2
8.0
ppm

Figure 13. 400-MHz DQF-phase sensitive COSY of cyclo^{7,10}[Nle^{7,10}]-α-factor in DMSO-$_{d_6}$ at 25 °C. Peptide concentration was 5 mg/ 0.5 ml. Displayed is weak COSY crosspeak for ϵNH to ϵCH of Lys^{7}.

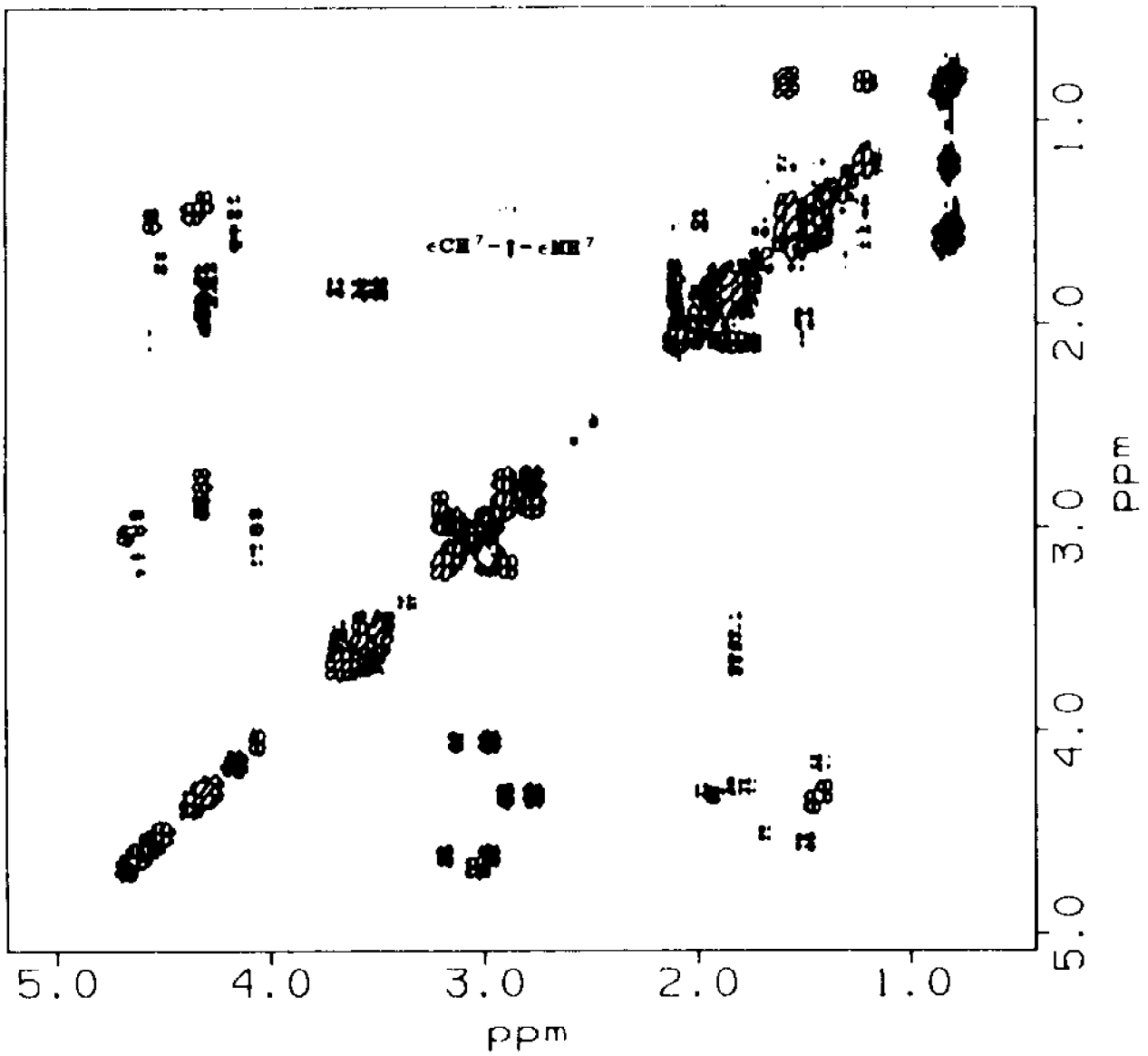
5.0
4.0
3.0
2.0
1.0
ppm
5.0
4.0
3.0
2.0
1.0
ppm

Figure 14. 400-MHz 400-msec NOESY of cyclo^{7,10}[Nle^{12}]-α-factor in DMSO-$_{d_6}$ at 25 °C. Peptide concentration was 5 mg/ 0.5 ml. Displayed are sequential αCH^{n}-NH^{n+1} NOE's for Gly^{9} and εCH^{11}- εNH^{11} for Lys^{11}.

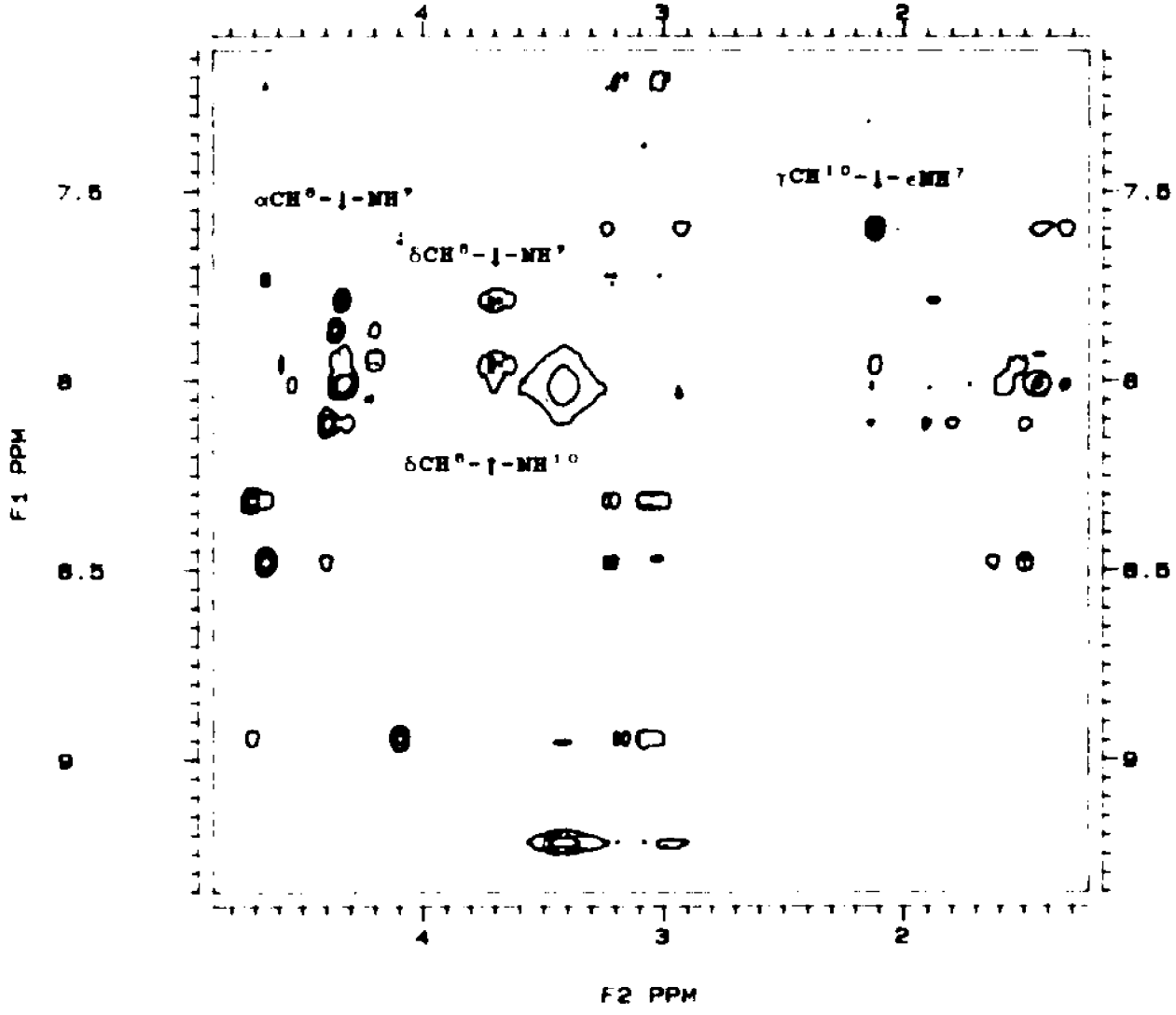
4
3
2
7.5
8
8.5
9
αCH°-↓-NH'
δCH°-↓-NH'
γCH'°-↓-εNH'
δCH°-↓-NH'°
F1 PPM
F2 PPM

Table 4. Peak assignments for 400 MHz spectrum of cyclo^{7,10}[Nle^{8}]-α-factor in DMSO-d_6 at 25 °C. Peptide concentration was 5 mg/ 0.5 ml.

Table 4

Peak assignments for cyclo[-Trp[1]-His[2]-Trp[3]-Leu[4]-Gln[5]-Leu[6]-Lys[7]-Pro[8]-Gly[9]-Glu[10]-Pro[11]-Nle[12]-Tyr[13]-]-α-factor

Residue	NH	αCH	βCH	γCH	δCH	Other
Trp[1]	7.95	4.06	3.14 2.98			N^1- 10.92 C_2- 7.15 C_4- 7.57 C_5- 6.80 C_6- 7.00 C_7- 7.32
His[2]	8.88	4.68	3.04			C_2- 8.92 C_4- 7.32
Trp[3]	8.26	4.63	3.19 2.98			N^1- 10.82 C_2- 7.17 C_4- 7.68 C_5, C_6 7.00 C_7- 7.32
Leu[4]	8.41	4.37	1.46	1.59	0.84	
Gln[5]	8.05	4.28	1.87 1.75	2.11		NH_2- 7.25 6.80
Leu[6]	7.95	4.31	1.41	1.56	0.82	
Lys[7]	7.98	4.51	1.71 1.54	1.28-	1.43-	$^{\varepsilon}CH_2$- 3.23 2.93 NH_2- 7.54
Pro[8]		4.30	1.96 1.92	1.82	3.69 3.54	
Gly[9]	7.73	3.66 3.60				
Glu[10]	7.89	4.56	1.44 1.38	2.09 1.97		
Pro[11]		4.33	1.96 1.92	1.83	3.60 3.47	
Nle[12]	7.82	4.16	1.58 1.44	1.21	1.21	$^{\varepsilon}CH_3$- 0.87
Tyr[13]	7.87	4.32	2.93 2.78			C_{δ}, 6.98 C_{ε}, 6.62 OH 9.20

- Due to severe overlap, this resonance can't be assigned unequivocally.

Pro^{8} residue have strong NOE connectivities to the $^{\alpha}$NH of Gly^{9}. In addition, a strong sequential NOE can also be observed between the $_{\gamma}CH_2$ of Glu^{10} to the $^{\epsilon}$NH of the Lys^{7} amide linkage (7.54,2.09). The assignments based on the COSY spectra are listed in Table 4.

In order to provide supporting evidence for the spectral assignments of this cyclic agonist, Relayed-COSY experiments were also performed (149). As described earlier, a COSY experiment can yield information on the chemical shift of neighboring protons in a particular residue. However problems can arise when well-resolved amide protons correlate into a number of mutually overlapping αCH resonances. For example, in AMX and BNY spin systems, spins A and B as well as X an Y are well resolved, however spins M and N overlap. In such a case the COSY experiment can not correlate A to X or B to Y. To circumvent this problem, a Relayed-COSY experiment can be performed, allowing correlation of A to X and B to Y.

In this type of experiment, magnetization is transferred from spin A to spin M, as in the typical COSY experiment. However, instead of detecting the A-labeled magnetization on spin M, a delay period before and subsequent to the application of a 180° pulse results in refocusing of the magnetization on spin M. Application of the final 90° mixing pulse results in transferring the

A-labeled magnetization to spin X. The end result of such an experiment enables the transfer of magnetization from Spin A through a relay spin M to a third spin X, where X is not directly coupled to spin A. Consequently not only is a COSY-type amide to αCH crosspeak observed, but more importantly an NH to βCH crosspeak is detected as well. Hence the Relayed COSY experiment can allow correlation between two neighboring protons which are separated up to 3 or 4 bonds in the same spin system(151). Higher order Relayed-COSY experiments such as Double Relayed and Triple-Relayed-COSY are also available, which can correlate neighboring protons as being separated by 5 or even 6 bonds, respectively(150). These types of experiments allow protons to be assigned to their respective residues, even though a number of centrally located resonances are mutually overlapped, and have been successfully applied in the spectral assignment of peptides and sugars (145). In order for the Relayed-COSY experiment to work efficiently, the delay period must be optimized with respect to the magnitude of the coupling constant for the relay spin. It must be short enough with respect to the largest coupling, such that $\cos \pi J \Delta t \leq 0$, or otherwise this passive coupling leads to disappearance of the relayed signals(149). Furthermore, long delays should be avoided in order to keep signal intensity losses due to relaxation processes at a minimum. In general, the maximum efficiency for the relay transfer occurs when the delay period is $\Delta t = 0.5/J$.

Although this type of experiment is particularly useful in spectral assignments, a TOCSY experiment can ideally yield crosspeaks between all the nuclei in a spin system. The number of nuclei to which magnetization is distributed is controlled through the spin-lock periods. Short mixing times produce crosspeaks practically between vicinally coupled nuclei, whereas longer mixing times result in relayed and multiple-relayed crosspeaks (145). At the time of these studies, the 200-MHz Brucker spectrometer was not capable of applying a spin-lock field, hence it was decided to perform the relayed COSY experiments instead.

The choice of delay times were such that maximum relay transfer would occur for peaks exhibiting coupling constants of 3, 5, 6, 7, 8.3, 10, 12.5, 16.5, and 25 Hz. As illustrated in Figures 15 and 16, the 200-MHz Relayed-COSY for optimal 12.5-Hz magnetization transfer displayed numerous relayed signals which were quite useful in supporting the reported spectral assignments. As can be easily seen, the His^{2} residue not only displays the typical NH-αCH COSY-type correlation (8.88, 4.68), but more importantly a NH-βCH relayed-type crosspeak as well (8.88, 3.04). In addition, relayed signals for Leu^{4} (8.41, 1.46), Trp^{3} (8.26, 3.19) (8.26, 2.98), Glu^{10} (7.89, 1.44) (7.89, 1.38), Tyr^{13}(7.87, 2.93) (7.87, 2.78), and Nle^{12} (7.83, 1.44) can be readily identified in this figure.

This type of data circumvents the problem of mutually overlapping resonances and allows peak assignments for individual residues in highly crowded regions of the spectrum. The results of all nine Relayed-COSY experiments are consistent with the reported assignments listed in Table 4. It is also quite interesting to note that both the 3 Hz and 5 Hz relayed experiments did not yield any observable relayed signals, even though these experiments were optimal for the amide triplets of the Gly^9 and Lys^7 residues respectively. In general, smaller coupling constants require longer delay times for the relay process to work efficiently. Consequently, short relaxation times for a given molecule can become a prominent factor in reducing the relayed signal intensity to an undetectable level. This may be one explanation for the absence of relayed signals in the two above experiments.

Although the results of the COSY, NOESY, and ROESY experiments can circumstantially support the peak assignments for the Gly^9 and Lys^7 residues, these results by themselves are not sufficient to unequivocally assign these two residues. The failure of the Relayed COSY experiments to remove this ambiguity led us to try a series of spin-decoupling experiments. However, this approach was unsuccessful because of severe resonance overlap. In order to conclusively assign the Gly^9 and Lys^7 residues, synthesis

of α-deuterated Boc-Gly was undertaken and completed. This derivative will be used in future syntheses of the cyclic-agonist, and will result in the unequivocal assignment for these residues when the α-deuterated-Gly^{9}-cyclic agonist is completed.

In order to gain further insight on the conformation for this cyclic agonist, both 400-MHz NOESY and ROESY experiments were applied. To this point, the experiments described dealt with coherent magnetization transfer, or "through bond" interactions. These techniques have proven most useful in the spectral assignments of peaks located in the 1D-spectrum. However, one of the most important consequences of modern NMR spectroscopy is the ability to determine the spatial proximity of groups relative to one another. This type of data provides major constraints on the possible folding patterns for a given molecule. Just as the COSY experiment is a fundamental approach for spectral assignments, so the NOESY experiment is preeminent for determining conformational features for a given molecule.

Figure 15. 400 MHz Relayed COSY of cyclo^{7,10}[Nle^{12}]-α-factor in DMSO-$_{d_6}$ at 25 °C. Peptide concentration was 5 mg/ 0.5 ml. Optimal magnetization transfer was 12.5 Hz for this experiment.

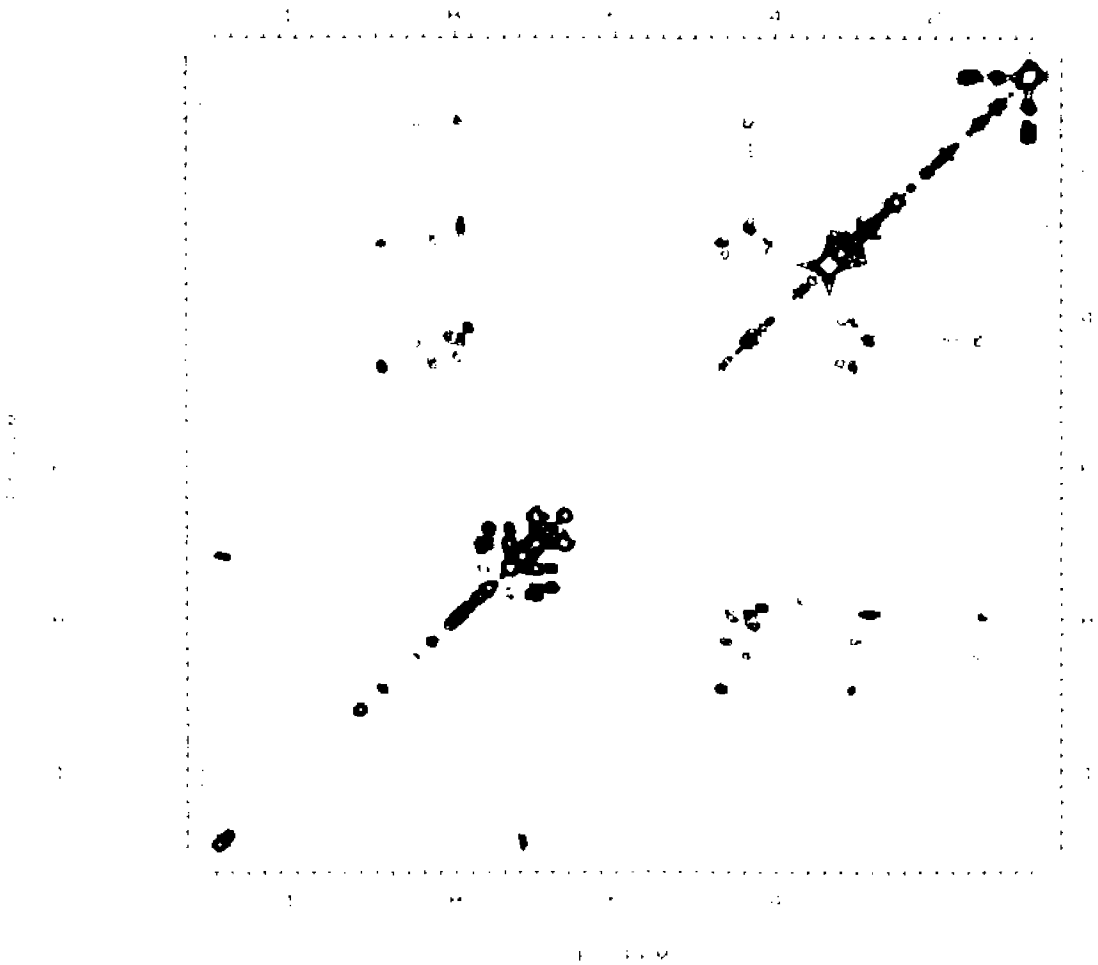

Figure 16. Amide and alpha proton region of 400 MHz Relayed COSY of cyclo^{1,6}[Nle^{4}]-a-factor in DMSO-$_{d_6}$ at 25 °C. Peptide concentration was 5 mg/ 0.5 ml. Optimal magnetization transfer was 12.5 Hz for this experiment.

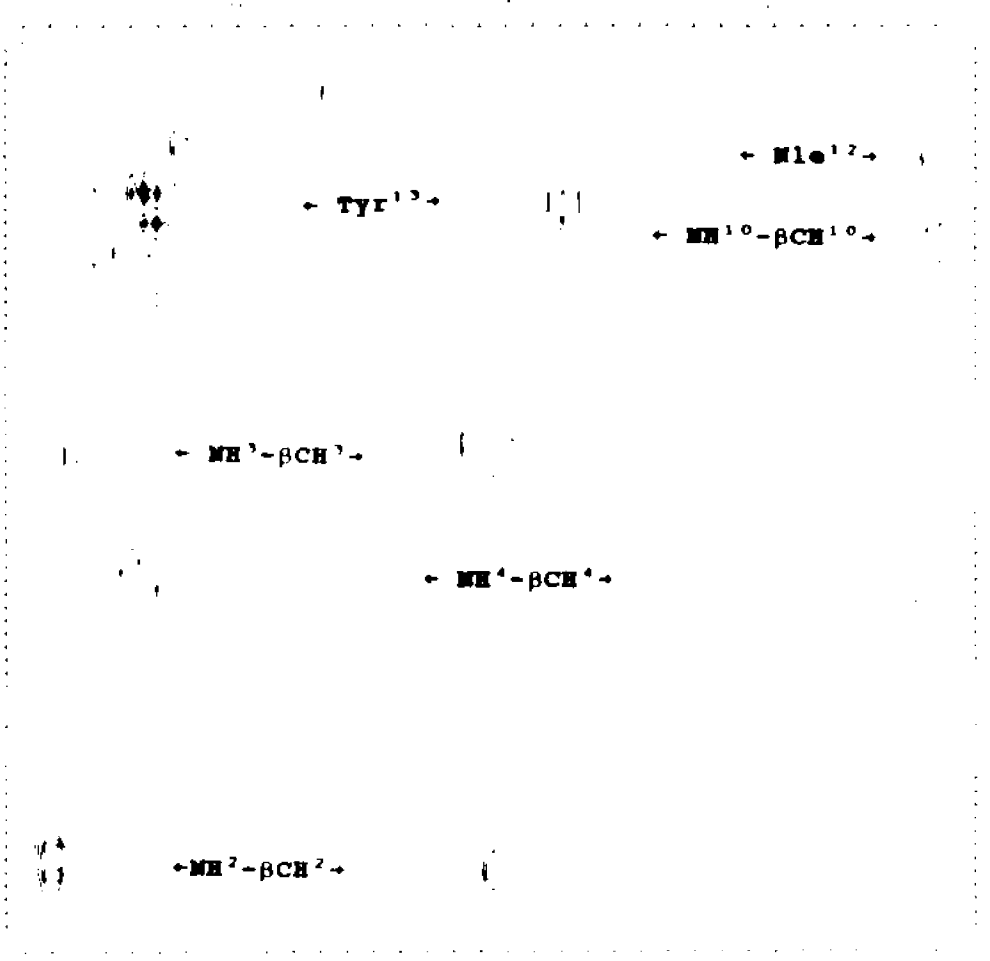
← Ile¹²→
← Tyr¹³→
← NH¹⁰-βCH¹⁰→
← NH³-βCH³→
← NH⁴-βCH⁴→
←NH²-βCH²→

In a NOESY experiment, incoherent magnetization transfer results from dipolar coupling. Dipolar coupling is the interaction of the magnetic moments of two spins through space, which is both distance and orientation dependent, and results in the practical consequence of line broadening. Due to dipolar coupling, the two spins do not relax independently, but influence each other. Hence, each deviation of a spin state from equilibrium is transferred to the other spin state, which therefore also deviates from equilibrium. This results in incoherent magnetization transfer, leading to the Nuclear Overhauser Enhancement (NOE) effect(145).

As in previous two-dimensional experiments, peaks located on the diagonal correspond to resonances found in the one-dimensional spectrum. Any off-diagonal NOESY crosspeak correlates the two perpendicularly related diagonal peaks as being in close spatial proximity. The maximum distance for which a NOESY crosspeak can be observed between two interacting nuclei is dependent on the mixing time if the molecule is considered to be rigid. Longer mixing times result in the observation of NOE connectivities for nuclei which are separated by larger distances. The upper limits for the spatial separation of the two nuclei on the 400-MHz spectrometer with a 400 msec NOESY mixing time is approximately 3.5 angstroms. Not only has this technique been successfully applied to the qualitative analysis of

distances in number of peptides and proteins (155-157), but more importantly quantitative estimates of distances between two nuclei can be determined from a series of NOESY experiments with different mixing times. This type of analysis can also monitor the undesirable effect of spin diffusion(152). Spin diffusion is the transfer of magnetization from nucleus A to a distant nucleus C through a relay nucleus B, because B is close to both nuclei A and C. This phenomenon results in the erroneous determination that nuclei A and C are close in space, even though they are quite distant.

The NOESY experiment is sensitive to the motional properties for the molecule under investigation. In particular, a flexible peptide can exhibit rapid internal motions of its backbone and side-chain protons, which leads to a small motional correlation time, τ_c. This results in NOE's which are positive and are in phase with the diagonal, since the rate of these motions are quicker than its resonance frequency. This property may also alter the maxiumum observable distance between two nuclei. In contrast, a rigid protein exhibits slow internal motions, which leads to a large correlation time. This results in NOE's which are negative or 180° out of phase with respect to the diagonal, since the rate of these motions are slower than its resonance frequency(145). When the rate of these internal motions approximately equals its resonance

frequency $\omega_o \tau_c \sim 1.$, then no observable NOE's will result. Under such nulling conditions the NOESY experiment fails to reveal any through space connectivities. For the 400-MHz spectrometer, a correlation time of approximately 0.44 nsec would lead to this condition.

In order to circumvent this problem, investigators have developed several strategies including lowering the sample temperature and/or increasing the solvent viscosity to slow down these internal motions to a level that allows detection of NOE's (159). In addition, the sample could be analyzed on a higher or lower field spectrometer, which would alter the Larmor frequency ω_o for the sample. However, recent advances utilizing spin-locking fields have generated a powerful variant to the NOESY experiment. The ROESY experiment, Rotating-frame Overhauser Enhancement Spectroscopy, also yields spatial connectivities for a molecule. However the sign of the NOE is always positive and its amplitude increases with τ_c (153,154). This experiment is particularly useful for small liner peptides.

In both the 400 msec NOESY and 300 msec ROESY at 400-MHz, a number of long range connectivities can be observed for the cyclo^{7,10}[Nle^{12}]-α-factor peptide. The most significant long range connectivities are summarized in Table 5. As can be seen in Figure 17, the N-terminal region for this peptide (His^{2}-Trp^{3}-Leu^{4}-Gln^{5}) exhibits strong

sequential NH_i-NH_{i+1} connectivities. These connectivities can be indicative of a helical type structure(160). Furthermore, the C_7 ring-proton for either $Trp^{1,3}$ exhibits a connectivity to the side-chain amide of Gln^5, which would be consistent in a helical type of structure. Moreover, the αCH of Leu^6 exhibits connectivities to both the C_7 of $Trp^{1,3}$ and to the C_2 of Trp^3 in the ROESY experiment. In addition, a connectivity between the C_7 ring protons of $Trp^{1,3}$ and the αCH of Gln^5 can also be observed in the ROESY experiment. These connectivities are highly suggestive for a helical type of structure spanning residues 1-6. A significant long range interaction between the Phenolic OH of Tyr^{13} and the NH of either Lys^7 and/or Leu^6 can be readily observed in Figure 17.

A number of long-range connectivities were also observed for the centrally cyclized region spanning residues Lys^7-Pro^8-Gly^9-Glu^{10}, and these are summarized in Table 6. Connectivities observed in the NOESY experiment include: the αCH of Pro^8 to the NH of Gly^9, αCH of Gly^9 to the NH of Glu^{10}, αCH of Pro^8 to the NH of Glu^{10}, the δCH's of Pro^8 to the NH of Gly^9, the NH of Gly^9 to the NH of Glu^{10}, the δCH of Pro^8 to the NH of Glu^{10}. the γCH's of Glu^{10} to the εNH of Lys^7, the αCH of Glu^{10} to the βCH of Lys^7, the αNH of Lys^7 to the NH of Gly^9. In addition, strong connectivities between the δCH's of Pro^8 to the αCH of Lys^7 indicate a *trans*-peptide bond between these two residues. In a

trans-peptide bond the distance between the αCH_i and the δCH_{i+1} would range 2.0-3.9 angstrom whereas in a *cis*-peptide bond this distance would range 4.3-5.0 angstrom(166).

The above connectivities are consistent for a β I- or β II-type turn structure spanning residues 7-10 (79). Displayed in Figure 18 is the characteristic sequential $amide_{i,1}$-$amide_{i,2}$ connectivity between the Gly^9 and Glu^{10} residues in this peptide, which supports a β-turn in this region(79,80). However, connectivities between the NH of Gly^9 to both the α and δCH's protons of Pro^8 indicate that a mixture of type I and type II β-turns may be present in DMSO. These connectivities are summarized in Table 6, along with the observed intensities. Long range connectivities are observed between the β-turn region and the postulated helical region. In the NOESY spectrum, the αCH of Glu^{10} has a connectivity to the αCH of Leu^4, and in the ROESY, the αCH of Pro^{11} exhibits a connectivity to the NH of Leu^4. These connectivities are depicted in Figures 19 and 20. These long range connectivities are particularly useful in the construction of a model, since they may begin to orient regions of the peptide relative to another.

Table 5. Interresidue NOE connectivities observed in 400-MHz 400 msec NOESY for cyclo^{7,10}[Nle^{14}]-α-factor, in DMSO-d_6 at 25 °C. Peptide concentration was 5 mg/ 0.5 ml.

Table 5

Interresidue NOE's(i to j) for cyclo[7-10][Nle[7]]-α-factor

residue i	proton i	residue j	proton j	structure (nm)
1	αCH	2	NH	α 0.35, 3_{10} 0.34 β/extended 0.22
1,3	C,	5	γNH	>0.45 ordered str
1,3	C,	5	αCH	>0.45 ordered str
1,3	C,	6	αCH	>0.45 ordered str
2	αCH	3	NH	
2	NH	3	NH	α 0.28, 3_{10} 0.26
3	αCH	4	NH	
3	NH	4	NH	α 0.28, 3_{10} 0.26
3	C,	6	αCH	>0.45 ordered str
1,3	C,	5	γNH	
1,3	C,	5	γCH	
1,3	C,	6	γCH	
4	αCH	5	NH	
4	NH	5	NH	α 0.28, 3_{10} 0.26
4	NH	11	εCH	>0.45 ordered str
4	αCH	10	εCH	>0.45 ordered str
5	αCH	6	NH	
5	NH	6	NH	α 0.28, 3_{10} 0.26
6,7	NH	13	ΦOH	>0.45 ordered str
7	αCH	8	δCH	
7	NH	9	NH	>0.45 ordered str
7	βCH	10	εCH	>0.45 ordered str
7	εNH	10	εCH	>0.45 ordered str
8	αCH	9	NH	β-turn 0.34-0.22
8	αCH	10	NH	β-turn 0.35-0.33
8	δCH	10	NH	β-turn 0.39-0.43
8	δCH	9	NH	β-turn 0.25-0.48
9	αCH	10	NH	β-turn 0.32
9	NH	10	NH	β-turn 0.23-0.24
10	αCH	11	δCH	
10	NH	12	εCH	>0.45 ordered str
11	αCH	12	NH	
12	αCH	13	NH	
12	NH	13	NH	

Figure 17. Sequential amid- -mide NOE connectivities observed in 400 MHz 400 msec NOESY for cyclo^{1,10}[Nle^{12}]-α-factor, in DMSO-$_{d_6}$ at 25 °C. Peptide concentration was 5 mg/ 0.5 ml.

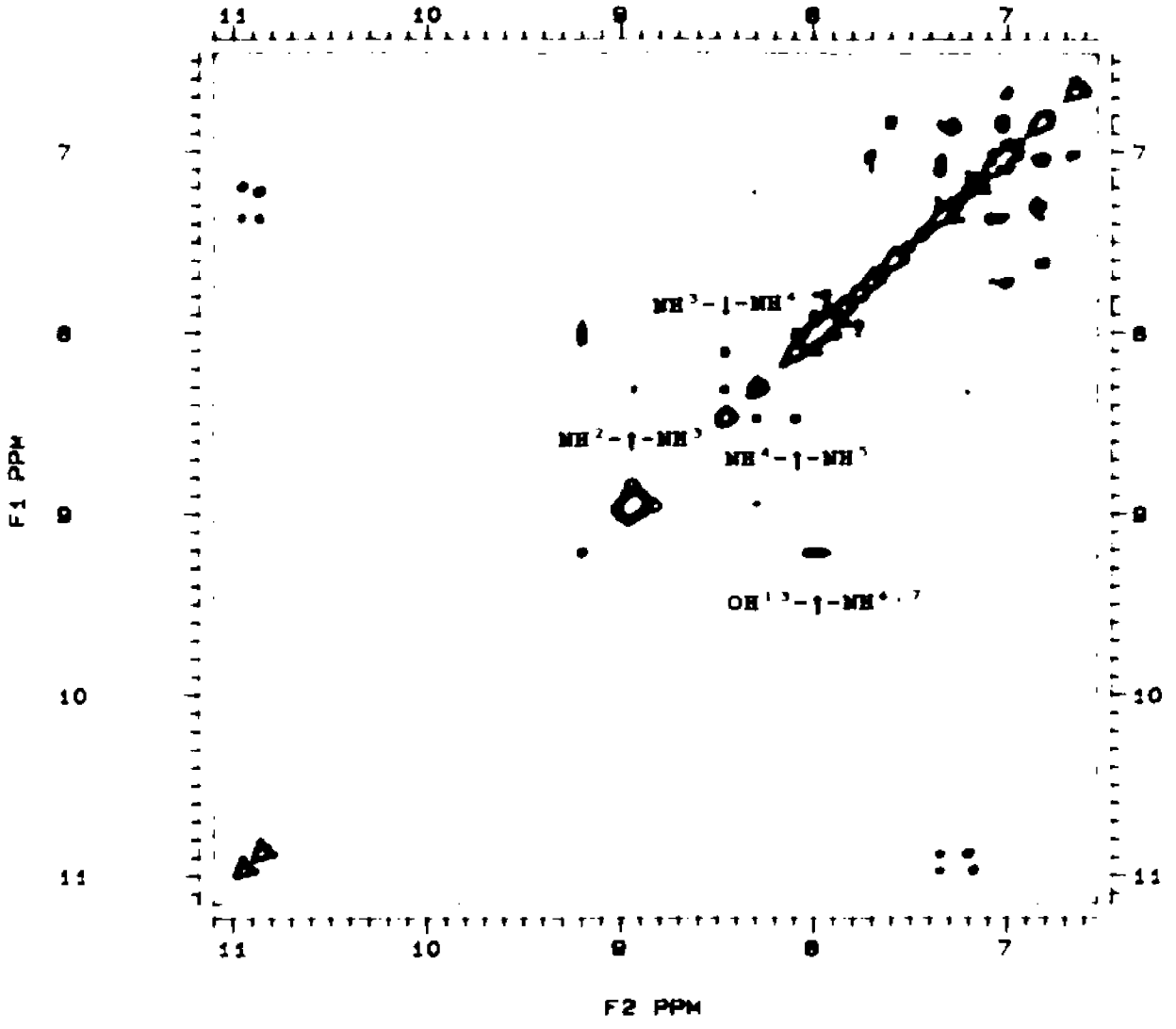
11
10
9
8
7
F1 PPM
F2 PPM
NH3-1-NH4
NH2-1-NH3
NH4-1-NH5
OH13-1-NH4,7

Figure 18. Expanded sequential amide NOE connectivities observed in 400-MHz 400-msec NOESY for cyclo[1-5][Nleu[11]]-α-factor, in DMSO-d$_6$ at 25°C. Displayed is Gly[7] to Glu[5] connectivity. Peptide concentration was 5 mg/ 0.5 ml.

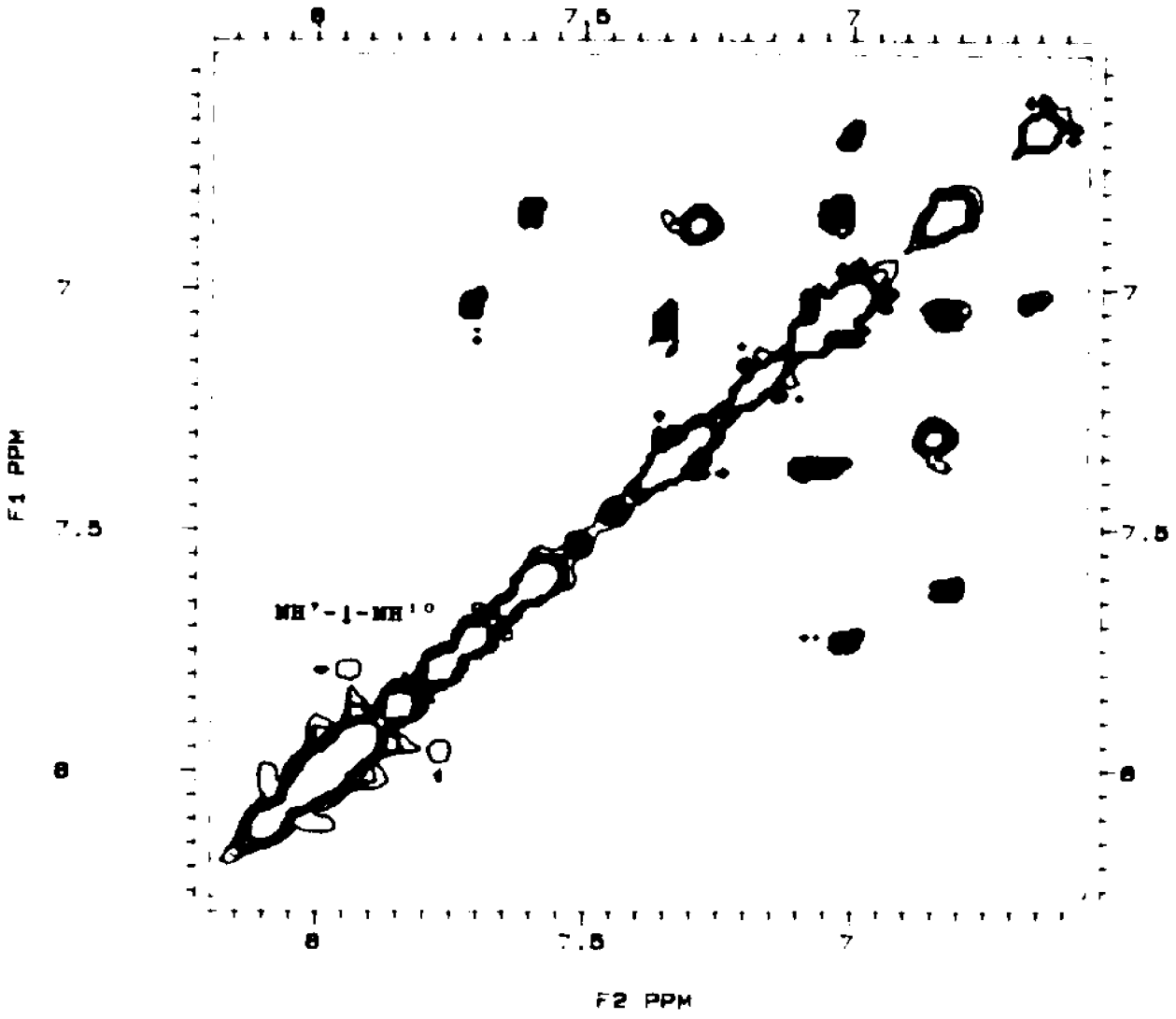
8
7.5
7
F1 PPM
7
7.5
8
MH'-1-MH'°
8
7.5
7
F2 PPM

Table 6. Interresidue NOE connectivities observed in 400-MHz 400-msec NOESY for cyclo^{7,10}[Nle^{4}]-α-factor, in DMSO-d$_6$ at 25°C. Peptide concentration was 5 mg/ 0.5 ml. Listed are the expected distances for residues in a β-turn, along with our observed NOE intensities for the cyclic agonist.

Table 6

Connectivity	Interproton distance β-turns (Angs.) Type I[a]	Type II[a]	β-sheet (extended chain)[a]	Lys^{7}-Pro Gly-Glu^{10} NOE's observed[b]
$d_{\alpha N}(2,3)$	3.4	2.2	2.2	strong
$d_{\alpha N}(3,4)$	3.1	3.1	2.2	strong
$d_{\alpha N}(2,4)$	3.5	3.3	5.5	weak
$d_{\beta N}(2,3)$	2.5	4.8	4.7	weak
$d_{NN}(3,4)$	2.3	2.4	4.1	medium
$d_{\beta N}(2,4)$	3.9	4.3	6.8	weak

[illegible] ated values [illegible] bserved experimentally for the [illegible]

Figure 19. Long range NOE connectivity observed between Glu^{10} and Leu^{4} in 400-MHz 400 msec NOESY for cyclo$^{7-10}$[Nle^{12}]-α-factor, in DMSO-$_{d_6}$ at 25 °C. Peptide concentration was 5 mg/ 0.5 ml.

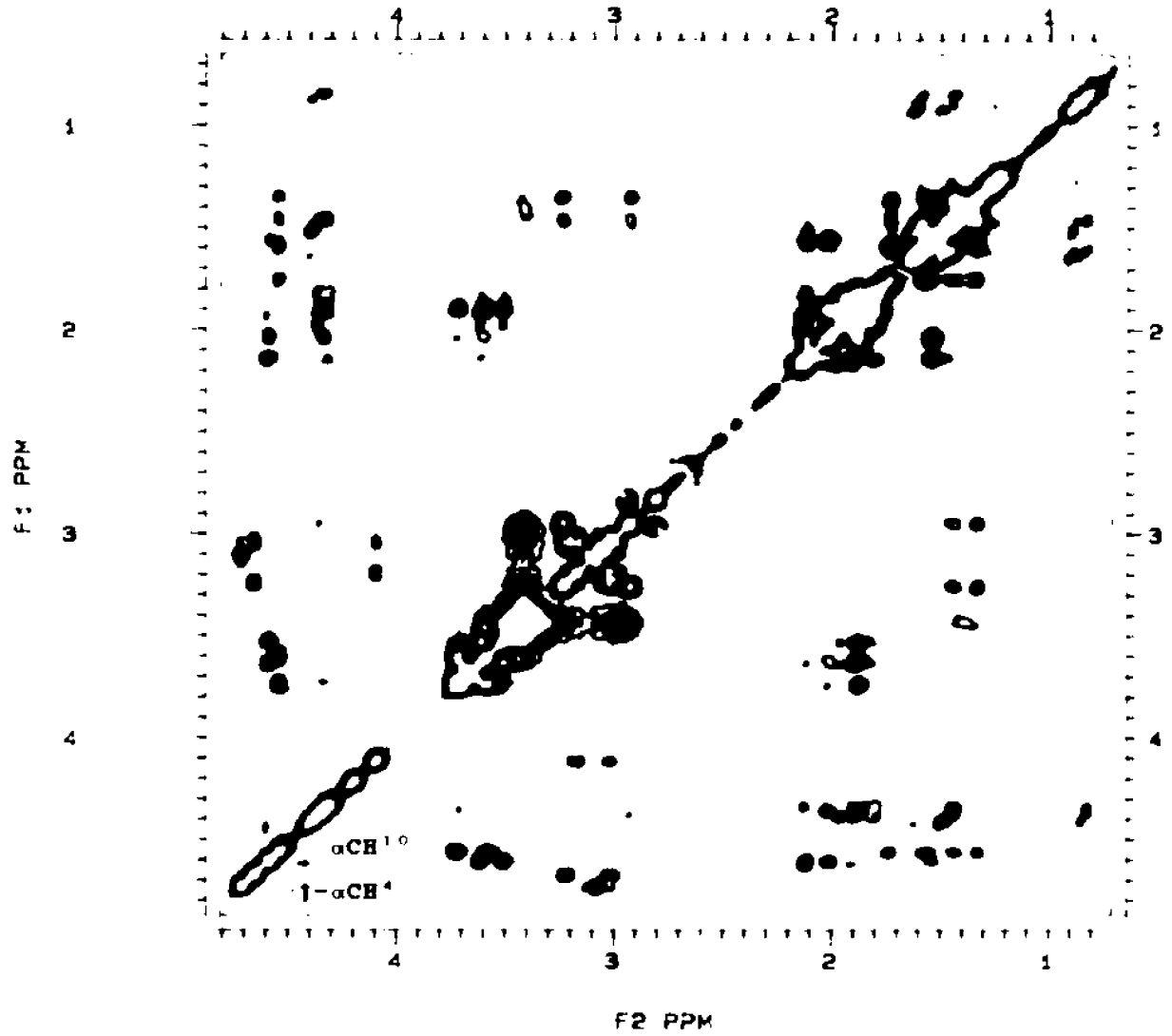
F1 PPM
F2 PPM
αCH 10
1-αCH 4

Figure 20. Long range NOE connectivity observed between Pro[3] and Leu[4] in 400-MHz 300-msec ROESY for cyclo[1,5]-[Nle[5]]-α-factor, in DMSO-d$_6$ at 25 C. Peptide concentration was 5 mg/ 0.5 ml. Depicted in this figure is the NH-αCH region of the ROESY spectrum.

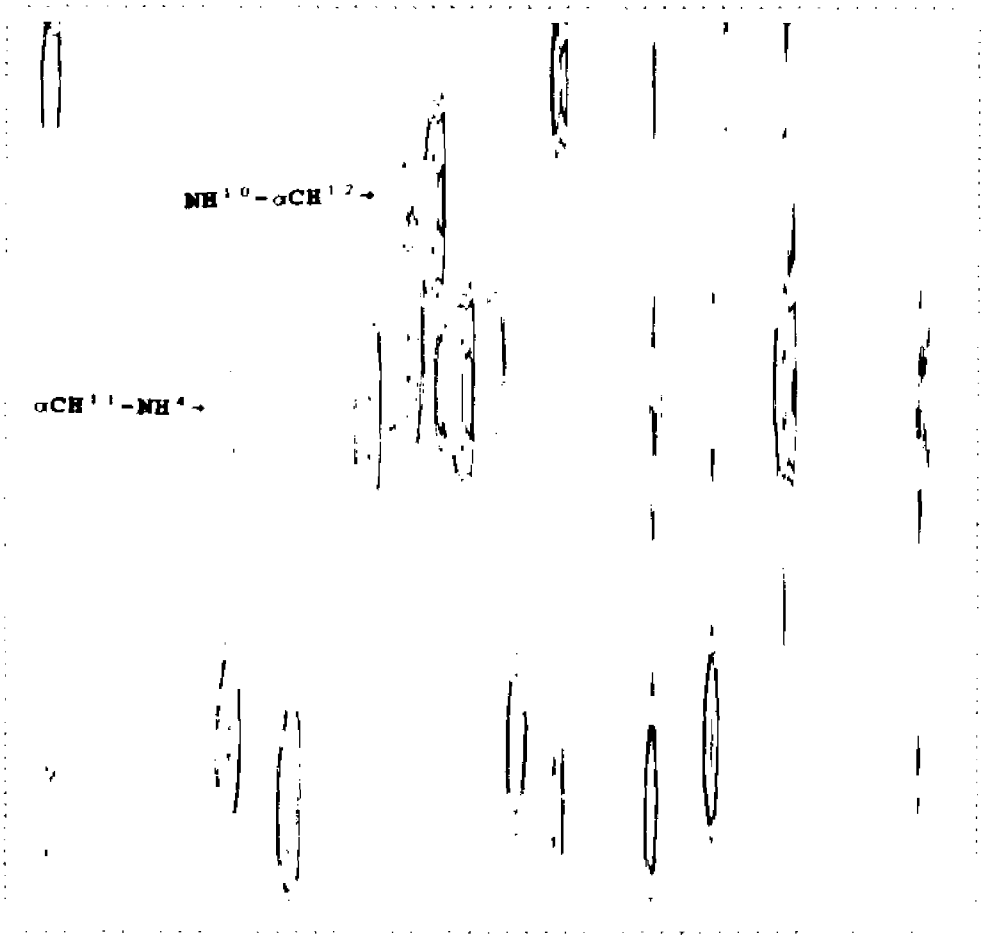
NH 10 – αCH 12 →
αCH 11 – NH 4 →

For the C-terminal region of this peptide spanning residues Glu^{10}-Pro^{11}-Nle^{12}-Tyr^{13}, several long range connectivities are observed which may suggest that a second turn structure may be present as well. These connectivities include the NH of Nle^{12} to the NH of Tyr^{13}, the αCH of Nle^{12} to the αCH and NH of Tyr^{13}, the αCH of Nle^{12} to the NH of Glu^{10}, the αCH of Pro^{11} to the NH of Nle^{12}. In addition, strong connectivities between the δCH's of Pro^{11} and the αCH of Glu^{10} indicate that this peptide bond is also *trans*. These NOE connectivities may be consistent for a turn similar to a type II β-turn spanning the C-terminus. However, not all of the NOE's expected for such a structure are present in these experiments. This result may be a consequence of conformational averaging in this flexible peptide. It is also most noteworthy that a long-range connectivity between the phenolic OH of Tyr^{13} and the NH of Leu^{6} and/or the $^{\alpha}$NH of Lys^{7} can also be observed in the NOESY experiment. These connectivities are summarized in Tables 5 and 7.

To further characterize this peptide, $J_{NH-\alpha CH}$ coupling constants were calculated from the 400-MHz spectrum, after applying resolution enhancement weighting functions. Furthermore, amide temperature shift coefficients were measured from a series of six two dimensional absolute-value COSY experiments at 200-MHz (see experimental section). The

results of these experiments are reported in Table 8. Although most of the backbone amide protons exhibited coupling constants which may be indicative of conformational averaging (158), several amide coupling constants were significantly lower. Most notably, the Gly^{9} and the Glu^{10} backbone amides (3.93, 5.13) and 5.91 Hz, respectively. These were noticeably lower than all other backbone NH's(6.90-8.21 Hz). In addition the side chain $^{\epsilon}N$ amide of Lys^{7} was also rather low (4.9 Hz). The low value obtained for the vicinal coupling constant of the Gly^{9} residue was to be expected, since the Pro-Gly sequence has a high propensity to form a type II β-turn (79,80). In such a structure, glycine would occupy the i+2 position and would generally exhibit a NH-αCH coupling constant of approximately 5 Hz(158). In contrast, the low value for the Glu^{10} amide is not easily rationalized. This value does, however, suggest that the Glu^{10} residue may also participate in a turn type structure which would be consistent with the NOE data, and that a turn structure in the C-terminal end may also be present.

Table 7. Interresidue NOE connectivities observed in 400-MHz 400-msec NOESY for cyclo^{7,10}[Nle^{10}]-α-factor, in DMSO-d_6 at 25°C. Peptide concentration was 5 mg/ 0.5 ml. Listed are the expected distances for residues in a β-turn, along with our observed NOE intensities for the cyclic agonist.

Table 7

Connectivity	Interproton distance (Angs.) β-turns		β-sheet (extended chain)	Glu^{10}-Pro Nle-Tyr^{13} NOE's observed[b]
	Type I	*Type II'*		
$d_{\alpha N}(2,3)$	3.4	2.2	2.2	strong
$d_{\alpha N}(3,4)$	3.1	3.1	2.2	strong
$d_{\alpha N}(2,4)$	3.5	3.3	5.5	? weak
$d_{\beta N}(2,3)$	2.5	4.8	4.7	----
$d_{NN}(3,4)$	2.3	2.4	4.1	strong
$d_{\beta N}(2,4)$	3.9	4.3	6.8	overlap H_β

? = Indicates crosspeak in a region where severe resonance overlap occur. [illegible]

Table 8. Amide coupling constants and temperature shift coefficients for cyclo^{7,10}[Nle^{12}]-α-factor, in DMSO-$_{d_6}$ at 25 °C. Peptide concentration was 5 mg/ 0.5 ml.

Table 8

Amide coupling constants and temperature shift coefficients for cyclo^{7,10}[Nle^{12}]-α-factor

Residue	$^3J_{NH\alpha CH}$	$\Delta\delta/\Delta t$
Trp^1-^{1}NH		-8.1
His^2	7.75	-7.2
Trp^3-^{3}NH	6.95	-6.1
Trp^3-^{1}NH		-6.3
Leu^4	7.85	-11.4
Gln^5-^{5}NH	7.95	-6.5
[a]Gln^5-^{1}NH		-1.4
[b]Gln^5-^{3}NH		-7.3
Leu^6	7.39	-6.9
Lys^7-^{7}NH	7.42	-6.3
Lys^7-^{6}NH	4.90	-6.4
Gly^8	3.93, 5.13	-3.1
Glu^9	5.91	-6.3
Nle^{10}-^{2}NH	8.29	-6.2
Tyr^{11}-^{11}NH	7.71	-9.6
Tyr^{11}- OH		-8.1

[a] side chain amide at 7.55 ppm

[b] side chain amide at 7.03 ppm

The results for the amide temperature shift coefficients appear to be extremely interesting. In particular, the backbone amide of Gly^9 and the side-chain amide of Gln^5 appear to be involved in potential hydrogen-bond interactions, -3.1 and -1.4 ppb/K respectively. These values were significantly lower than all other NH's, which were in the range for solvent exposed protons (6.1-9.6 ppb/K). The results of this study may begin to explain the significant upfield shift for the Gly^9 amide, since hydrogen bonding has also been associated with an upfield shift in a recent report (139). The extremely low value obtained for the side-chain amide of Gln^5 (-1.4 ppb/K) is particularly significant. To date, this finding has not been previously reported. It is possible that this hydrogen bond may be crucial in stabilizing the overall structure, which will be discussed further in the discussion section in the light of generating a potential model.

Discussion:

From the results of the DQF-phase sensitive COSY, nine Relayed-COSY's, the 400 msec NOESY, and 300 msec ROESY experiments, the assignments reported herein should be quite reliable. The only ambiguities that appear to exist at present are the chemical shift assignments for the Gly^9 and Lys^7 residues. Strong sequential NOE's from the αCH of Pro^8 to the NH of Gly^9, and from the γCH's of Glu^{10} to the NH of Lys^7 suggest that these residues have been properly assigned. Failure of the spin-decoupling experiments to distinguish between these two residues, due to severely overlapping side-chain protons from other residues, have hampered our efforts to conclusively assign these resonances. Synthetic efforts to α-deuterate the Gly^9 position in order to resolve this ambiguity have already been initiated.

The assignment of the Trp^1 and Trp^3 side-chain resonances is complicated by the lack of COSY connectivities between main chain and side-chain protons. The NH and αCH of Trp^1 and Trp^3 were distinguished on the basis of sequential αCH_i-NH_{i+1} NOESY connectivities, the presumed absence of the αNH_3' signal for Trp^1, and the use of [^{2}H-Trp^3]-α-factor. In order to assign side-chain resonances, NOESY connectivities to the NH and αCH protons were utilized. I attribute the downfield indole resonance to Trp^1(10.92), whereas previous

reports assign the downfield indole to the Trp^3 residue(10.91) (84). My assignments rely upon intraresidue NOE's from both the C_2-proton and the C_4-proton of the indole ring to the βCH's within the same residue. The maximum separation that both βCH's can simultaneously assume from the C_2-proton would be 3.7 angstroms, as judged from the molecular modeling program PCMODEL. However, when this is the case, the βCH's are then 2.8 angstroms from the C_4-proton. When these distance relationships are reversed, the βCH's are 3.7 angstroms from the C_4-proton and 2.95 angstroms from the C_2-proton. The upper and lower limits that any one β-proton can assume from the indole C_2-proton of the same residue is 4.11 and 2.83 angstroms, respectively. Since the maximum observable separation in a NOESY or ROESY experiment is approximately 3.5 angstroms, one would expect to observe at least one βCH to C_2-connectivity or one βCH to C_4-connectivity within the same residue. In the ROESY experiment, clearly observable C_2H to βCH and C_4H to βCH connectivities are present for each residue. No interresidue NOE's can be seen between either the C_2 or the C_4 protons to the βCH's of the other tryptophan residue. Intraresidue NOE's between the C_2-proton and its αCH, and the C_4-proton to its αCH can also be observed for each of the tryptophan residues. Once the C_2H and C_4H protons were assigned as above, the COSY spectra correlates the ring CH to the indole NH. We believe that

although our assignments differ from those in the literature, we have sufficient experimental evidence to feel confident that they are correct.

With the exception of the Gly^9 amide, the remaining spectral assignments are strikingly similar to those previously reported for the linear pheromone(89), and this is probably reflected in its comparable activity(92). It does not appear that cyclization of the central residues 7-10 results in a dramatic alteration of the overall structure for this α-factor analog, in comparison to the native pheromone. This conclusion is supported by both the comparable activity of this analog with respect to the linear α-factor, and the similar chemical shifts observed for the linear versus the cyclic peptide. I conclude that the observed similarities reflect the fact that a turn spanning residues 7-10 is a biologically significant structural feature for the α-factor molecule.

Despite the similarities in assignments there are several significant differences in the present study compared with those previously reported for the linear α-factor(89). In particular, the α-amide of Gly^9 is shifted upfield by 0.47 ppm in the present report, and the assignment of the αNH and αCH of both the His^2 (αNH 8.88, αCH 4.68) and the Trp^3 (αNH 8.26, αCH 4.63) resonances appear to be reversed. In order to check the consistency of

the reported assignments for this cyclic peptide, an [α-deuterated Trp^3]-α-factor was analyzed. The results with the deuterated-peptide confirm the chemical shifts found in this study.

The significant upfield shift for the Gly^9 amide resonance may have resulted from its participation in hydrogen-bonding as deduced from the temperature-shift coefficient studies (139). However, this result could have also arisen from local magnetic field anisotropies. More importantly, this upfield shift of 0.47 ppm from the native pheromone may reflect a different conformational environment, which may explain the modest reduction of biological activity exhibited by this cyclic agonist. However, the remarkable similarity in chemical shifts for all residues except Gly^9 suggest that the overall conformation of the linear and cyclic α-factors appear to be extremely similar.

The results of the NOESY and ROESY experiments have generated a highly speculative model, which is consistent with the observed NOE connectivities in this study (Figure 21). In this model, the N-terminal region spanning residues 1-6 is helical, residues 7-10 form a β-turn, and residues 10-13 form an additional turn structure. The molecule may be stabilized by hydrogen-bonds between the side-chain amide of Gln^5 to the terminal

carboxylate of Tyr^{13}, and between the imidazole ring of His^{2} to the side-chain carbonyl of Gln^{5}. Since the phenolic OH of Tyr^{13} may be in close proximity to Leu^{6} and Lys^{7}, it is possible that in the native pheromone an additional hydrogen-bond between the phenolic OH and the side-chain $^{\epsilon}NH_3^{\cdot}$ of Lys^{7} may also be present. This would place the side-chains of His^{2}, Gln^{5}, and the terminal carboxyl group of Tyr^{13} all on one side of the molecule. This orientation which is depicted in Figure 21 may be consistent with the previous SAR results indicating that His^{2} and Tyr^{13} appear to be important residues for activity of the α-factor. In particular, the imidazole ring of His^{2} is required for activity, as judged by the antagonistic results obtained on a truncated pheromone, [des-Trp^{1},des-His^{2}] -α-factor, whereas the terminal carboxylate of Tyr^{13} may be required for binding, since removal of residues 12 and 13 in the [des-Tyr^{13}, des-Nle^{12}]-α-factor peptide resulted in loss of pheromone binding (73). It is interesting that the gamma-carboxamide of Gln^{5} and the terminal carboxylate of Tyr^{13} are close in proximity in this hypothetical model, and may reflect Gln^{5} participation in the potential hydrogen bond interactions deduced from our temperature coefficient studies. Also illustrated in this figure are the long range connectivities observed in this study depicted by the double-sided arrows. This model is by no means proven by the NMR data; however, it is consistent with our results and provides readily testable hypotheses that can be determined

experimentally, through the design of structurally constrained analogs. The results of these subsequent analyses may shed some insight into the biologically active state for this pheromone.

For the N-terminal region of this peptide, strong and clearly resolvable sequential NH_i-NH_{i+1} connectivities can easily be observed spanning residues (His^2 - Trp^3 - Leu^4 - Gln^5), as well as a less resolvable Gln^5 - Leu^6 connectivity (Figure 17). Jelicks et al.(89,90) also observed several amide-amide connectivities in the *N*-terminus. These connectivities are highly suggestive of a helical type of secondary structure spanning these residues (160). In an extended type of structure this connectivity should be approximately 4.68 angstroms (158). Consequently, these connectivities should not be observed under the conditions of our experiment. In addition, potential NOE connectivities between the $C_7^{1,3}$ ring protons to the αCH and γCH of Gln^5, as well as a $C_7^{1,3}$ connectivity to the αCH of Leu^6 were observed. These connectivities would lend further support to this hypothetical folding pattern. However, since these NOE's appear in crowded regions of the spectrum, the NOE interpetations cannot be considered irrefutable. The N-terminus of this peptide was reported to have a high propensity to form an α-helix according to Chou-Fasman considerations(76). Jelicks et al.(90) also reported similar connectivities when α-factor was bound to lipid vesicles.

Several of the earlier NMR reports on this pheromone in solution or in lipid suspensions also indicated that these residues may be in close proximity, and that Trp^1 and His^2 may be close to Leu^4 and Gln^5 respectively(84-88).

Although there are several pieces of evidence to suggest a helical structure for the *N*-terminus, not all of the expected connectivities for such a structure were observed. Specifically, connectivities such as $d_{NN}(i, i+3)$ = 2.5-3.1 angstroms and $d_{\alpha N}(i, i+3)$ = 3.3-3.4 angstroms were not detected. Furthermore, both the amide coupling constants and temperature coefficients for this region of the peptide would not support the predominance of this structure in DMSO. Thus it seems clear that significant conformational averaging is occurring for this peptide and the J and $\Delta\delta/\Delta T$ values reflect a weighted average structure for cyclo^{7,10}[Nle^{12}]-α-factor. Since the NH_i-NH_{i+1} NOE's we do observe have also been associated by some investigators with a random peptide these connectivities cannot be used definitively at present, and this model is only presented to suggest the possibility of such a folding pattern.

Figure 21. Model for cyclo[[illegible][Nle^{12}]-α-factor, illustrating observed NOE connectivities in DMSO-d$_6$ at 25 °C.

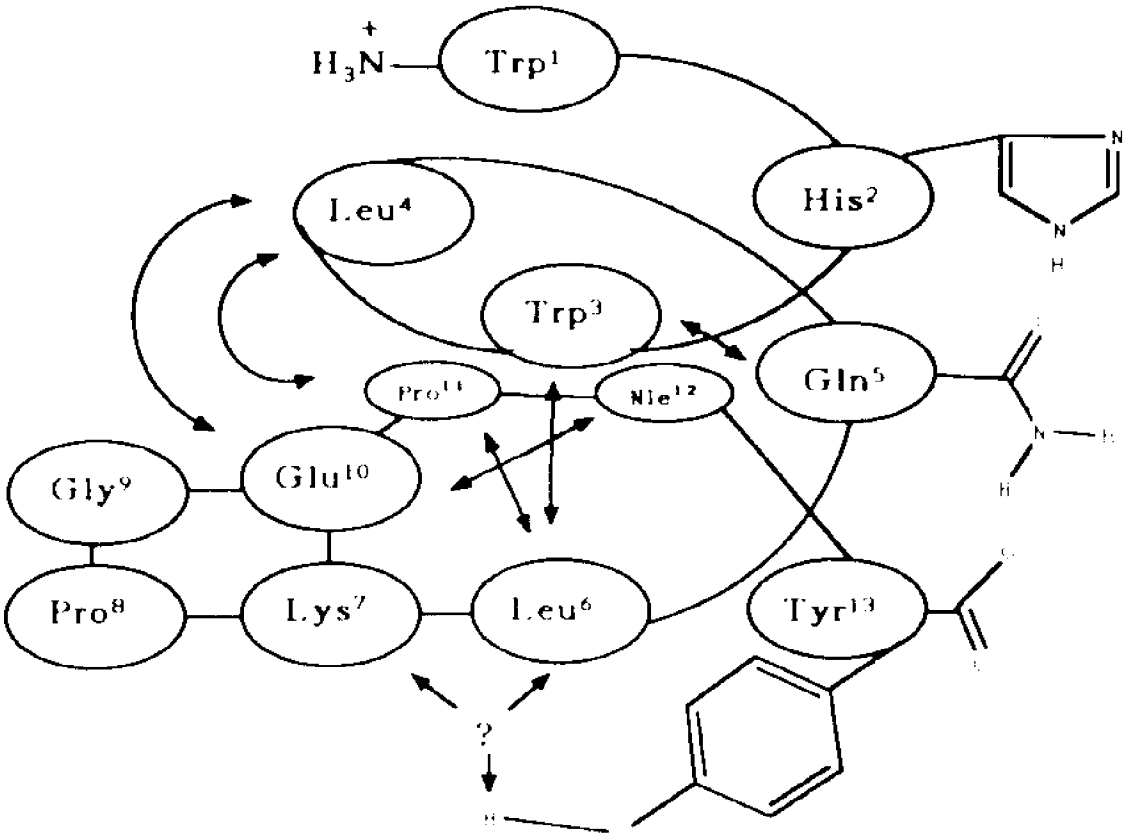
H_3N^+
Trp¹
His²
Leu⁴
Trp³
Gln⁵
Pro¹¹
Nle¹²
Gly⁹
Glu¹⁰
Pro⁸
Lys⁷
Leu⁶
Tyr¹³
?

In contrast to the N-terminus, the central portion of this peptide 7-10 appears to form a β-turn. This is supported by observing all NOE connectivities expected for such a structure. Most notably, the medium range dαN(i,i+2) connectivity between $Pro^{8}$and Glu^{10}residues and the connectivity between a δCH of Pro^{8} and the NH of Glu^{10} are expected for a turn. Moreover, the coupling constant of the Gly^{9}amide is approximately 5 Hz, as would be expected for the residue in the i+2 position of this turn. However, the observation of connectivities between both the NH of Gly^{9} and the αCH of Pro^{8}, and between the NH of Gly^{9} and the δCH of Pro^{8}, indicates that a mixture of type I and type II β-turns is present in this peptide. Since a mixture of β-turns is present, this result may reflect the modest reduction in activity exhibited by this cyclic peptide.

Cyclization may have influenced this region of the peptide since the amide temperature coefficient for the Gly^{9} residue was -3.1 ppb/K, whereas the Glu^{10} residue was -6.3 ppb/K. A low value of the temperature coefficient is suggestive of an NH which participates in a hydrogen bond. Generally, values of -2ppb/^{0}K or lower are taken as an indication of hydrogen bonded amides(158). In both type I and type II β-turns, the Glu^{10} amide, and not the Gly^{9} NH should be involved in a stabilizing hydrogen bond. It is possible that in a type I β-turn, the amide of Gly^{9} may

hydrogen bond to another region of the peptide, or may be involved in an inverse γ-type turn structure. In an inverse γ-turn structure, the $i+2$ residue is involved in a hydrogen bond to the carbonyl of the i^{th} residue, whereas in a β-turn the $i+3$ residue hydrogen bonds to the carbonyl of the i^{th} residue.Although this result is equivocal, we favor the conclusion that a β-turn structure spanning residues 7-10 is the most probable conformation for this peptide.

For the C-terminal end of this peptide, Glu^{10}-Tyr^{13}, there is evidence to suggest that a second turn may be present in this molecule. Connectivities between the αCH of Nle^{12} and the NH of Glu^{10}, and the NH of Nle^{12} to the NH of Tyr^{13} are suggestive of a turn. However, these potential NOE connectivities are in highly crowded regions of the spectrum, and are not sufficient to conclusively define the conformation of this region of the peptide.

In contrast, a long range NOE connectivity between the phenolic OH of Tyr^{13} and either the NH of Leu^{6} or the NH of Lys^{7} would orient the side-chain of Tyr^{13} towards Leu^{6} and Lys^{7}, and may result in orienting the terminal carboxylate group toward the His^{2} and Gln^{5} residues. This carboxylate group may be involved in the potential hydrogen bond interaction observed for the side-chain amide of Gln^{5}, and explain its low temperature coefficient. Earlier reports on protonation of the carboxylate of Tyr^{13} resulted in a

noticeable change in chemical shift for the NH proton of Leu^{6}, whereas protonation of the imidazole ring of His^{2} resulted in changes in chemical shift for the side-chain amides of Gln^{5}, and the NH's of Trp^{3}, Leu^{4}, Gln^{5}, and Leu^{6}(84). These results suggest that Tyr^{13} may be in close proximity to Leu^{6}, and that His^{2} may be near Gln^{5}.

An important result from the ROESY/NOESY analysis is the observation of long range connectivities between the β-turn region and the postulated helical region. In the NOESY, the αCH of Glu^{10} has a connectivity to the αCH of Leu^{4}, and in the ROESY, the αCH of Pro^{11} to the NH of Leu^{4} connectivity can be observed. A long range NOE connectivity between the phenolic OH of Tyr^{13} and either the NH of Leu^{6} or the NH of Lys^{7} was also observed. These results may orient the turn region(7-10) to the potential helical region (1-6) and indicate that residues far apart in the main chain are interacting. Hence the turn about residues 7-10 not only results in a chain reversal, but most importantly it may allow the ends of this peptide to interact. These results extend previous studies on the α-factor and may begin to elucidate the bioactive conformation.

Although we have presented one possible folding pattern for this cyclic peptide which would be consistent with the observed NOE's, the ultimate test of this hypothetical model will be derived from structure/function type studies.

In particular, this model can be used to design analogs to support its biological relevance. In this model, His^{2}, Gln^{5}, and Tyr^{13} would appear to be the critical residues for interaction with the STE-2 receptor. The helical structure spanning residues 1-6 may only be required for proper alignment of residues 2 and 5. If this interpretation is valid residues Trp^{1}, Trp^{3}, Leu^{4}, and Leu^{6} may be replaced by residues which are readily accommodated in a helical type structure with retention of biological activity. A number of studies have indicated that the α-aminoisobutyric acid (Aib) represents an excellent choice for building up 3_{10} helices, α-helices, and type III/I β-turns (161). Accordingly, analogs in which residues 1, 3, 4, or 6 have been replaced by one or more Aib residues should be quite active, and would lend further support to this hypothesis.

It appears that Gln^{5} participates in stabilizing the whole structure and maintains proper alignment of the Tyr^{13} and His^{2} residues through hydrogen bonding with the Tyr^{13} COO^{-}. Substitution of Gln^{5} with glutamic acid should result in an analog ($[Glu^{5}]$-α-factor) with diminished activity, since the side-chain carboxylate should destabilize this structure. Further support could be derived by comparing the activity of a $[Asn^{5}]$-α-factor versus $[Asp^{5}]$-α-factor. It would be also interesting to determine the relative activity of a $[Ser^{5}]$-α-factor and $[Cys^{5}]$-α-factor with regard to potential hydrogen bond interactions.

In conclusion, a detailed conformational analysis has been performed on a cyclic agonist of the α-factor. The results of this study has generated a model, in which the *N*-terminal region is helical, and the central and C-terminal regions forms two turns. Although cyclization has reduced the conformational flexibility for this α-factor agonist, this peptide still exhibits significant conformational averaging in DMSO. Consequently, this hypothetical model can only describe one out of potentially many other possible folding patterns for this molecule. Analogs which can further restrict this freedom have been proposed. Due to the flexibility of this pheromone in solution, future conformational analyses are planned in the presence of the α-factor receptor and will be aimed at determining the biologically active form of this pheromone while it is bound to its receptor.

V) 2D-NMR studies on [Glu^{6}, NMePhe^{8}, Aib^{9},]-Substance P $^{6-11}$ in DMSO-d_6

Introduction:

Substance P is an undecaneuropeptide, Arg-Pro-Lys-Pro-Gln-Gln-Phe-Phe-Gly-Leu-Met-NH_2, which is thought to be involved in pain-perception within the mammalian brain. This neuromodulator is an important member in a family of neuropeptides known as the tachykinins. All of these peptides share a common C-terminal sequence Phe-X-Gly-Leu-Met-NH_2, and are widely distributed in different regions of the mammalian nervous system, where they exert different actions(94). Two other naturally occurring mammalian tachykinins have been elucidated, and these decapeptides have been classified as Neurokinin A (NKA) and Neurokinin B (NKB).

These molecules have been shown to interact with at least three independent receptors designated as NK1, NK2, and NK3, where the preferred agonist is substance P, NKA and NKB respectively (30). However only modest selectivity is exhibited by these peptides, since each one shows appreciable activity on the other two receptors. Recently, several independent studies on the synthesis and characterization of Substance P analogs which are selective for individual receptors have been reported (64,65). Among

the most selective of these are Ac-Arg^{6}-Phe-Phe-Gly-Leu-Met^{11}-NH_2 and pGlu^{6}-Phe-NMe Phe-Aib-Leu-Met^{11}-NH_2. These hexapeptides are 1000 fold and 30,000 fold more active against NK1 and NK3 receptors respectively.

An important problem in the field of endocrinology is determining the biologically active conformation of the signal molecule. Many mammalian peptides interact with a variety of receptors, and it is difficult to extend studies on the conformation of such molecules in solution to the biologically active state. In such cases it would be very advantageous to examine analogs which are highly selective for a given receptor. Since [pGlu^{6}-NMe Phe^{8}]SP6-11 has been found to interact specifically with the NK3 receptor, it would appear to be an ideal model for determining the conformation of Substance P bound to this receptor subtype. However, [pGlu^{6},NMePhe^{8}]SP6-11 is a relatively flexible molecule and probably assumes a distribution of conformations in solution. Recently, a new analog of Substance P, pGlu-Phe-NMePhe-Aib-Leu-Met-NH2, which is also highly selective for NK3 has been generated. Since this molecule contains both Aib and N-MePhe residues, its conformation is expected to be significantly more restricted than any of the other hexapeptide analogs. In the following section, a detailed NMR analysis on pGlu-Phe-NMePhe-Aib-Leu-Met-NH_2 in DMSO-d_6 is presented.

Results:

Upon first inspection of the one-dimensional proton spectrum for pGlu-Phe-NMePhe-Aib-Leu-Met-NH2,, which is illustrated in Figure 22, it was noticed that the spectrum exhibited significantly more peaks than expected based on the primary structure for this peptide. As shown in Figure 23 which focused on the 7-9 ppm region of the spectrum, at least 10 resonances were observed which can be attributed to NH protons. Similar complexity was observed in the αCH region of the spectrum which is depicted in Figure 24. At least seven αCH resonances were observed, even though the primary structure would predict five. This additional multiplicity was also observed throughout the rest of the spectrum. Furthermore, the integration ratios of the peaks did not correlate with the expected peak ratio. The observation of small peaks with integration values of less than one proton was indicative of the existence of more than one averaged conformation for this hexapeptide in DMSO. The proton NMR spectra were also examined at different concentrations, from 12 mM to 0.1 mM. No differences in chemical shift or linewidths were observed, suggesting that aggregation did not occur at the concentrations examined. Furthermore the peak multiplicity was not a result of aggregation which leads to dissymmetric structure.

A small peptide in solution can exist in a number of low-energy conformations (162). As well documented in the literature, a peptide which contains N-alkylated amino-acids such as proline or N-methylated residues can exhibit *cis-trans* isomerization about their peptide bond (163-165). Our original hypothesis was that the additional peaks were the result of *cis-trans* isomerism about the Phe^{7}-NMePhe^{8} peptide bond. To provide supporting evidence that *cis-trans* isomerization resulted in two distinct populations of structures, the proton spectrum was measured over a range of temperature. As illustrated in Figure 25 , when the temperature was raised from 300K to 400K the two sets of peaks in the αCH region and the βCH region coalesced. This coalescence was reversible upon cooling the sample back to 300 K.

The substance P(SUBP) analog was homogeneous on reversed phase HPLC and a FAB-mass spectrum gave an experimental molecular ion which agreed nicely with the calculated value,(calculated 765, found 766). Thus the peak multiplicity was not due to a side-product from the chemical synthesis, and it is reasonable that it is due to *cis-trans* isomerization about the Phe^{7}-NMePhe^{8} peptide bond. Careful inspection of various peaks suggested that the two isomers are present in a 60/40 ratio.

Figure 22. 400-MHz ^{1}H-NMR spectrum of [pGlu^{5}, NMePhe^{8}, Aib^{9}]-SP$^{5-11}$ in DMSO-d_6 at 25 °C. Peptide concentration was 5 mg/ml.

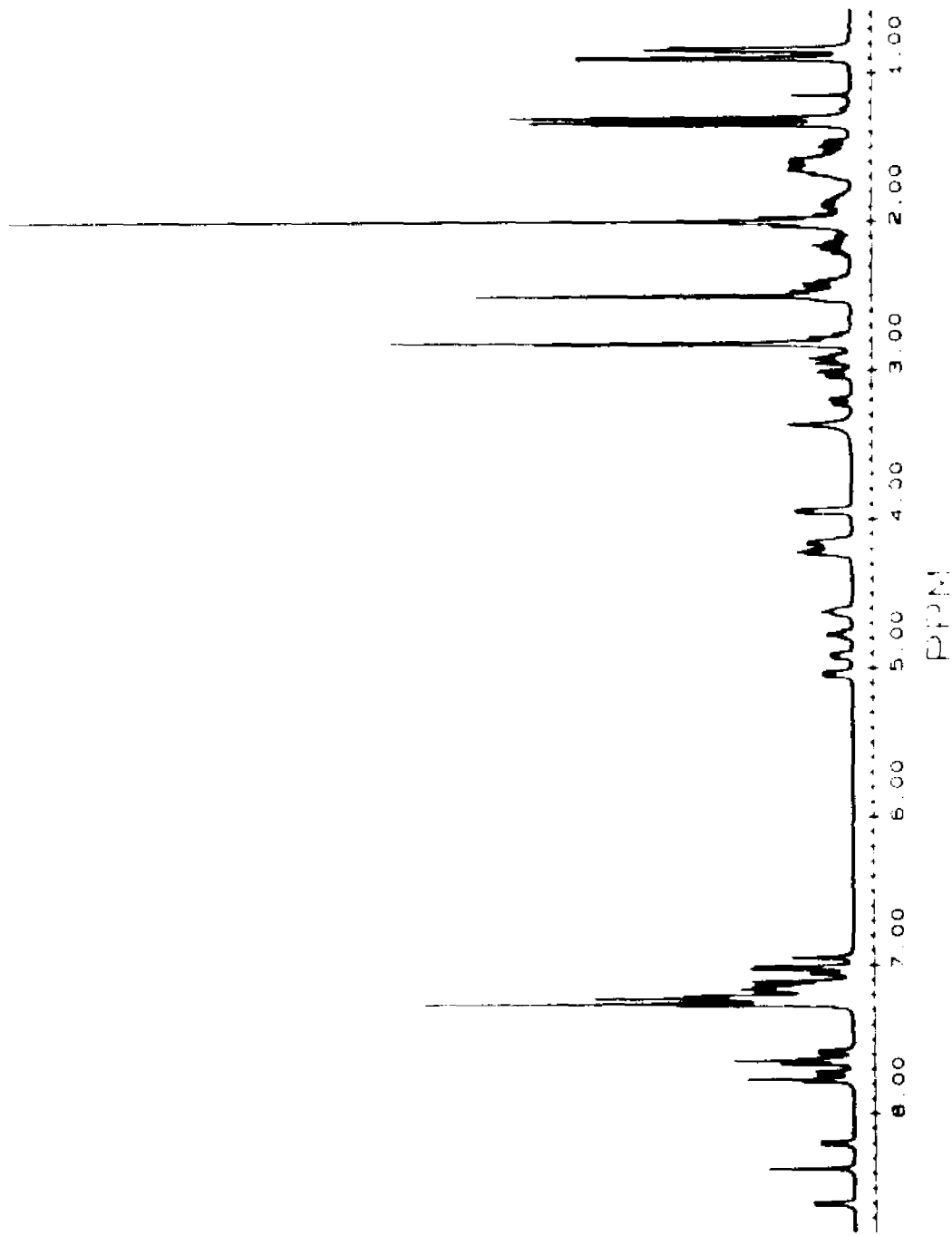
8.00
7.00
6.00
5.00
4.30
3.00
2.00
1.00
PPM

Figure 23. Amide region of 400-MHz ^{1}H-NMR spectrum of [pGlu^6, NMePhe^8, Aib^9]-SP$^{6-11}$ in DMSO-d_6 at 25 °C. Peptide concentration was 5 mg/ml. Displayed are 10 amide resonances where the primary structure would indicate 7 amide signals.

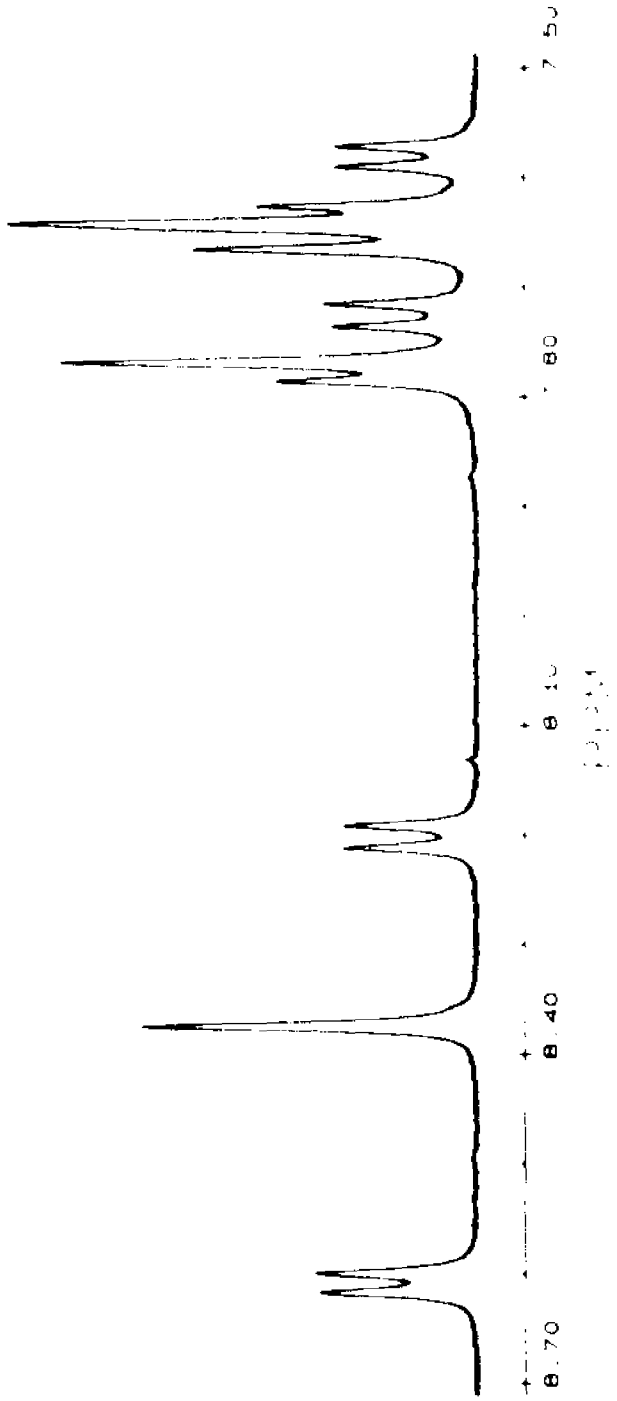
8.70
8.40
8.10
7.80
7.50

Figure 24. Expanded alpha proton region of 400-MHz ^{1}H-NMR spectrum of [pGlu^{6}, NMePhe^{8}, Aib^{9}]-SP$^{6-11}$ in DMSO-d_6 at 25 °C. Peptide concentration was 5 mg/ml. Displayed are 7 alpha proton resonances where the primary structure would indicate 5 alpha proton signals.

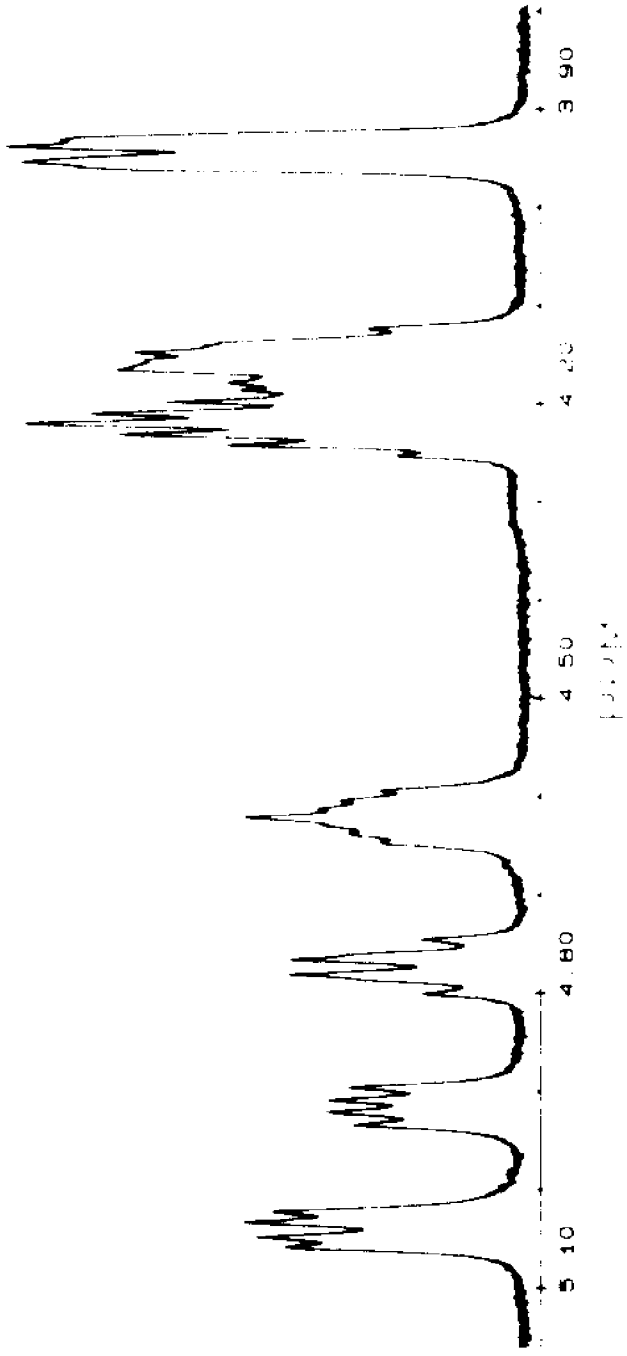
5.10
4.80
4.50
4.20
3.90

Figure 25. Expanded proton region of 200-MHz ^{1}H-NMR spectrum of [pGlu^6, NMePhe^8, Aib^9]-SP$^{6-11}$ in DMSO-d_6 at 300 K(top) and at 400 K(bottom). Peptide concentration was 5 mg/ml. Reversible coalescence of *cis/trans* resonances are exhibited at higher temperature.

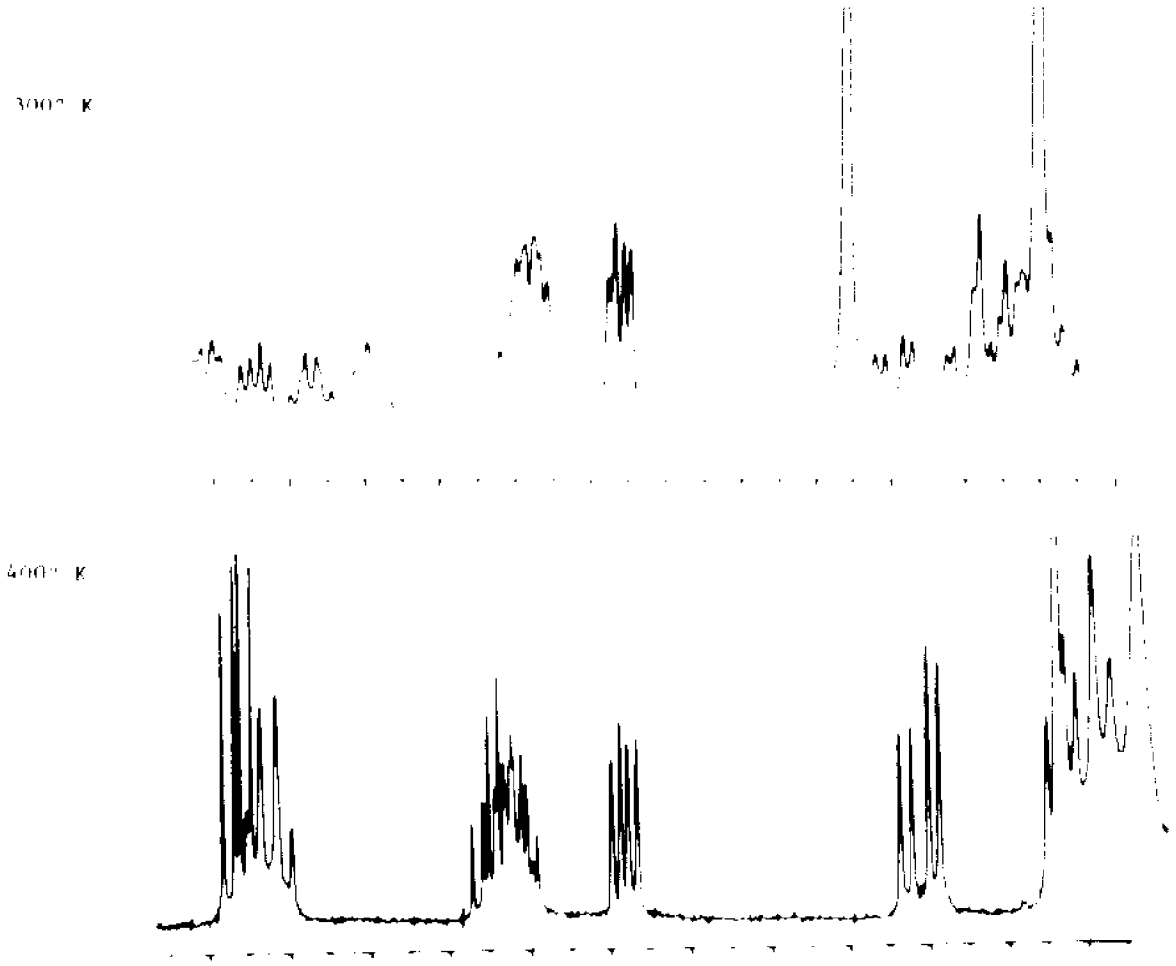

Peak assignment of the proton NMR spectrum was accomplished by a combination of two-dimensional homonuclear DQF-phase sensitive-COSY(Figure 26), Relayed-COSY(Figure 27), and ROESY experiments(Figure 28). The DQF-phase sensitive-COSY and Relayed-COSY spectra were interpreted assuming the presence of a mixture of *cis/trans* diastereomers for this hexapeptide. ROESY connectivities were also very helpful in distinguishing between these isomers. As depicted in Figure 29, when the Phe7-NMe Phe8 peptide bond is *cis*, the αCH of both residues 7 and 8 are close in space, whereas the αCH of residue 7 is much farther from the N-CH3 on residue 8. Conversely, when the peptide bond is *trans*, the distance relationships are reversed. Hence, a strong ROESY connectivity between resonances at 5.03 ppm and 4.61 ppm, indicates that these αCH's are associated with the *cis* isomer. This conclusion is supported by the fact that the resonance at 4.61 ppm does not exhibit a connectivity to the $N\text{-}CH_3$ of residue 8. In contrast, the resonance for the *trans* αCH of residue 7 at 4.76 ppm, has a strong connectivity to the $N\text{-}CH_3$ group of residue 8 at 2.82 ppm. Using the above reasoning, peak assignments for all residues in both diastereomeric forms of this hexapeptide are reported in Table 9. The results are consistent with a mixture of diastereomers in DMSO, corresponding to 60% *cis* and 40% *trans*. The chemical shifts for the NH protons for the Phe^{7} and Aib^{9} residues of the *cis* diastereomer are shifted downfield by more than 0.5 ppm in comparison to

those in the *trans* isomer. Furthermore, the βCH protons of Phe^{7} in the *cis* isomer differ in chemical shift by more than 1 ppm. These differences may reflect conformational preferences which are characteristic of the individual diastereomers.

To further characterize this hexapeptide, a detailed analysis of $J_{\alpha CH-NH}$ and $J_{\alpha-\beta}$ coupling constants was performed. Coupling between α and β protons was measured by utilizing selective-saturation experiments to simplify αCH-βCH spin-systems, and processing the resultant FIDs to optimize peak resolution. Analysis of the coupling constants demonstrated that the $J_{\alpha CH-NH}$ values are between 6 and 8 Hz for residues 7-11, and less than 1 Hz for the pGlu^{6} residue (Table 10). These values were then corrected for electronegativity effects(166) and utilized in a Karplus type equation to generate possible ϕ and φ angles(158), which are also listed in Table 10. In order to determine the most likely ϕ angle that a particular residue may assume, we utilized intraresidue NH_i-αCH_i NOE connectivities to distinguish the relative angle between the two nuclei involved. Those values listed in boldface in Table 10 are the most likely candidate angles assumed by this peptide.

Figure 26. 200-MHz DQF-phase sensitive COSY of [pGlu^{6}, NMePhe^{8}, Aib^{9}]-SP$^{6-11}$ in DMSO-d_6 at 25 °C. Peptide concentration was 5 mg/ml.

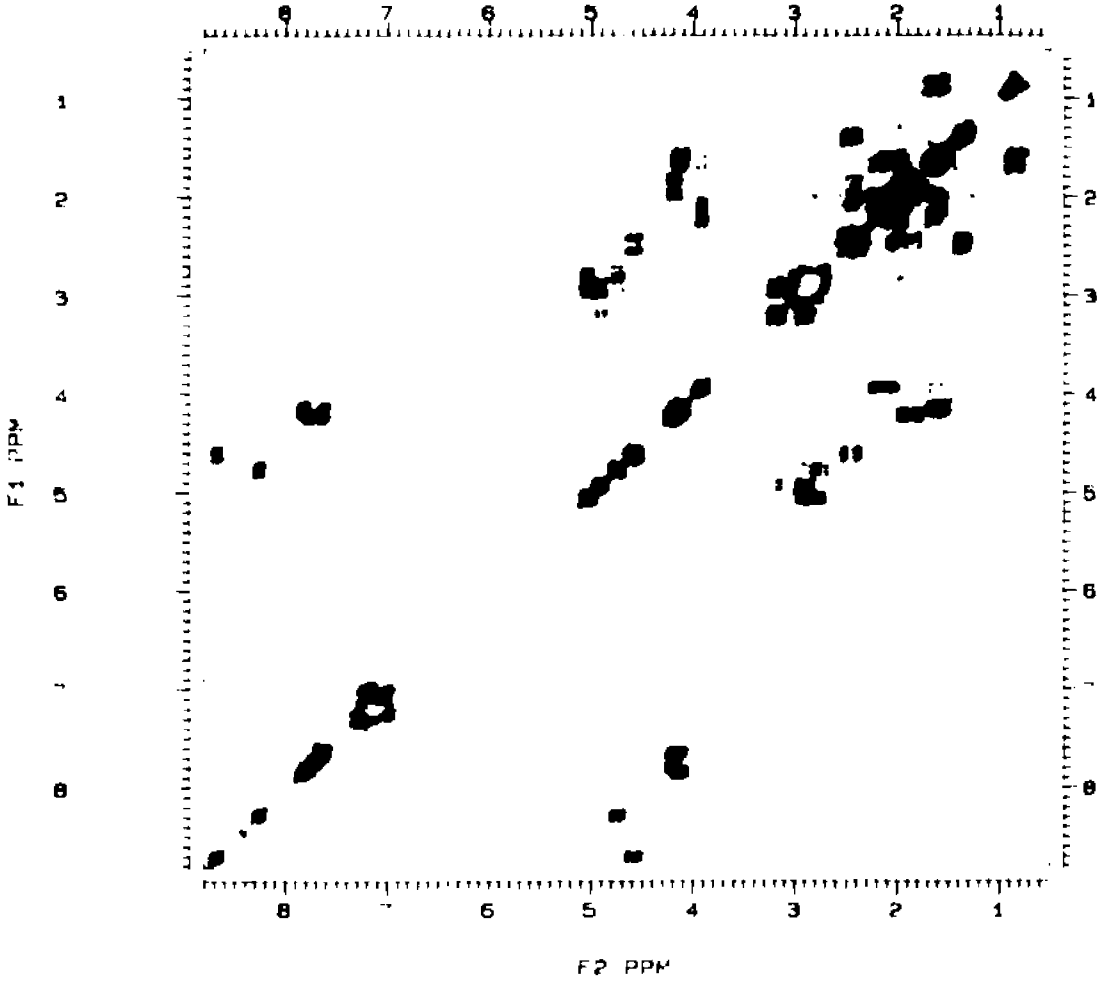
F1 PPM
F2 PPM

Figure 27. 7.5 Hz Relayed COSY at 200-MHz for [pGlu^{6}, NMePhe^{8}, Aib^{9}]-SP$^{6-11}$ in DMSO-d_6 at 25 °C. Peptide concentration was 5 mg/ml.

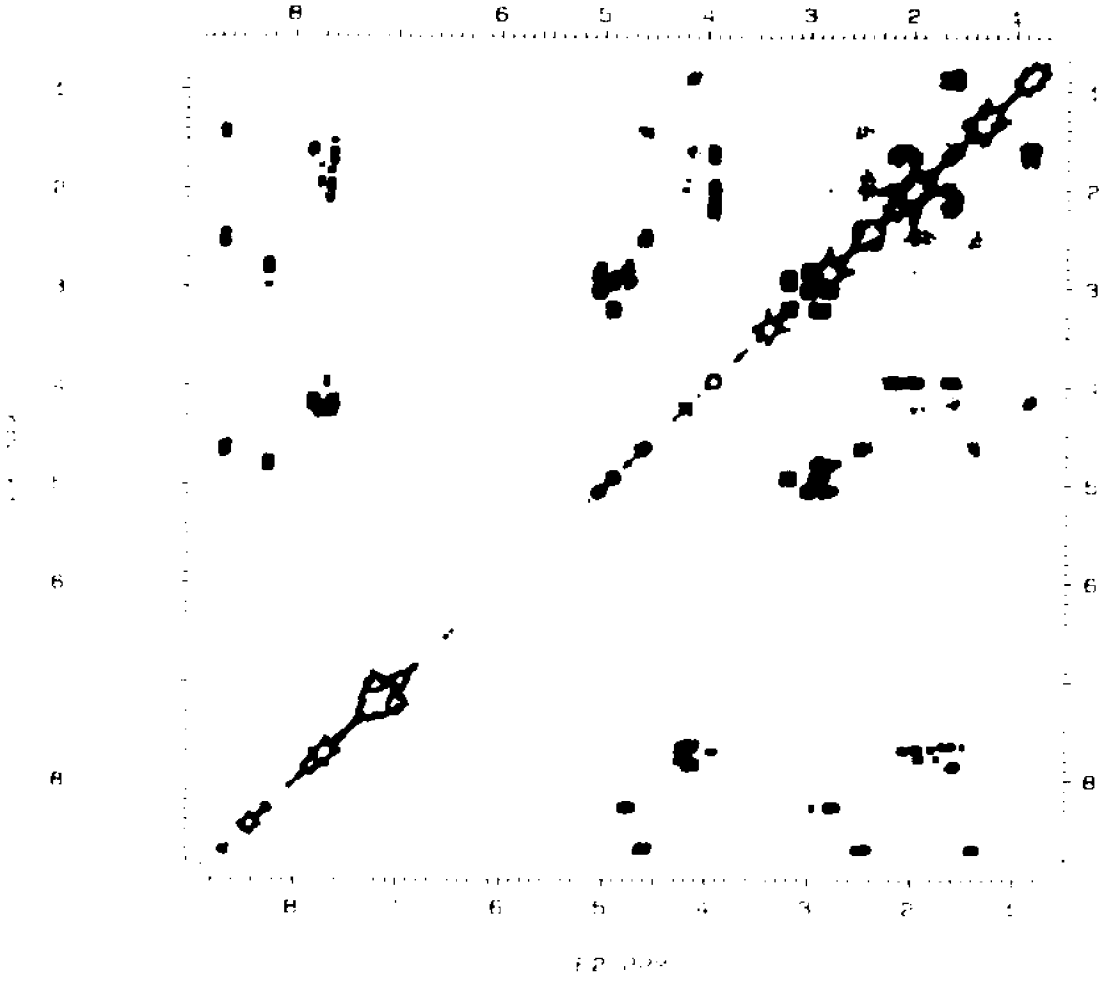
8
6
5
4
3
2
1
1
2
3
4
5
6
8

Figure 28. 400-MHz 250 msec ROESY of [pGlu$^{\alpha}$, NMePhe$^{\beta}$, Aib$^{\gamma}$]-SP$^{\delta\ 11}$ in DMSO-d_6 at 25 °C. Peptide concentration was 5 mg/ml.

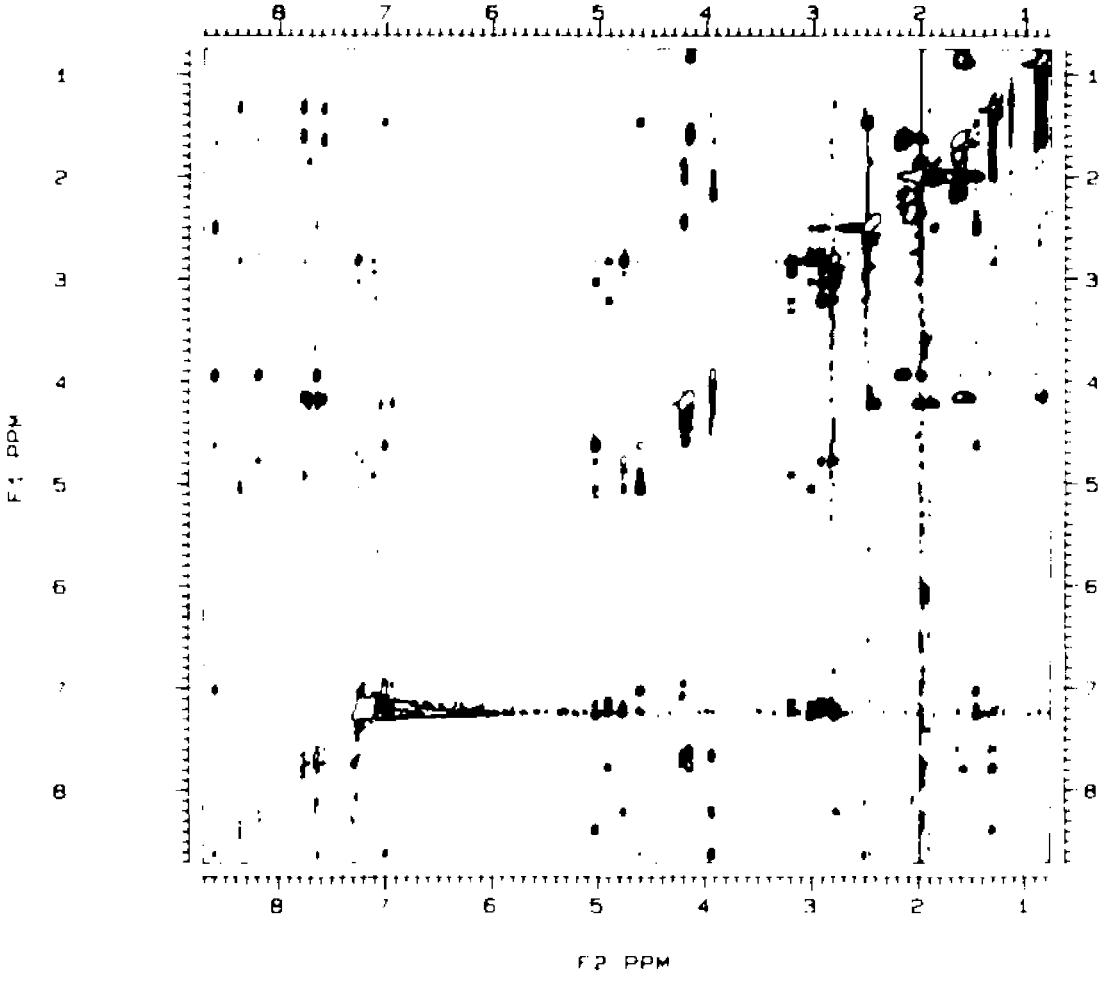
F1 PPM
F2 PPM

Figure 29. Expanded alpha proton region of 400-MHz 250 msec ROESY of [pGlu^{5}, NMePhe^{8}, Aib^{9}]-SP$^{6-11}$ in DMSO-d_6 at 25 °C. Peptide concentration was 5 mg/ml. Characteristic NOE connectivities observed for *cis/trans* isomerism about the Phe^{7}-NMePhe^{8} peptide bond.

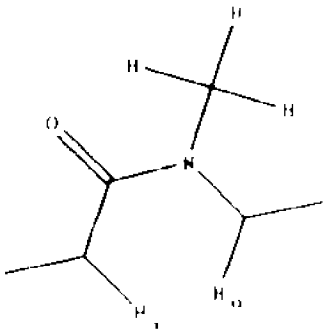

Cis peptide bond

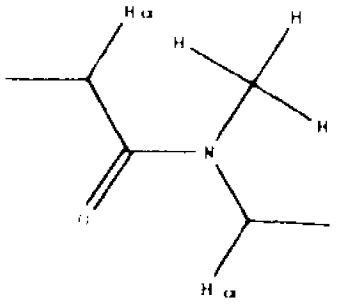

Trans peptide bond

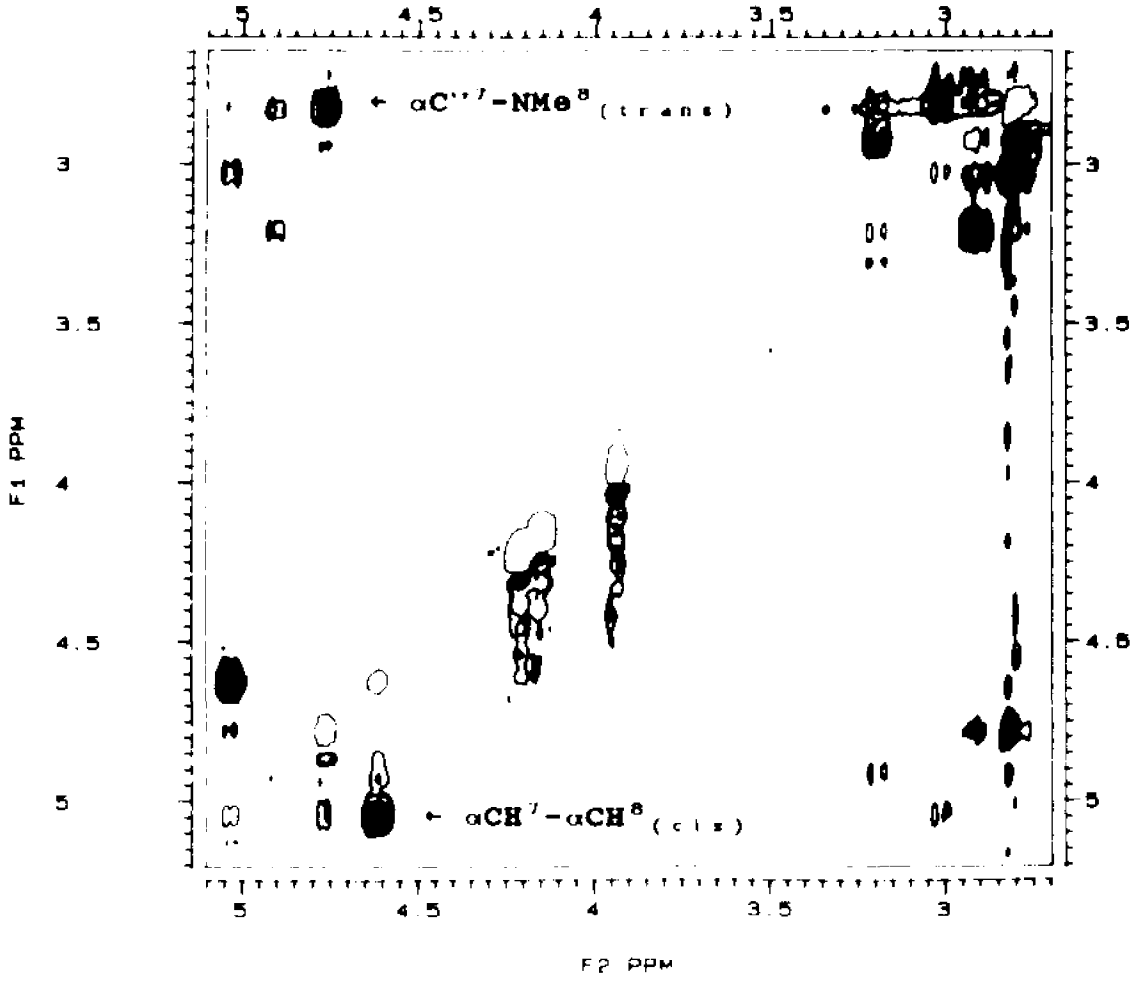

As illustrated in Figure 30, if approximately equivalent values of less than 4 Hz were obtained for both $J_{\alpha\beta 1}$ and $J_{\alpha\beta 2}$, one could assign the side-chain of Phe^{7} in the *trans* diastereomer as being predominantly in rotamer-state III. In contrast, both rotamer I and II would exhibit $J_{\alpha\beta}$ values of less than 4 Hz and greater than 9 Hz. To differentiate between rotamer I and II, distance dependent through space connectivities from the ROESY spectra can be applied. All spatial connectivities with the expected intensities were observed for this rotamer, supporting our assignment that the Phe^{7} *trans* isomer assumes χ^{1}-angles which are consistent with the rotamer III state, these results are depicted in Figures 31-33.

Specifically, equivalent αβ1 (4.76,2.91) and αβ2 (4.76,2.77) through space connectivities were observed(Figure 31), whereas only the NHβ2 (8.19,2.77) connectivity could be detected in the ROESY(Figure 32). Furthermore, an NH-ortho-ring proton (8.19,7.11) connectivity was also observed(Figure 33).

NOE's and coupling constants consistent with the rotamer II state were observed for the *cis*-Phe^{7} residue. For example, only the αβ2 (4.61,1.47) connectivity(Fig. 32) and the NHβ1 (8.60,2.52) connectivity(Fig. 32) could be observed in the ROESY. Furthermore, the magnitude of the αβ1 (9.92 Hz) coupling constant was greater than the αβ2 (3.87 Hz)

coupling constant. Moreover, an NH-side-chain (8.60,7.00) and αCH-side-chain (4.61,7.00) connectivities were also observed (Figure 32 and 33, respectively).

Support for both isomers of the NMePhe^{8} residue residing predominantly in the rotamer I state was obtained by observing equivalent NHβ1 (4.91,3.20)^{trans},(5.02,3.02)^{cis} and NHβ2 (4.91,2.93)^{trans},(5.03,2.91)^{cis} connectivities, whereas only the αβ1 (4.91,3.20)^{trans},(5.03,3.02)^{cis} connectivities could be detected for the *trans* and *cis* isomers, respectively(Figure 31). Moreover, the βCH coupling constant for the αβ1 connectivity was less than 4 Hz, whereas the αβ2 value was greater than 9 Hz in both isomers, see Table 10. In addition, an αCH-side-chain (4.91,7.14)^{trans},(5.03,7.25)^{cis} connectivity was also observed for both diastereomers(Figure 32). By employing this strategy, we have also concluded that the Leu^{10} and Met^{11} residues are predominantly in the rotamer III state within both diastereomeric forms of this peptide.

Figure 30. Expected coupling constants and NOE connectivities for each of the side-chain rotamer states.

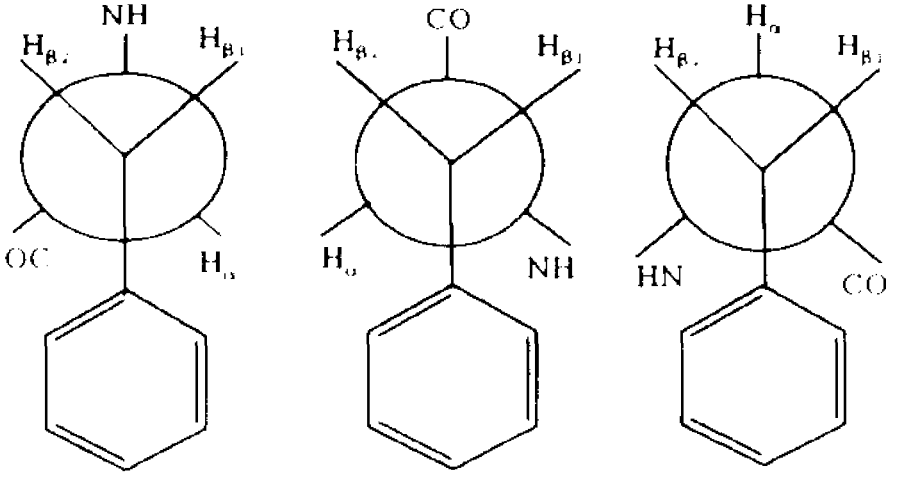

I II III

$J_{\alpha\beta 1}$	< 4Hz	> 10 Hz	< 4 Hz
$J_{\alpha\beta 2}$	> 10 Hz	< 4 Hz	< 4 Hz
NOEs	$\alpha\beta 1 > \alpha\beta 2$	$\alpha\beta 1 < \alpha\beta 2$	$\alpha\beta 1 \approx \alpha\beta 2$
NOEs	$NH_{\beta 2} \approx NH_{\beta 1}$	$NH_{\beta 2} < NH_{\beta 1}$	$NH_{\beta 2} > NH_{\beta 1}$

Figure 31. Evidence for diastereotopic configuration of beta-methylene protons for [pGlu^{6}, NMePhe^{8}, Aib^{9}]-SP$^{6-11}$ in DMSO-d_6 at 25 °C, the αCH-βCH region of 400-MHz 250 msec ROESY is displayed.

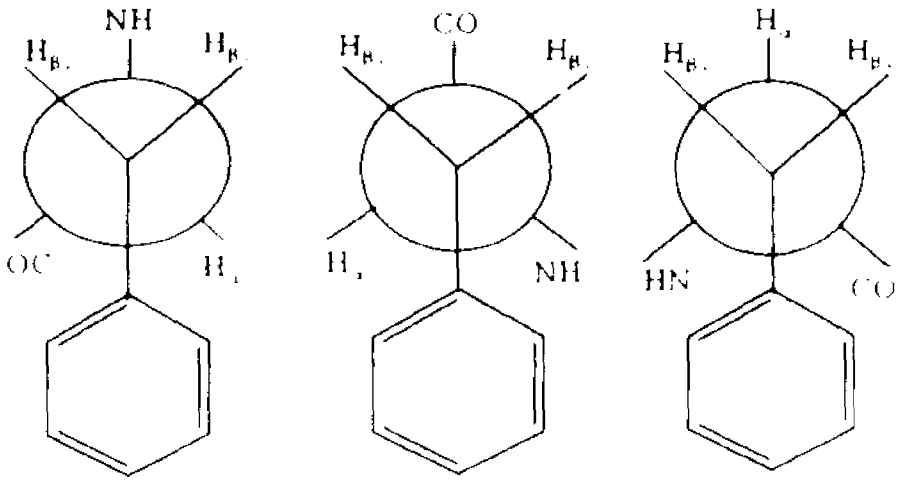
NH
H_{β_1}
H_{β_2}
OC
H_α
CO
H_{β_1}
H_{β_2}
H_α
NH
H_α
H_{β_1}
H_{β_2}
HN
CO

I II III

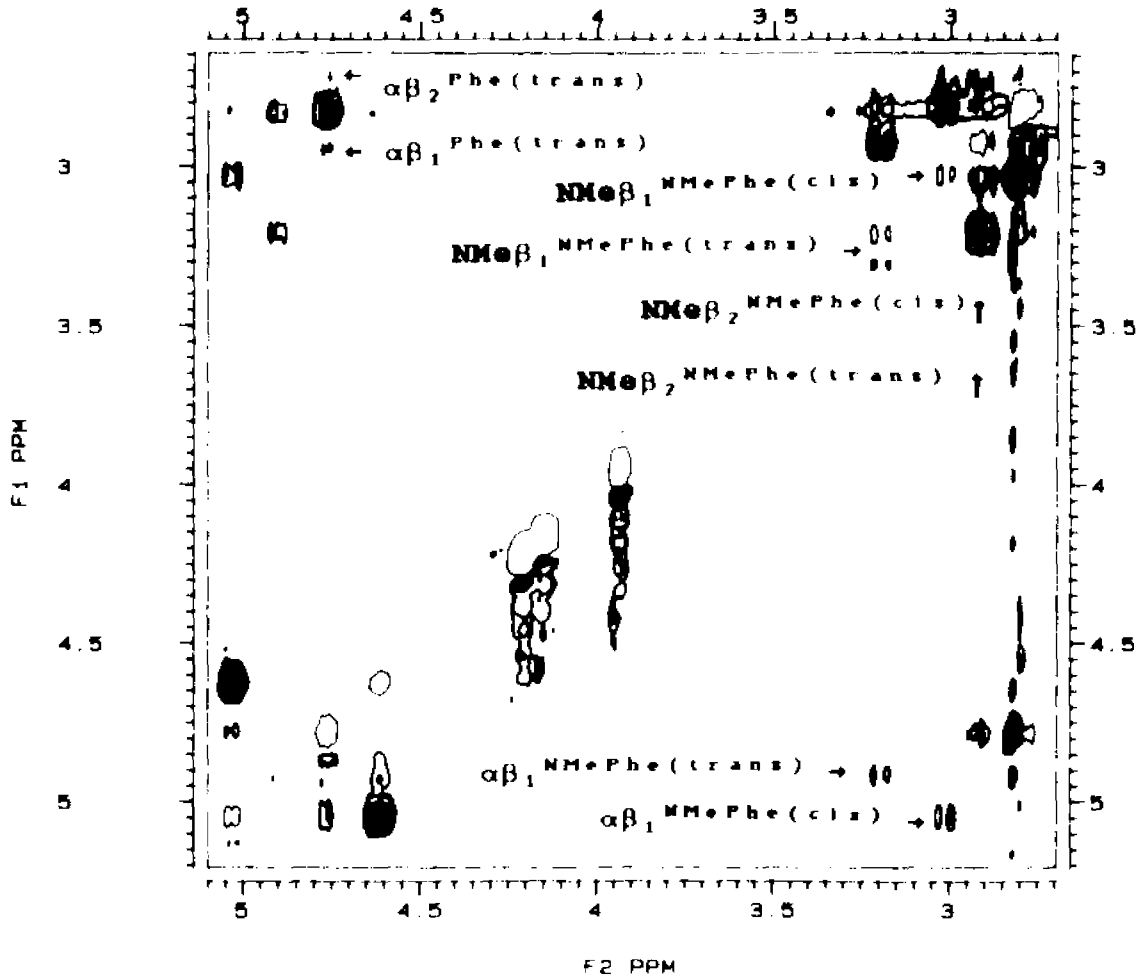
$\alpha\beta_2$ Phe(trans)
$\alpha\beta_1$ Phe(trans)
NMeβ_1 NMePhe(cis)
NMeβ_1 NMePhe(trans)
NMeβ_2 NMePhe(cis)
NMeβ_2 NMePhe(trans)
$\alpha\beta_1$ NMePhe(trans)
$\alpha\beta_1$ NMePhe(cis)
F1 PPM
F2 PPM

Figure 32. Evidence for diastereotopic configuration of beta-methylene protons for [pGlu$^{\alpha}$,NMePhe$^{\beta}$, Aib$^{\gamma}$]-SP$^{6\ 11}$ in DMSO-d_6 at 25 °C, the NH-αCH NH-βCH region of 400-MHz 250 msec ROESY is displayed.

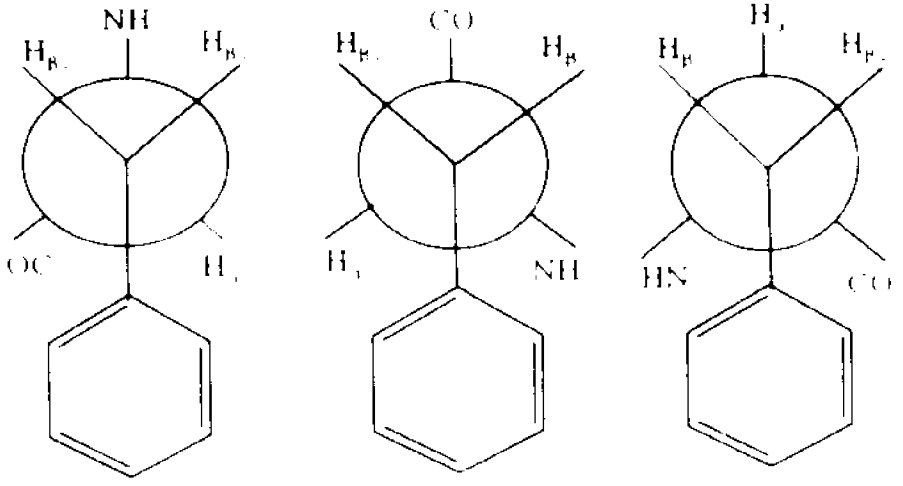
NH
H_β
H_β
OC
H_α
CO
H_β
H_β
H_α
NH
H_α
HN
CO

I II III

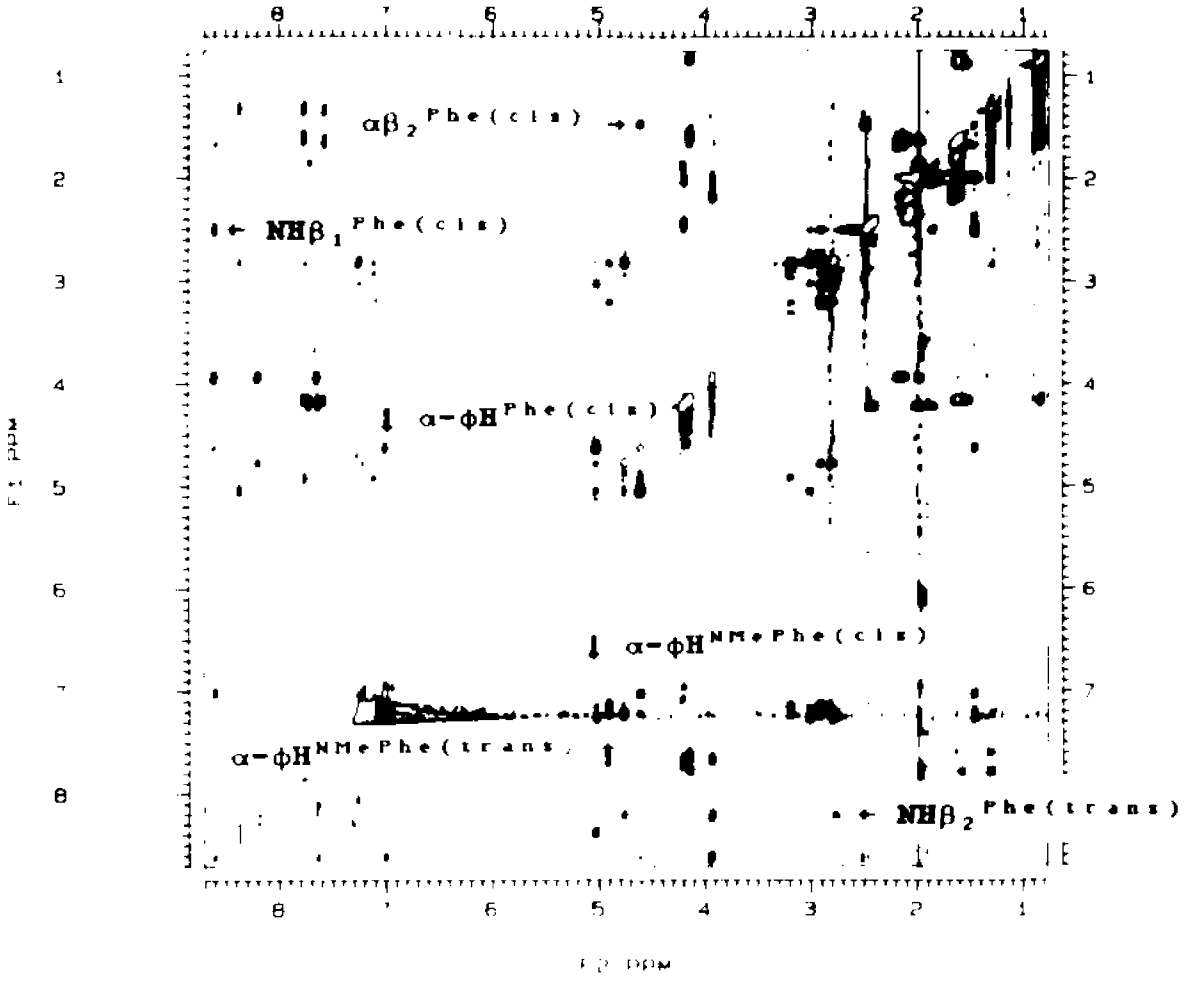
$\alpha\beta_2$ Phe(cis)
$NH\beta_1$ Phe(cis)
$\alpha-\phi H$ Phe(cis)
$\alpha-\phi H$ NMePhe(cis)
$\alpha-\phi H$ NMePhe(trans)
$NH\beta_2$ Phe(trans)
F1 ppm
F2 ppm

Figure 33. Evidence for diastereotopic configuration of beta-methylene protons for [pGlu^{5}, NMePhe^{8}, Aib^{9}]-SP$^{5-11}$ in DMSO-d, at 25 °C, the NH-side-chain ring proton region of 400-MHz 250 msec ROESY is displayed.

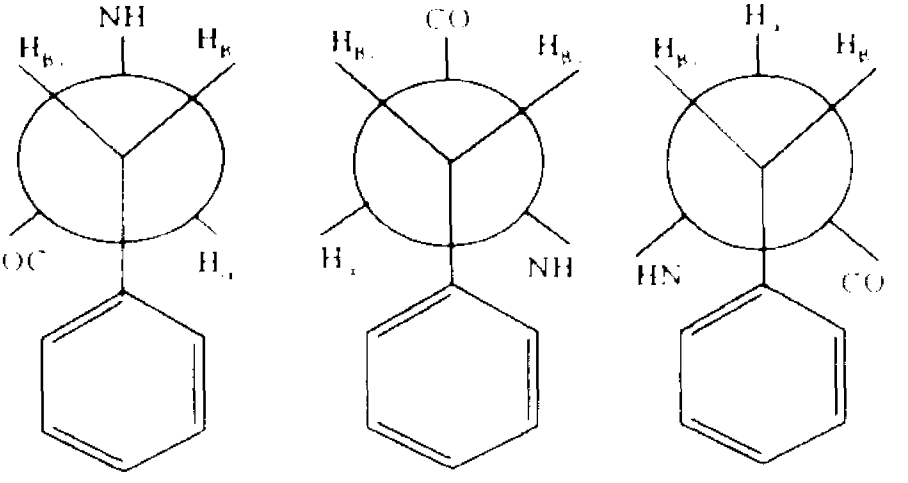
NH
$H_{\beta'}$
H_{β}
OC
H_{α}
CO
$H_{\beta'}$
H_{β}
H_{α}
NH
H_{α}
$H_{\beta'}$
H_{β}
HN
CO

I II III

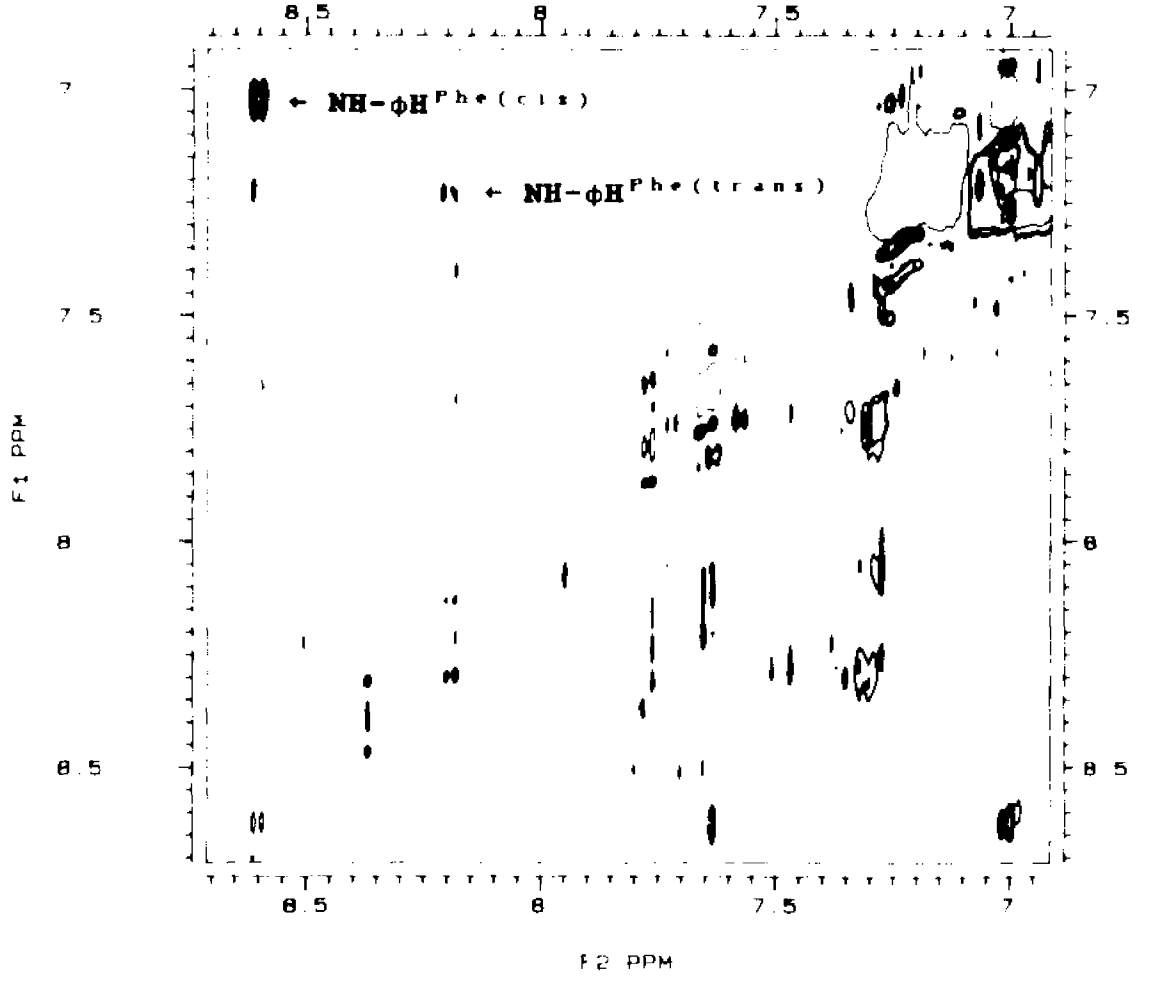
← NH-φH Phe (cis)
← NH-φH Phe (trans)
8.5
8
7.5
7
F1 PPM
F2 PPM

Table 9. Spectral assignments for [pGlu^{5}, NMePhe^{8}, Aib^{9}]-SP$^{5-11}$ in DMSO-d_6 at 25 °C.

Table 9.

Peak Assignments for Protons of

[pGlu^{6},NMePhe^{8},Aib^{9}]SP$^{6-11}$ in DMSO-$_{d6}$*

Residue		HN	αHC	βHC	γHC	δHC	Other
pGlu#6	(t)	7.66	3.94	2.18- 1.66-	2.01-		
pGlu#6	(c)	7.63	3.94	2.10- 1.62-	1.95-		
Phe#7	(t)	8.19	4.76	2.91 2.77			φ7.26,7.24→7.13 7.11-
Phe#7	(c)	8.60	4.61	2.52 1.47			φ 7.27,7.20→7.02 7.00-
N-Me-Phe#8	(t)		4.91	3.20 2.93			N-Me 2.82
N-Me-Phe#8	(c)		5.03	3.02 2.91			N-Me 2.80
Aib#9	(t)	7.76					α-Me 1.34,1.29-
Aib#9	(c)	8.36					α-Me 1.33,1.30-
Leu#10	(t)	7.57	4.14	1.63 1.54	1.58		δ-Me 0.89,0.84
Leu#10	(c)	7.77	4.14	1.63 1.52	1.58		δ-Me 0.89,0.83
Met#11	(t)	7.72	4.21	2.03- 1.87-	2.38 2.45		S-Me 1.99 amide 7.05- 7.20-
Met#11	(c)	7.62	4.21	2.03- 1.87-	2.38 2.45		S-Me 1.99 amide 6.93 7.13-

*[illegible] assigned.
[illegible] parentheses [illegible]

Table 10. Vicinal coupling constants and potential dihedral angles for [pGlu^{6}, NMePhe^{8}, Aib^{9}]-SP$^{6-11}$ in DMSO-d$_{6}$ at 25 °C.

Table 10.

Vicinal Coupling Constants (Hz) and Calculated Angles

for [pGlu°,NMe Phe°,Aib°]SP° [1]

Residue	JHN-αHC	φ Angles*	Jαβ	χ1 Angles¢	Jβγ	χ2 Angles
pGlu#6 (t)	< 1 Hz		3.05	+/-61	7.06	+/-31,135
			3.86	" 54		
pGlu#6 (c)	< 1 Hz		3.78	" 55	8.57	"17,144
			4.86	"122		
Phe#7 (t)	8.18	-148,-92	3.35	" 58		
			2.60	" 65		
Phe #7 (c)	7.20	-156,-84	9.92	"152		
			3.87	" 54		
N-Me-Phe#8 (t)			8.85	"146		
			6.51	" 35		
N-Me-Phe#8 (c)			8.24	"142		
			5.14	" 44		
Leu#10 (t)	7.45	-154,-86	5.45	"126	< 1 Hz	
			3.97	" 54		
Leu#10 (c)	6.96	-158,-82	4.19	"118	< 1 Hz	
			3.38	" 58		
Met#11 (t)	8.30	-150,-94	4.53	" 120	6.22	+/-129
			2.68	" 64	3.66	" 114
					3.39	" 58
Met#11 (c)	6.23	-164,-76, 40,80	4.56	" 49	"	"
			3.62	"114	"	"

* J values were corrected for electronegativity effects
¢ Both positive and negative values will yield the same J value. Values in this table indicate magnitude only; enantiomeric angle assumed to rest due

Table 11. Coupling constants and rotamer populations for aromatic side-chains of [pGlu^{6}, NMePhe^{8}, Aib^{9}]-SP$^{6-11}$ in DMSO-d_6 at 25 °C.

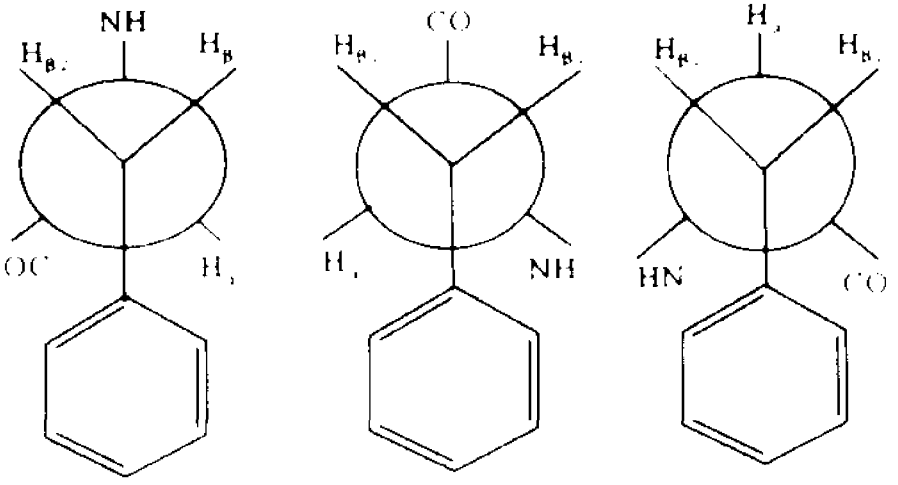

I II III

Table 11.
Rotamer populations of Phe' and
NMe Phe* side-chains in DMSO-d_6*

Residue	$J_{a,}$	$J_{b,}$	Rotamer I	Rotamer II	Rotamer III
Phe#7 (t)	3.45	2.68	< 1 %	< 1 %	99 %
Phe#7 (c)	10.22	3.99	< 1 %	78 %	21 %
N-Me-Phe#8(t)	9.12	6.71	60 %	39 %	< 1%
N-Me-Phe#8(c)	8.49	5.50	55 %	29 %	16 %

*J values corrected for electronegativity effects.

Analysis of coupling constants and ROESY connectivities have not only resulted in determination of the side-chain orientation for residues in this hexapeptide, but more importantly, they have also allowed the stereospecific assignments for the β-protons as well. These assignments are very useful in the construction of a model for the tachykinin analogs.

The rotamer populations are interesting in that the Phe^{7} side-chain in the *trans* diastereomer is calculated to be exclusively in Rotamer III, which is the most sterically hindered of the three staggered forms. In contrast, the same side-chain in the *trans* isomer prefers Rotamer II. In both isomers, the NMe Phe^{8} side-chain appears to assume a much broader distribution of $\chi 1$ angles, but appears to prefer the Rotamer I state. These rotamer populations were calculated by the method of Pachler(105) and are listed in Table 11. In addition, both the Leu^{10} and Met^{11} side-chains seem to prefer the Rotamer III state, in both diastereomers. However, since these residues are located in very crowded regions of the spectrum, the assignments for their predominant rotamers can not be considered unequivocal, and are not listed in Table 11.

To determine the possible involvement of amide protons in hydrogen bond interactions, temperature coefficients for the NH protons were measured from 300K to 325K, low

coefficients, ~ -2 ppb/K, were observed for the Met[11] NH of the *trans* diastereomer,and for the terminal carboxamide in both diastereomers. The coefficient of the Met[11] NH for the *cis* isomer -3.75 ppb/K, was significantly lower than those measured for the remaining NH's in this isomer. However this value is not in the definitive range for hydrogen bonding. The values for all other residues were in the range expected for solvent exposed protons, 6-9 ppb/K. In addition, the standard deviation of each slope was calculated, and these values are reported in Table 12.

Through space interactions are used to gain information which helps define the conformational space available to a linear peptide. NOESY experiments have been widely employed to determine such connectivities (155-157). The NOESY spectra for pGlu[6]-Phe-NMePhe-Aib- Leu-Met[11]-NH_2 in DMSO-d_6 at both 200-MHz and 400-MHz exhibited almost no connectivities. It is believed this was due to a correlation time problem, and 91 connectivities were observed for this hexapeptide in a 250 msec ROESY at 400-MHz. The most significant of these dipolar interactions are summarized in Tables 13 and 14.

Several long-range interactions are observed within both diastereomeric forms of this peptide. Most notably, the long range connectivity between the pro-S βCH of Phe^{7}and the γCH of Met^{11} in the *cis* isomer(1.46,2.45), and between the αCH of pGlu^{6} with both methyl groups of Aib^{9} in the *trans* diastereomer (3.94,1.34), and (3.94,1.30). These connectivities indicate that both diastereomers of this hexapeptide exhibit a predominant conformation which must be bent in solution.

Several other connectivities can circumstantially support our contention that the hexapeptide is bent in DMSO. However, since these regions are very crowded, these connectivities could not be used definitively. For the *cis* isomer, these connectivities include: the βCH of pGlu^{6} with the NH of Leu^{10}(1.61,7.75), the NH of Phe^{7} with the βCH of Leu^{10}(8.60,1.64), and the S-CH_3 of Met^{11} with both methyls of Aib^{9}(1.99,1.34 and 1.30). Long range connectivities associated with the *trans* diastereomer are the ring protons of either Phe^{7,8} with the NH of Met^{11}(7.26,7.71), and much weaker connectivities observed include the NH of pGlu^{6}(3.94) with the methyls of Aib^{9}(1.34,1.30), the αCH of pGlu^{6} with the NH of Aib^{9}(7.65,7.74), and the NH's of Leu^{10} and Met^{11} with the αCH of NMe-Phe^{8}(7.56,4.90)(7.71,4.90).

Table 12. Amide temperature shift coefficients for [pGlu^{6}, NMePhe^{8}, Aib^{9}]-SP$^{6-11}$ in DMSO-d_6 at 25 °C.

Table 12.
Temperature Shift Coefficients for
{pGlu^{6},NMe Phe^{8},Aib^{9}}SP$^{6-11}$ in DMSO-$_{d6}$

Residue	$\Delta\delta/t$ ppb/K	on
pGlu#6 (t)	-6.44	+/- 0.22
Phe#7 (t)	-7.75	+/- 0.35
Aib#9 (t)	-8.76	+/- 1.03
Leu#10 (t)	-5.59	+/- 0.39
Met#11 (t)	-2.29	+/- 0.66
amide (t)	-2.14	+/- 0.28
pGlu#6 (c)	-6.35	+/- 0.34
Phe#7 (c)	-9.23	+/- 0.46
Aib#9 (c)	-7.32	+/- 0.24
Leu#10 (c)	-7.60	+/- 0.34
Met#11 (c)	-3.75	+/- 0.31
amide (c)	-2.74	+/- 0.91

Discussion:

In this study, aggregation has been ruled out as a contributor for the observed NOE connectivities found in pGlu^{6}-Phe-NMePhe-Aib- Leu-Met^{11}-NH_2. Furthermore, this peptide exhibits *cis-trans* isomerization due to the presence of the Phe^{7}-NMePhe^{8} peptide bond. Support for this conclusion has been derived from both the reversible coalescence of the two distinct sets of peaks in the one-dimensional spectrum and ROESY connectivities which also allowed us to distinguish between the two isomers.

Based on the results of the DQF-phase sensitive-COSY, Relayed-COSY, and ROESY experiments, complete resonance assignments for all residues in this peptide have been determined. The results of the ROESY experiment allowed us to complement our spectral assignments through the use of sequential connectivities. Since some of the αCH's and amide protons were well resolved in the 1-D spectrum, integration ratios for each diastereomer were calculated indicating that a 60/40 mixture of *cis-trans* isomers is present in DMSO at 25°C. When ambiguities arose for peak assignments in highly crowded regions of the spectrum, the final criterion for assigning resonances to either the *cis* or *trans*-diastereomer was based on the integration ratios of the respective peaks. This has led us to the reported values listed in Table 9. This resulted in assigning the

downfield set of peaks to the *cis*-isomer, whereas the upfield set of resonances are attributable to the *trans* diastereomer.

In the ROESY experiment, unique NOE connectivities were observed which can be attributed to either the *cis* or *trans* diastereomer. As previously stated, all NOE's expected for a *cis*-peptide bond were observed, most importantly, an intense αCH^{7} - αCH^{8} crosspeak, which was also the strongest connectivity observed in both the NOESY and ROESY experiments. Furthermore, a strong αCH^{7} - NMe^{8} crosspeak was observed for the *trans* diastereomer. Conversely, an extremely weak αCH^{7} - αCH^{8} connectivity was observed for the *trans* isomer, as well as an extremely weak αCH^{7} - NMe^{8} crosspeak for the *cis*-isomer. We believe these unique NOE connectivities are sufficient to assign the two diastereomeric forms of this peptide.

Since both the βCH's of Phe^{7} and NMe-Phe^{8} were well resolved in the one-dimensional spectrum for this hexapeptide, we also calculated the rotamer population of the aromatic side-chains (105). The data could be used to refine the model for the solution-state conformation of the NK3 selective agonist. Utilizing selective saturation experiments to simplify αCH-βCH spin systems, α-β1 and α-β2 coupling constants were calculated. In this study, the most unusual finding was that the Phe^{7} side-chain for the

trans-isomer was almost exclusively in its highest energy rotamer state (Table 11). This result must represent a unique conformational feature present in the *trans*-diastereomer. The aromatic side-chains in all other isomers exhibited a wider distribution of rotamer values. In addition, diastereotopic assignment of the β-protons were determined from unique NOE connectivities; see results section. From these results, we were able to determine that the Met residue is also predominantly in its highest energy rotamer state within both diastereomers. All values for the α-β1 and α-β2 coupling constants were corrected for electronegativity effects (166) and used in a Karplus equation to generate possible χ^1 angles (158), which are reported in Table 10.

Although the angular dependence of the vicinal coupling constant can relate the spatial proximity of protons attached to adjacent carbon atoms, the results of these calculations cannot uniquely define a particular angle. At least two and possibly four angles can be calculated for a given coupling constant(158). In general, these angles are reported as possible ranges assumed by protons on neighboring carbon atoms. Upon first inspection, these angular values would appear insignificant; however, these values can be utilized to either corroborate or negate possible conformations. In order to reduce the number of possible angles assumed by a pair of vicinal protons, we

utilized through space connectivities to distinguish between various possibilities. In particular, if two protons have a small angle between them, then one would expect a strong through space connectivity, whereas a larger angle between these protons should result in a weaker connectivity. Of the values listed in Table 10, those which appear in boldface are believed to be the most likely candidates for angles assumed by this peptide as determined by ROESY connectivities. Most notably, a weak NH_i-αCH_i connectivity is observed for the Phe^7 residue. In contrast, both the Leu^{10} and Met^{11} residues have strong intraresidue NH_i-αCH_i connectivities. Hence we believe that the Leu^{10} and Met^{11} residues assume a much smaller angle than the Phe^7 residue. As such, we believe that the Leu^{10} residue assumes a ϕ angle in the approximate range of -80, whereas the Met^{11} residue is in the approximate range of -80 to 80 degrees. In contrast, we believe the Phe^7 residue assumes an angle in the range of -156° .

In order to determine the possible involvement of amide protons participating in hydrogen-bond interactions, temperature shift coefficients were measured. The terminal carboxamide of Met^{11} exhibited very low values in both diastereomers, -2.74 ppb/K (*cis*) and -2.14 ppb/K (*trans*). The peptide NH of Met^{11} in the *trans*-isomer was also in the range for hydrogen-bonding, -2.29 ppb/K. Although the peptide NH for the *cis* Met^{11} residue is low, -3.75 ppb/K, this value

is not definitive. Nevertheless, we believe that the Met^{11} NH is probably involved in a weak hydrogen bond, since all other NH's are significantly higher and are in range for solvent exposed protons. The participation of the amide and carboxamide of the Met^{11} residue in hydrogen-bonded interactions is a significant structural feature which must be accounted for in any model of the NK3 selective agonist. Many other tachykinin peptides also exhibited low temperature coefficients for the terminal carboxamide of the C-terminal methionine residue(30), and this may be a common structural feature for this class of peptides. These values are listed in Table 12.

In contrast to the carboxamide, involvement of the NH of Met^{11} in a hydrogen bond was not previously reported for NK3 selective neurokinins. In a previous report, the temperature coefficient for this group was in the same range as those ascribed to be solvent exposed(158). However, in the same report, analysis of an NK1 selective agonist suggested the possible involvement of the Met^{11} NH as well as the terminal carboxamide in hydrogen bonding. It is still not clear how one should interpret these results. It may be possible that the flexible nature of the Gly^{9} residue in the NK3 selective agonist studied previously(30) promotes a wider distribution of possible conformations for this

Table 13. NOE connectivities observed in NOESY/ROESY analysis of [pGlu^{6}, NMePhe^{8}, Aib^{9}]-SP$^{6-11}$ in DMSO-d_6 at 25 °C, for the *cis*-diastereomer.

Table 13 NOE connectivities observed for the *cis* diastereomer of [pGlu^4, NMePhe^8, Aib^9] SP$^{4-11}$ in $(DMSO)_{d_6}$ at 25 °C.

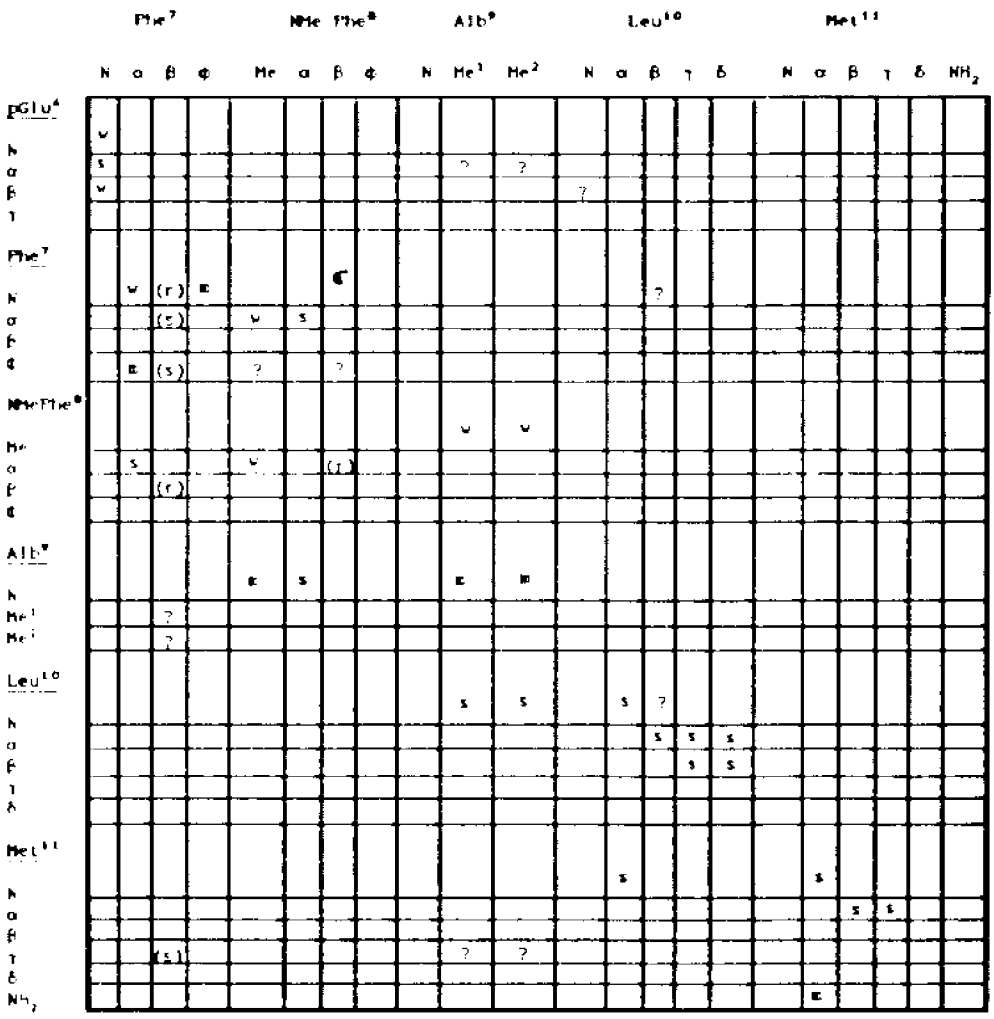

Letters in parentheses indicate the pro-R or pro S configuration of the β protons letters without a parenthesis indicates intensity of the observed NOE, where s denotes strong, m = medium, and w = weak NOE. ? denotes that the NOE observed is not unequivocal le

Table 14. NOE connectivities observed in NOESY/ROESY analysis of [pGlu^{6}, NMePhe^{8}, Aib^{9}]-SP$^{6\ 11}$ in DMSO-d_6 at 25 °C, for the *trans*-diastereomer.

Table 14 NOE connectivities observed for the *trans* diastereomer of [pGlu^{6}, NMe-Phe^{8}, Aib^{9}] SP$^{6-11}$ in DMSO$_{d_6}$ at 25 °C.

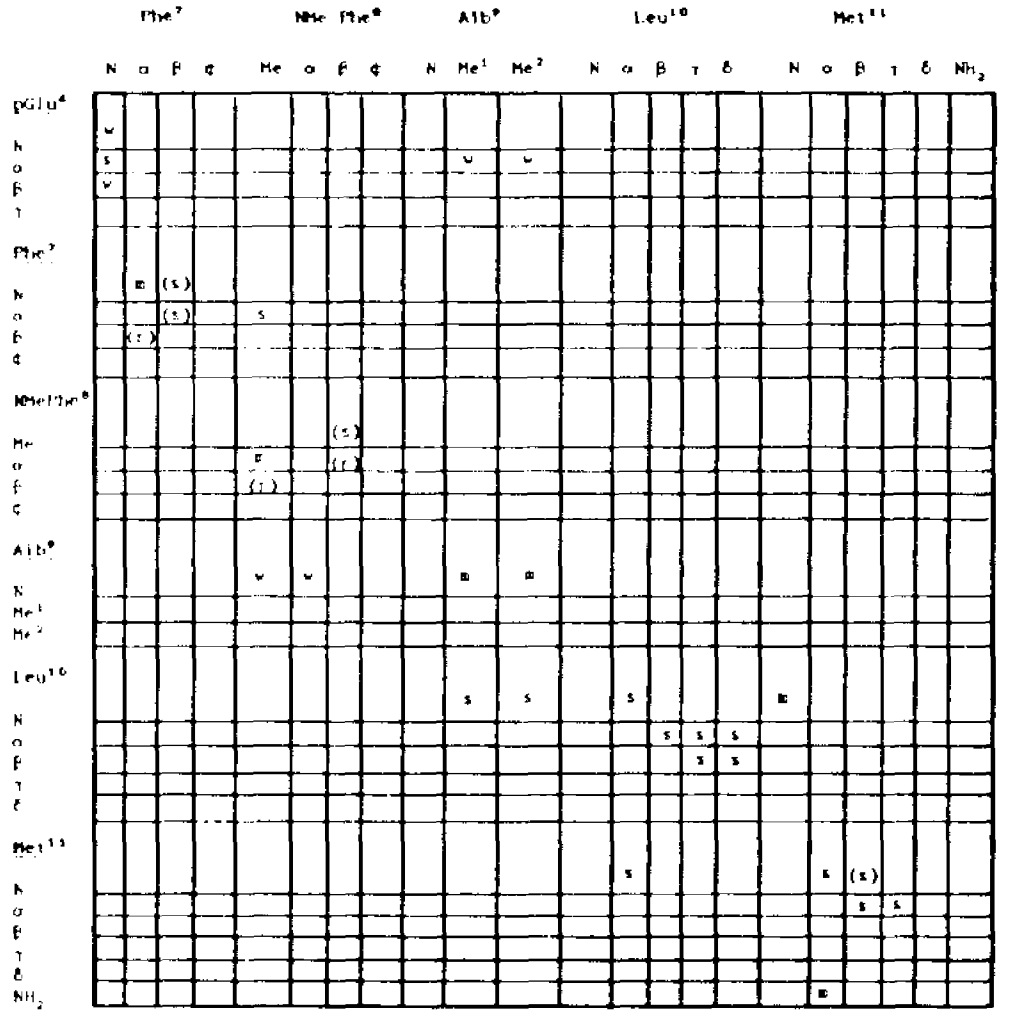

Letters in parentheses indicate the pro R or pro S configuration of the β-protons. Letters without a parenthesis indicate intensity of observed NOE, where s denotes strong, m = medium, and w = weak NOE.

peptide, thus leading to a higher value for the temperature coefficient. In the NK1 selective agonist, a proline residue occupies the Gly^9 position and may reduce the distribution of allowable conformations to a level which permitted detection of this group's involvement in hydrogen bonding.

Although conjecture, this may be one plausible reason for the observed results in the earlier report. It may be interesting to compare the receptor selectivity of an Ala^9 versus Val^9 analog. If the Ala^9 analog were an agonist for both the NK1 and NK3 receptors, whereas the Val^9 analog was an agonist only for the NK1 receptor, one could argue that both the Val^9 and Pro^9 analogs are blocking association of these peptides as a result of steric factors due to this particular position within the binding pocket of NK3 receptor. Furthermore, if both the peptide NH and carboxamide of the Met^{11} residue in both of these analogs display characteristic hydrogen-bonding values, then it is possible that all of these analogs have a similar C-terminal conformation which may be required for activity.

As previously mentioned, several long range through space connectivities were observed for this hexapeptide. Most notably, the connectivity between the αCH of pGlu^6 and the methyl groups of Aib^9 in the *trans*-isomer, and between the pro-S βCH of Phe^7 to the γCH of Met^{11} in the *cis*-isomer. These connectivities are indicative of a chain reversal or

"turn" conformation for the backbone atoms of this peptide. To gain further insights into the nature of the turn, the ROESY experiment was carefully inspected for NOE connectivities which were indicative for a classically defined type of secondary structure. These structures included β-turns, γ-turns, 3-10 helix, α-helix, β-sheet, etc. A number of interresidue NOE's were observed for the N-terminal region of pGlu^{6}-Phe-NMe Phe-Aib^{9}, which at first glance would predict a type II β-turn spanning these residues in the *trans* isomer, and a type β VIb for the *cis*-isomer(Tables 15 and 16). These types of turns can readily accommodate an N-methylated residue in the i+2 and i+3 positions, and are consistent with the peptide bond between Phe-NMe Phe assuming a *trans* and *cis* conformation respectively (79,80,167). However the most diagnostic connectivity, $d_{\alpha N}(2,4)$ = 3.3 angstroms for the β II turn and 1.9 angstroms for the β VI b turn were not observed. Furthermore, the temperature coefficient for the amide of Aib^{9} is not in the range for a hydrogen bond, which would be expected in this type of structure. In addition, the most likely candidate φ angle for the Phe^{7} residue is ~ -160, which would be inconsistent for this type of turn.

Moreover, the intensity of the observed NOE's did not correlate well to the expected distances in these types of turns. Although these turns were the best-fit model for the empirically observed NOE's, I believe this region of the

peptide does not assume the angles which classically define these types of turns. However, many β-turns do not require a stabilizing hydrogen bond to generate these types of structures (80). There appears to be an inherent stability in a β-turn, possibly arising from the orientation of bulky side chains in the i+1 and i+2 positions into conformations which are equatorial and axial respectively to the plane of the turn. Hence the Phe^{7}-$NMePhe^{8}$ side chains may be oriented in a similar fashion to reduce steric interactions between these bulky side-chains, which may result in a lower energy state. I believe this is particularly relevant for the *trans*-isomer, where the observed αCH-$pGlu^{6}$- $Methyls^{9}$ connectivity reflects that the N-terminal region must be bent in order for this connectivity to be generated.

Turning our attention to the C-terminal end of this hexapeptide, the Leu^{10} and Met^{11} residues appear to be in the same local conformational environment in both diastereomeric forms of this peptide. This is evidenced by the fact that for each diastereomer, well resolved peaks are observed for the Phe^{7}, $NMePhe^{8}$, and Aib^{9} residues, whereas the Leu^{10} and Met^{11} residues do not exhibit this trait. It is reasonable that the ends of this peptide would be more flexible than the conformationally restricted residues in the center of the peptide. This possibility is supported by the fact that the $pGlu^{6}$ resonances in both diastereomers are

extremely similar, and that similar coupling constants and psi angle ranges are found for the terminal residues in both diastereomers.

The connectivity between the pro-S βCH of Phe^{7} to βCH of Met^{11} in the *cis*-diastereomer supports our contention that this hexapeptide must be bent in DMSO. However, the "turn" structure proposed for the N-terminal domain is not sufficient to bring these two residues into close proximity.

As such, we believe there may be an additional turn structure for the C-terminal domain. Supporting evidence for a turn structure in the *cis*-isomer comes from NOE connectivities between the βCH of $pGlu^{6}$ with the NH of Leu^{10}(1.61,7.75), the NH of Phe^{7} with the βCH of Leu^{10}(8.60,1.64), and the $S-CH_3$ of Met^{11} with both methyls of Aib^{9}(1.99,1.34 and 1.30). Long range connectivities associated with the *trans* diastereomer are the ring protons of either $Phe^{7,8}$ with the NH of Met^{11}(7.26,7.71), and much weaker connectivities observed include both NH's of Leu^{10} and Met^{11} with the αCH of NMe-Phe^{8}(7.56,4.90)(7.71,4.90).

Table 15. Theoretical interresidue distances for type I and type II β-turns, and observed NOE connectivities for the *trans*-diastereomer of [pGlu^{5}, NMePhe^{6}, Aib^{9}]-SP$^{6-11}$ in DMSO-d_6 at 25 °C.

Table 15.

Connectivity	Interproton distance β-turns (Angs.)		β-sheet (extended chain)	pGlu⁵-Phe NMePhe-Aib NOE's, (trans)[b]
	Type I[a]	*Type II*[a]		
$d_{\alpha N}(2,3)$	3.4	2.2	2.2	strong
$d_{\alpha N}(3,4)$	3.1	3.1	2.2	medium
$d_{\alpha N}(2,4)$	3.5	3.3	5.5	------
$d_{NN}(2,3)$	2.6	4.5	4.7	medium
$d_{NN}(3,4)$	2.3	2.4	4.1	weak
$d_{NN}(2,4)$	3.8	4.3	6.8	------

--- Indicates no observable NOE connectivity.

[a] [illegible] values [illegible] observed experimentally [illegible] the [illegible] analog

Table 16. Theoretical interresidue distances for type VIa and type VIb β-turns, and observed NOE connectivities for the *cis*-diastereomer of [pGlu^{6}, NMePhe^{8}, Aib^{9}]-SP$^{6\ 11}$ in DMSO-d_6 at 25 °C.

Table 16.

Connectivity	Interproton distance β-turns (Angs.) *Type VIa*[a]	*Type VIb*[a]	β-sheet (extended chain)[a]	pGlu°-Phe NMePhe-Aib NOE's, (cis)[b]
$d_{\alpha\alpha}(2,3)$	1.9	1.6	5.5	strong
$d_{\alpha N}(2,3)$	4.5	4.0	2.2	weak
$d_{\alpha N}(2,4)$	1.9	2.8	5.5	------
$d_{\alpha N}(3,4)$	2.5	2.3	2.2	medium
$d_{NN}(3,4)$	4.3	5.4	4.1	weak
$NH^{4}..OC^{1}$	2.6	2.9		
$^{3}J_{NH(3)-H}(2)$	2.3 Hz	7.9 Hz		

--- Indicates no observable NOE connectivity

[a] Calculated values for ideal experimentally for the GTBP analog

From analysis of the above NOE's we have concluded that in both diastereomers of this hexapeptide there is probably a turn structure spanning the C-terminal region as well. I believe the most important NOE's to distinguish the turn type are the following: strong intraresidue αCH_i-NH_i and sequential CH_i-NH_{i+1} connectivities for both the Leu[10] and Met[11] residues were observed. A medium strength connectivity between the NH of Leu[10] and NH of Met[11] was found in the *trans* diastereomer, and the absence of any other NOE connectivity to the terminal carboxamide except for its own sequential connectivity. This latter finding is most significant because in any of the classical β-turn structures, the terminal carboxamide would be in close proximity to the methyls of Aib[9], as well as to the NMePhe[8], and Leu[10] residues. However, interactions between the carboxamide and these residues were not observed. Moreover, bulky β-branched hydrophobic residues are not tolerated well in the i+2 position of β-turns, which would suggest that Leu[10] or Met[11] would not assume this position(79,80). Although I conclude that a classical β-turn is not indicated, all of the observed NOE connectivities would be consistent with a consecutive C_7 conformations spanning residues Aib[9]-Leu-Met[11]-NH_2.

A consecutive C_7 conformation is comprised of two fused $_1$-turn structures, where Aib[9] would occupy the i position, Leu[10] the i+1, and Met[11] the i+2 position for the first

inverse γ-turn. The peptide NH of Met^{11} would hydrogen-bond to the carbonyl of Aib^{9} to stabilize the first γ-turn. The second inverse γ-turn then overlaps the first where Leu^{10} would occupy the i position, Met^{11} the i+1, and the terminal carboxamide would occupy the i+2 position. The 3→1 stabilizing hydrogen bond would be formed between the carbonyl of Leu^{10} and the terminal carboxamide. Hence low temperature coefficients for both the peptide NH and the terminal carboxamide for the Met^{11} residue would be expected in such a structure, which is consistent with our observed results.

In a consecutive γ-turn conformation(168), strong intraresidue connectivities, $d_{NH\ \alpha CH}$=2.3 A, for the Leu^{10}and Met^{11} residues would be expected. In addition, strong sequential connectivities, $d_{\alpha CH_i\ NH_{i+1}}$=2.4A, should also be observed for the Leu^{10}, Met^{11}, and terminal carboxamide. Strong intraresidue connectivities, (dNH-αCH) are observed for the Leu ^{10} and Met^{11} residues, and strong sequential connectivities ($d_{\alpha CH_i\ NH_{i+1}}$) are observed for the Leu^{10}, Met^{11}, and terminal carboxamide. Furthermore, the relative intensities for both the intraresidue and sequential connectivities are all approximately equivalent, indicating the spatial distance between these groups are approximately the same, under the assumption that the flexiblity of this region is constant. These results are consistent with the expected distances for an inverse γ-turn structure.

Moreover, the psi and phi angles defining this type of structure ϕ = -80, φ_1= 80, ϕ_1= -80, φ_2= 80, are consistent with the psi angle ranges we propose for the Leu[10] and Met[11] residues,(-80)-(-90). In addition, these angles would orient the terminal carboxamide away from the Leu[10] residue, thus explaining the lack of interresidue NOE's. An earlier report also lists ϕ angle values, for both the NK1 and NK3 agonists that are compatible for this type of structure(30). Summing up all arguments, we believe that a pseudo β-turn or loop" structure, similar to a type II β-turn for the *trans*-isomer, and a type VIb β-turn for the *cis*-isomer, may be a predominant conformational feature for the N-terminal region spanning residues 6-9. In addition, we believe the C-terminal region may be assuming a consecutive inverse γ-turn conformation spanning residues 9-11 in both diastereomers of this hexapeptide. This results in bringing the ends of this hexapeptide in close proximity, and may reflect a biologically significant conformational feature for this class of peptides.

Interestingly, the consecutive γ-turn structure proposed for the C-terminal domain for this hexapeptide might begin to explain the receptor selectivity exhibited by several other analogs. In particular, modification of the Gly[9] position by bulky amino acids such as proline or sarcosine, results in a dramatic decrease in activity

towards the NK2 and NK3 receptors. However, these analogs are still potent agonists for the NK1 receptor. One hypothesis to explain these results is that the NK2 and NK3 receptors are sensitive to the size of the side-chain in position 9. Bulky amino acids at this position may not be readily accommodated within the binding pocket of these receptors.

However, the NK1 receptor is not as sensitive towards position 9 replacements in the peptide. In fact, replacement of the terminal carboxamide with either the free acid or a methyl ester accompanied by a bulky amino acid at position 9 or the entire Substance P sequence, respectively, gives rise to extremely potent NK1 agonists. In contrast, these same analogs are devoid of activity towards the NK2 and NK3 receptors. In the study by Teitelbuam et al.(30), a lower temperature coefficient was observed for the peptide NH of Met^{11} when proline occupied position 9. Temperature coefficients for both the peptide NH and the terminal carboxamide were -3.5 ppb/K and -3.2ppb/K respectively in the [$pGlu^{6}$, Pro^{9}] SP^{6-11} analog suggesting their involvement in hydrogen bonding. In addition, the vicinal coupling constants for the Leu^{10} and Met^{11} residues are consistent with a psi angle of $\sim$ -80. It is plausible that when a bulky or conformationally restricting residue (i.e. Pro^{9}, Aib^{9}, or Sar^{9}), occupies the 9 position, this results in favoring the inverse γ-turn spanning residue 9 to 11. This

γ-turn may be minimally sufficient for eliciting the proper conformation of these analogs for the NK1 receptor. According to this hypothesis, the activity of a [pGlu^{6}-Aib^{9}] SP$^{6-11}$-OMe analog should be active with at least the NK1 and NK3 receptors, since Aib may restrict the conformational flexibility of this analog,whereas the flexible [pGlu^{6}-Gly^{9}] SP$^{6-11}$-OMe should be inactive with the NK1 and NK3 receptors.

Several tachykinin peptides have been previously analyzed by NMR spectroscopy. In particular, the pGlu-Phe-NMePhe-Gly-Leu-Met-NH_2 analog studied by Teitelbuam et al (30) can be thought as the parent peptide to the present study, in which the Glycyl residue has now been replaced by Aib in the present report. Their study provides an opportunity to make direct comparisons with our analyses, which may result in elucidating common structural characteristics possessed by both of these NK3 selective analogs. These structural features may be critically important in the transmission of information from the peptide to the NK3 receptor, which has remained the central goal of both these studies.

A similar approach was employed in the previous report for the spectral assignments of [pGlu^{6},Pro^{9}]SP$^{6-11}$. This resulted in assignment the downfield set of peaks to the trans diastereomer, and the upfield set to the

cis-isomer. In contrast, we conclude that the downfield set of peaks is attributable to the *cis*-isomer, and the upfield set to the *trans* diastereomer. Although these peptides are intrinsically distinct, Gly^9 in the previous report versus Aib^9 in the latter, we do not believe this difference would lead to a complete reversal of chemical shifts for the two sets of isomers. The previous report distinguished between the two diastereomers based on the $J_{NH-\alpha CH}$ of Phe^7, and NOE's which were indicative of a type VIb β-turn. This type of turn is exclusive for a *cis*-proline (167) or N-methylated residue in the i+2 position. In addition, NOE's indicative of a γ turn were observed for the downfield isomer, which would be consistent with a *trans* peptide bond.

However we believe these conformations are still too speculative. The Φ angles for both isomers in the previous report are consistent with a γ turn conformation, where the i + 1 and i + 2 residue would be approximately -90° . Furthermore, the previous report never mentions the most prominent crosspeak, an intense αCH^7-α-CH^8 connectivity whose distance would range 1.6 - 1.9 angstroms apart in a β VI turn. Moreover, the models proposed for both diastereomers would involve the amide of Gly^9 in a stabilizing hydrogen bond. This appears contradictory to their own temperature coefficient data. The temperature coefficient for the Gly^9 amide, -4.4 (*trans*) and -5.3 (*cis*), is in the same range for all other peptide bond NH's, except

for the *trans* NH of Leu^{10}, which in even higher at -7.3. The only coefficient in the range for a possible hydrogen bond is the terminal carboxamide of Met^{11}, -2.9 (*trans*) and -0.5 (*cis*).

Although it must be emphasized that a H-bond is not mandatory for several beta-turns(80), we believe the previous results are not sufficient to conclusively define the conformations for these diastereomers. In order to refine the existing model for the NK3 selective agonist, the Gly^{9} residue was replaced by a conformationally restricting Aib moiety. This sterically hindered residue would restrict the distribution of allowable conformations for this hexapeptide to assume. The flexible nature of the Gly^{9} agonist may have been a shortcoming in the previous report, and may have led to the observed ambiguities in the earlier results.

It is particularly interesting to note that in the previous report a connectivity between the NH-pGlu^{6} and NH-Gly^{9} was observed in both of their diastereomers. These connectivities would further support our contention that the N-terminal region spanning residues 6-9 is bent in DMSO. Other long range connectivities observed in the earlier report include the NH of Met^{11} to the NH Phe^{7}, and the NH of

Phe^{7} to the NH of Leu^{10}, for their proposed-*trans* isomer. Whereas the proposed *cis*-isomer exhibited dipolar couplings between the NH-PGlu^{6} to the NH-Met^{11}.

The long range connectivities observed for the proposed *trans* isomer in the earlier report are the similar connectivities we observe for our *cis*-isomer in the present study. Connectivities associating residues 6 to 9 and 9 to 11 in their *cis* isomer, are the same interacting residues we observe for our *trans* isomer. Taking into consideration that similar chemical shifts were observed for both agonists by ignoring the *cis-trans* distinction, it appears that if one again ignores the *cis-trans* designation, similar NOE's are observed in both reports. Summing up these points, we believe that the *cis/trans* assignments in the previous report should be reversed(30).

In conclusion, we have presented a detailed conformational analysis for pGlu^{6}-Phe-NMePhe-Aib-Leu-Met^{11}-NH_2, utilizing a variety of spectroscopic approaches. The results of our studies are now being employed in internal energy minimization routines to generate a "first generation" model which accurately describes the conformation of this NK3 selective agonist. It is hoped these studies will lead to a better understanding on the activity of this NK3 selective agonist, as well as this whole class of tachykinin peptides.

VI) References

1) IUPAC-IUB (JCBN), (1983) J. Biol. Chem. **260**, 14

2) Cunningham B., Well J.A.(1991) Proc. Natl. Acad. Sci. USA. **88**, 3407

3) Veber D.F., Proc. 7th Am. Peptide Symp. (1981) 685

4) Milon A., Miyazawa T., Higashijima T. (1990) Biochemistry **29**, 65

5) Casey P.J., Gilman A.G. (1988) J. Biol. Chem. **263**, 2547

6) Dietzel C., Kurjan J. (1987) Cell **50**, 1001

7) Nakayama N.A., Miyajima A., Arai K. (1987) EMBO J. **6**, 249

8) Gilman A.G. (1987) **56**, 615

9) Dohlman H., Caron M., Lefkowitz R.J. (1987) Biochemistry **26**, No. 10, 2657

10) Wooley P., Clark F.C. (1989) Biotechology, **7**, 913

11) Bourne H., (1989) Nature **337**, 504

12) Lochrie M.A., Simon M.I. (1988) **27**, 4953

13) Stryer L., Bourne H.R. (1986) Annu. Rev. Cell Biol. **2**, 391

14) Jennings M...., (1989) Annu. Rev. Biochem. **58**, 999

15) Lodish H.F. (1988) TIBS **13**, 332

16) Marx J.L. (1987) Science **238**, 615

31) Naider F., Becker J.M. (1986) Crit. Rev. Biochem. **21**, 225

32) Dolan J., Fields S. (1991) Biochim. Biophys. Acta **1088**, 155

33) Blumer K.J., Thorner J. (1991) Annu. Rev. Physiol. **53**, 37

34) Herkoswitz I. (1988) Microbiol. Rev. **52**, 536

35) Betz R., Manney T.R., Duntze W. (1981) Gamete Research **4**, 571

36) Becker J.M., Marcus S., Kundu B., Shengbagamurthi P., Naider F. (1987) **7**, 4122

37) Marcus S., Caldwell G., Xul C., Naider F., Becker J.M. (1990) Biochem. Biophys. Res. Commun. **172**, 1310

38) Manney T.R., Duntze, Betz R. (1981) in Sexual Interaction in Eukaryatic Microbes, Acad. Press, pp.21

39) Goodenough V., Thorner J. (1983) in Cell Interactions and Development, John Wiley & Sons, 29

40) Kurjan J., Herskowitz I. (1982) Cell **30**, 933

41) Othniel E., Mechler B., Achstelter T., Muller H., Wolf D., (1983) Biochem. Biophys. Res. Commun. **116**, 822

42) Julius D., Blair L., Brake A., Sprague G., Thorner J. (1983) Cell **32**, 839

43) Julius D., Brake A., Blair L., Kunisawa R., Thorner J. (1984) Cell **37**, 1075

44) Achstetter T., Wolf D. (1985) EMBO J., **4**, 173

45) Tallon M., Shengbagamurthi P., Marcus S., Becker J.M., Naider F. (1987) Biochemistry **26**, 7767

46) Schafer W., Trueblood C., Yang C., Mayer M. (1990) Science **249**, 1133

47) Lowy D.R., Willimsen B. (1989) Nature **341**, 384

48) Gibbs J. (1991) Cell **65**, 1

49) Reiss Yuval, Goldstein J., Seabra M., Casey P., Brown M. (1990) Cell **62**, 81

50) Chan R.K., Otte C.A. (1982) Mol. Cell. Biol. **2**, 11

51) Chan R.K., Otte C.A. (1982) Mol. Cell. Biol. **2**, 21

52) Jenness D., Burkholder A.C., Hartwell L.H. (1983) Cell **35**, 521

53) Hagen H.C., McCaffrey G., Sprague G. (1986) Proc. Natl. Acad. Sci. USA **85**, 1418

54) Blumer K., Thorner J. (1990) Proc. Natl. Acad. Sci. USA **87**, 4363

55) Herskowitz I., Marsh L. (1987) Cell **50**, 995

56) Blinder D., Bourier S., Jenness D. (1989) Cell **56**, 479

57) Blumer K., Reneke J., Thorner J. (1988) J. Biol. Chem. **263**, 10836

58) Yu I., Blumer K., Davidson N., Lester H., Thorner J. (1989) J. Biol. Chem, **264**, 20847

59) Naider F., Yaron A., Ewenson A., Tallon M., Xue C., Srinivasan J., Bargiota E., Becker J. M. (1990) Biopolymers **29**, 237

60) Kyte J., Doolittle R.J. (1982) J. Mol. Biol. **157**, 105

61) Konopka J.B., Jenness D., Hartwell L. (1988) Cell **54**, 609

62) Reneke J., Blumer K., Courchesne W., Thorner J. (1988) Cell **55**, 221

63) Courchesne W., Kunisawa R., Thorner J. (1989) Cell **58**, 1107

64) Rovero P., Pestellini V., Patacchini R., Santiciollo P., Maggi C., Meli A. (1989) Biopolymers **28**, 65

65) Regoli D., Dior S., Rhaleb N., Rouissi N., Tousignant C., Juric D., Juste D. (1989) Biopolymers **28**, 81

66) Masui Y., Tanaka T., Chino N., Kita H., Sakakibara S. (1979) Biochem. Biophys. Res. Commun. **86**, 982

67) Stotzler D., Duntze W. (1976) Eur. J. Biochem. **65**, 257

68) Masui Y., Chino N., Sakakibara S., Tanaka T., Murakami T., Kita H. (1977) Biochem. Biophys. Res. Commum. **78**, 534

69) Ciejek E., Thorner J., Geier M. (1977) Biochem. Biophys. Res. Commun. **78**, 952

70) Shengbagamurthi P., Baffi R., Khan S., Lipke P., Pousman C., Becker J.M., Naider F. (1983) Biochemistry **22**, 1298

71) Ciejek E., Thorner J. (1979) Cell **18**, 623

72) Tanaka T., Kita H. (1978) Biochem. Biophys. Res. Commun. **83**, 1319

73) Bargiota E., Becker J.M., Xue C.-B., Naider F. (submitted for publication)

74) Thorner J. (1980) in The Molecular Genetics of Development, Academic Press, pp.119

75) Baffi, R., Shenghagamurthi P., Terrance K., Becker J.M., Naider F., Lipke P.N. (1984) J. Bacteriol. **158**, 1152

76) Chou P.Y., Fasman G.D. (1978) Adv. Enzymol. **47**, 45

77) Gierasch L., Deber C., Madison V., Niu C., Blout E. (1981) Biochemistry **20**, 4730

78) Venkatachalam C. (1968) Biopolymers **6**, 1425

79) Dyson J., Rance M., Houghten R., Lerner R., Wright P. (1988) J. Mol. Biol. **201**, 161

80) Rose G. Gierash L., Smith J. (1985) Adv. Prot. Chem. **37**, 1

81) Higashijima T., Fujimura K., Masui Y., Sakakibara S., Miyazawa T. (1983) FEBS Lett. **159**, 229

82) Shengbagamurthi P., Kundu B., Raths S., Becker J. M., Naider F. (1985) Biochemistry **24**, 7070

83) Baffi R., Becker J.M., Lippe P.N., Naider F. (1985) Biochemistry **24**, 3332

84) Higashijima T., Masui Y., Chino N., Sakakibara S., Kita H., Miyazawa T. (1984) Eur. J. Biochem. **140**, 163

85) Higashijiama T., Miyazawa T., Mausi Y., Chino N., Sakakibara S., Kita H. (1979) Peptide Chemistry, 155

86) Wakamatsu K., Okada A., Miyazawa T., Masui Y., Sakakibara S., Higashyima T. (1987) Eur. J. Biohem. **163**, 331

87) Miyazawa T., Higashijima T. (1981) Biopolymers **20**, 1949

88) Wakamatsu K., Okada A., Suzuki M., Higashijima T., Masui Y., Sakakibara S., Miyazawa T. (1986) Eur. J. Biochem **154**, 607

89) Jeliks L., Broido M., Becker J.M., Naider F. (1989) Biochemistry **28**, 4233

90) Jelicks L., Naider F., Shengbagamurthi P., Becker J.M., Broido M. (1988) Biopolymers **27**, 431

91) Naider F., Jelicks L., Becker J.M., Broido M. (1989) Biopolymers **28**, 487

92) Xue C.-B., Bargiota E., Miller D., Becker J.M., Naider F. (1989) J. Biol. Chem. **264**, 19161

93) Pernow B. (1983) Pharmacol. Rev. **35**, 85

94) Costa M., Furness J.B. (1982) Br. Med. Bull **38**, 147

95) Henry J., Couture R., Cuello A., Pelletier G., Quirion R., Regoli D. (1987) in Substance P and Nuerokinins, Springer-Verlag, N.Y.

96) Warmser V., Laufer., Hart Y., Chorev M., Gilon C., Selinger Z. (1986) EMBO J. **5**, 2805

97) Laufer R., Gilon C., Chorev M., Selinger Z. (1986) J. Biol. Chem. **22**, 10257

98) Buck S., Burcher E., Shults C., Lovenberg W., Donohue T. (1984) Science 226, 36

99) Kaiser E., Colescott R., Bossinger C., Cook P. (1970) Anal. Biochem. 34, 595

100) Stewart J.M., Young J.D. (1969) in Peptide synthesis, First Ed. W.H. Freeman and Company, San Francisco California

101) Mitchell A., Kent S., Engelhard M., Merrifield R.B. (1978) J. Org. Chem. 43, 2845

102) Tam J., Kent S., Wong T., Merrifield R.B. (1979) Synthesis 12, 955

103) Stewart J.M., Young J.D. (1984) in Peptide synthesis, Second Ed. Pierce Chemical Corp., Rockford Il.

104) Tam J., Merrifield R.B., (1987) In The Peptides: Analysis, Synthesis, and Biology Vol. 9, pp 185-248, Academic Press, N.Y.

105) Pachler K.G.R.,(1964) Spectrochimocta, 20, 581.

106) Marion D., Wuthrich K., (1983) Biochem. Biophys. Res. Commun.113, 967

107) Rance M., Sorenson O., Bodenhausen G., Wagner G., Ernst R., Wuthrich K. (1983) Biochem. Biophys. Res. Commun. 117, 479

108) Wagner G. (1983) J. Mag. Reson. 55, 151

109) Bax A., Drobny G. (1985) J. Mag Reson. 61, 306

110) Kopple K.D., Ohnishi M., Go A. (1969) Biochemistry 8, 4807

111) Kopple K.D., Ohnishi M. Go A. (1969) J. Am. Chem. Soc. **91**, 4264

112) Walter G., Doolittle R.F. (1983) in Genetic Engineering, Plenum Press N.Y., **5**, pp 61

113) Mariottino P., Chomyn A., Attardi G., Trovato D., Strong D., Doolittle R.F. (1983) Cell **32**, 1269

114) Cnomyn A., Mariottino P., Gonzalez N., Attardi G., Strong D., Trovato, Rieley M., Doolittle R.F. (1983) Proc. Natl. Acad. Sci. USA **80**, 5535

115) Brandolin G., Boulay F., Dalbon P., Vignais P. (1988) Biochemistry **28**, 1093

116) Mariottini P., Chomyn A., Doolittle R.F., Attardi G. (1986) J. Biol. Chem. **261**, 3355

117) Seckler R., Moroy T., Wright J., Overath P. (1986) Biochemistry **25**, 2403

118) Haspel H., Rosenfield M., Rosen O. (1988) J. Biol. Chem. **263**, 398

119) Maelicke A., Wilk-Plumer R., Fels G., Spencer S., Englehard M., Veltel D., Conti-Tronconi B. (1989) Biochemistry **28**, 1396

120) Neumann D., Barchan D., Safran A., Gershoni J., Fuchs S. (1966) Proc. Natl, Acad. Sci USA, **83**, 3008

121) Mulchahey J., Neill J., Dion D., Bost K., Blalock J.(1986) Proc. Natl, Acad. Sci USA, **83**, 9714

122) Gahmen V., Prinz H., Glatter V., Beyreuther K. (1985) EMBO J. **4**, 1731

123) Merrifield B. (1986) Science **232**, 341

124) Kent S. (1988) Annu. Rev. Biochem, **57**, 957

125) Young J.D., Huang A., Ariel N., Briuns J., Ng. D., Stevens R. (1990) Peptide Research **3**, 194

126) Matsueda G., Stewart J.M. (1981) Peptides **2**, 45

127) Orlowski R.C., Walter R., Winkler D. (1976) J. Org. Chem. **41**, 3701

128) Dyrberg T., Oldstone M. (1986) J. Exp. Med. **164**, 1344

129) Dimarchi R.D., Tam J.P., Kent S.B.H., Merrifield R.B. (1982) Int. J. Peptide Res. **19**, 88

130) Sklar L., Far S., Seligmann B., Freer R., Muthukumaraswamy N., Mueller H. (1990) Biochemistry **29**, 313

131) Kent S.B.H., Mitchell A.R., A.R. Engelhard M., Merrifield R.B., Proc. Natl. Acad. Sci USA **76**, 2180

132) Echeverria C., Molins A., Albericio F., Pions M., Giralt E. (1990) Int. J. Peptide Protein Res. **35**, 434

133) DiBello C., Gozzini L., Tonellato M., Corradini M., D'Auria G., Paolillo L., Trivellone E. (1989) Biopolymers **28**, 421

134) Langs D. (1989) Biopolymers 28, 259

135) Motta A. Picone D., Temussi P.A., Marastoni M., Tomatis R. (1989) Biopolymers **28**, 479

136) Sexena V.P., Wetlaufer D.B. (1971) Proc. Natl. Acad. Sci USA **66**, 969

137) Cantor C., Schimmel P. (1980) in Biophysical Chemistry Part II, W.H. Freeman and Co., San Francisco

138) Pardi A., Billeter M., Weuthrick K. (1984) J. Mol. Biol. **180**, 741

139) Williamson M.P. (1990) Biopolymers **29**, 1423

140) Jeener J., Meier H., Bachmann P., Ernst R. (1979) J. Chem. Phys. **71**, 4546

141) Macura S., Ernst R.R. (1980) Mol. Phys. **41**, 95

142) Keepers J.W., James T.L. (1984) J. Magn. Reson. **57**, 404

143) Gronenborn A.M., Clore G.M. (1985) Prog. Nucl. Mag. Reson. Spectroscopy **17**, 7

144) Suzuki E., Pattabiraman N., Zon G., James T.H. (1986) Biochemistry **25**, 6854

145) Kessler H., Gehrke M., Griesinger C. (1988) Angew. Chem. Int. Ed. Engl. **27**, 490

146) Neuhaus D., Wagner G., Vasak M., Kagi J., Weuthrick K. (1985) Eur. J. Biochem. **151**, 257

147) Bax A., David D.G. J. Magn. Reson. (1985) **65**, 355

148) Rance M. (1987) J. Magn. Reson. **74**, 557

149) Bax A., Drobny G. (1985) J. Magn. Reson. **61**, 306

150) Wagner G. J. Magn. Reson. (1983) **55**, 151

151) Kessler H., Oschkinat, Griesinger C., Bermel W. (1986) J. Magn. Reson. **70**, 106

152) Clore G.M., Gronenborn A.M. (1985) J. Mag. Reson. **61**, 158

153) Marion D. FEBS Lett. (1985) **19**, 99

154) Bax A., David D. (1985) J. Magn. Reson. **63**, 207

155) Wuthrich K. (1990) J. Biol. Chem. **265**, 22059

156) Kapstein R., Boelens R., Scheek R.M., Gunsteren W.F. (1988) Biochemistry **27**, No. 15 5395

157) Fesik S., Bolis G., Sham H., Olenjniczak T. (1987) Biochemistry **26**, 1851

158) Wuthrick K., in NMR of Proteins and Nucleic Acids (1986) John Wiley & Sons, N.Y.

159) Jardetzky O., Roberts G.C.K., in NMR in Molecular Biology, (1981), Academic Press, N.Y.

160) Dyson J., Rance M., Houghten R., Wright P., Lerner R. (1988) J. Mol. Biol. **201**, 201

161) Benedetti E. DiBlasio B., Pavone V., Pedone C., Santini A., Crisma M., Valle G., Toniolo C. (1989) Biopolymers **28**, 175

162) Kessler H., Bermel W. (1986) in NMR in Stereochemical Analysis, VCH Publishers Inc., pp. 179-205

163) Vitoux B., Aubry A., Cung T., Marraud M. (1986) Int. J. Peptide Protein Res., **27**, 617

164) Kessler H. (1979) Angew. Chem. Int. Ed. Engl. **9**, 219

165) Chou P.Y., Fasman G.D. (1977) J. Mol. Biol. **115**, 135

166) Bystrov V.F., Ivanov V.T., Portnova S.T., Blashiova T., Ovchinnikov Y. (1973) Tetrahedron **29**, 873

167) Hollosi M., Kawai M., Fasman G.D. (1985) Biopolymers **24**, 211

168) Rao B., Kumar A., Balaram H., Balaram P. (1983) J Am. Chem. Soc. **105**, 7423

169) Othniel E., Mechler B., Achstelter T., Muller H., Wolf D., Biochem. Biophy. Res. Commun. 116, 822